Doppler Flow Velocity System
User Manual
Version 1.70

DOPPLER FLOW VELOCITY SYSTEM

TABLE OF CONTENTS

INTRODUCTION

Cardiovascular System: Mice and Humans

The cardiovascular function in mice and other small animals is very similar to that in large animals and humans. Therefore methods used to make cardiovascular measurements in humans can be used in mice and small animals as well. The main difference between mice and human cardiovascular system is scaling. Table 1 below shows the similarities and differences of the cardiac parameters between mice and humans. Table 2 shows some cardiovascular and other general parameters in a mice, dogs, and humans. Note: ***The values shown are approximate with most of them calculated using allometric equations and should used only as a guide***.

Table 1. Comparison of cardiovascular parameters: mice vs.human.

Factor	Cardiovascular
Lower:	Volumes, Dimensions, Masses, Flows
Similar:	Pressures, Velocities, Wave shapes, Body temperatures
Higher:	Heart rates, Derivatives, Accelerations

Table 2.Cardiovascular and other physiological parameters in adult mice and humans

General		
Parameter	Mouse	Human
Body Weight (kg)	0.02-0.04	70-80
Body Temperature (°C)	36.5-38	36.1-37.2
Respiration Rate (breaths/min or BrPM)	80-220	12-20
Heart Rate (beats/min or BPM)	350-750	60-100
Heart Period (R-R interval) (msec)	80-171	600-1000

Systolic		
Parameter	Mouse	Human
Systolic Blood Pressure (mmHg)	95-125	95-140
Peak LVP (mmHg)	95	100-145
Maximum LVdP/dt (mmHg/s)	10000-15000	
Minimum LVdP/dt (mmHg/s)	-7000 - -12000	
Relaxation time constant, τ, (ms)	1-10	
LV End Diastolic Pressure (mmHg)	3-5	
Peak Ao Velocity (cm/s)	79-121	100-170
Mean Ao Velocity (cm/s)	19-27	18
Ao Acceleration (m/s^2)	111-277	
Rise Time (msec)	2.5-8.5	
Ejection Time (msec)	34-40	
Stroke Distance (cm)	22-36	
Cardiac Output (l/min)	0.011-0.016	4 - 5
Stroke Volume (ml)	0.025-0.035	56

Diastolic		
Parameter	Mouse	Human
Diastolic Blood Pressure (mmHg)	60-90	60-90
E Velocity (cm/s)	55-65	70-102
A Velocity (cm/s)	25-35	43-69
E/A Velocity Ratio	2.0-3.0	1.0-2.4
Linear Decelerating time of E (msec)	26-32	167-231
Decelerating rate of E (m/s^2)	21-24	

Other		
Parameter	Mouse	Human
Wave Speed (m/s)	2.5-4.0	4.0-6.5
Isovolumic Relaxation Time (msec)	13-20	55-90
Isovolumic Contraction Time (msec)	8-14	25-50

Dimensions		
Parameter	Mouse	Human
Body Weight (kg)	0.02-0.04	70-80
Empty Heart Weight (kg)	0.0009-0.0017	0.3-0.35
Total Blood Weight (kg)	0.00112-0.00115	4.9-5.7
Total Blood Volume (l)	0.0014-0.0025	4.7-5.5
Aortic Radius (mm)	0.45-0.50	20-30
Radius of Large Arteries (mm)	0.1-0.25	5-15
Length of Large Arteries (mm)	32.5-	200-250-
Number of Large Arteries	40	40
Radius of Capillaries (mm)	0.0025-	0.004-0.005
Length of Capillaries (mm)	0.092-	0.5-1.0
Number of Capillaries	$1.83*10^7$	$1.9*10^9$
LV Diastolic Dimension (mm)	2.5-3.5	36-52
LV Systolic Dimension (mm)	2.0-3.0	23-39
Septum (mm)	1.0-2.0	8-14
Posterior Wall Thickness (mm)	0.5-1.0	9-13
Left Atrium Wall Thickness (mm)	.025-.030	27-47

Application Areas

The following are the applications areas that are similar to those used humans and are most commonly used in mice.

Cardiac Flow Velocity Measurements
- o Signals measured - Asc. Aortic flow velocity, Mitral flow velocity, (pulmonary artery flow and tricuspid flow)

Pulse Wave Velocity Measurements
- o Signals measured - Aortic arch -Abdominal aortic flow velocities; Aortic sinus/root-R.Carotid flow velocities, Iliac-Femoral flow velocities

Transverse Aortic Constriction Measurements
- o Signals measured - Left & Right carotid and Stenotic jet velocity at arch

Coronary Flow Velocity and Coronary Flow Reserve Measurement
- o Signals measured - Left main coronary flow velocity (right coronary flow velocity)

Peripheral Flow Velocity Measurements
- o Signals measured - L & R carotid flow velocity, L & R renal flow velocity, iliac flow velocity, femoral flow velocity, caudal flow velocity, (other: hepatic artery, portal vein, umbilical artery), mid cerebral artery flow velocity

Parameters Measured with Doppler System

The following is a list of parameters that are measured in humans. In mice these parameters are extracted from the flow velocity signals listed under each of the above applications areas.

General	**Systolic Indices**
• Heart Rate	• Peak Velocity
• R-R Interval	• Mean Velocity
	• Peak Acceleration
Diastolic Indices	• Mean Acceleration
• E-Peak Velocity	• Pre-Ejection Time
• E-Stroke Distance	• Ejection Time
• E-Time Duration	• Rise Time
• E-Acceleration Time	• Stroke Distance
• E-Deceleration Time	
• E-Peak to ½E-Peak Time	**Peripheral Indices**
• E-Linear Deceleration Time	• Peak Velocity
• E-Linear Deceleration Rate	• Mean Flow Velocity
• A-Peak	• Minimum Flow Velocity
• A-Stroke Distance	• Pulsatility Index
• A-Time Duration	• Resistivity Index
• E-A Peak Velocity Ratio	
• Isovolumic Contraction Time	**Arterial Stiffness Index**
• Isovolumic Relaxation Time	• Pulse Wave Velocity (PWV)

SYSTEM OVERVIEW

System Hardware

The *Doppler Flow Velocity System* system hardware consists of three main subsystems:
1. Pulsed Doppler Transceiver, 2. Doppler Signal Digitizer, and 3. Doppler Workstation.
Shown here is a block diagram of the path of data flow. Each of these systems is described below.

Pulsed Doppler Transceiver

The Pulsed Doppler Transceiver (PDT) is a 2-channel (A & B) analog pulsed Doppler system, with each channel designed to operate (switchable) at either 10 or 20 MHz frequency. Both channels can operate simultaneously at 10 MHz, or at 20 MHz, or at combined 10 and 20 MHz. The figure below shows the front panel of the PDT system.
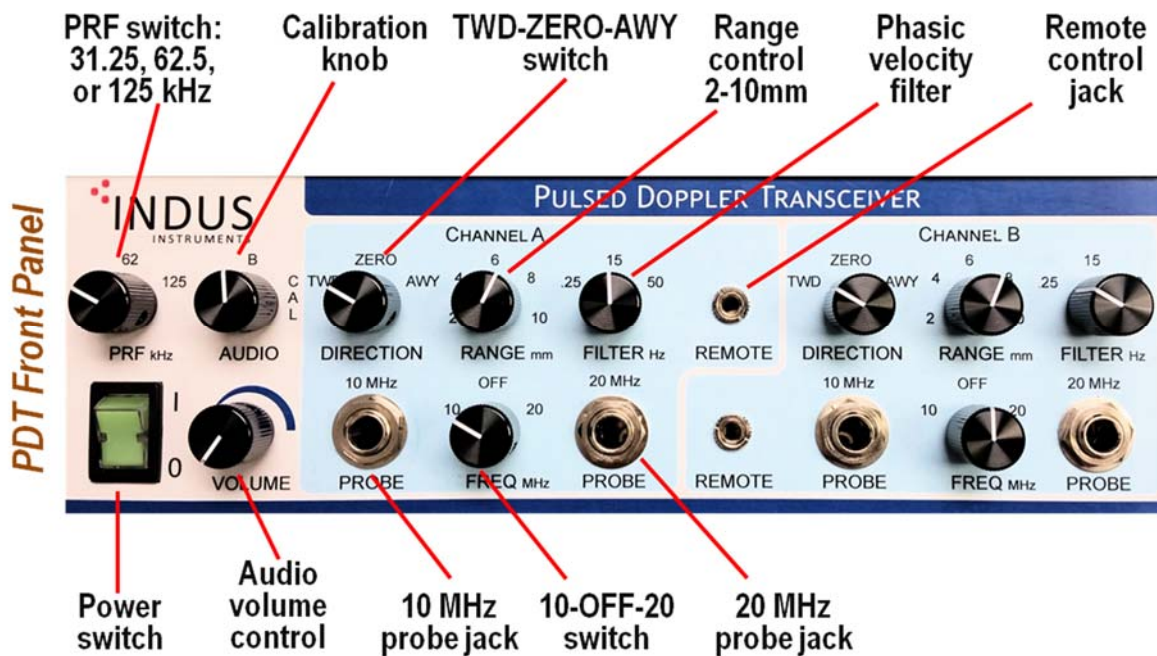
PDT Front Panel

The PDT system front panel has a main control part and Channels A and B.

Main Control

- The main control part (beige color) has a power switch, an audio VOLUME control knob, a PRF knob (pulse repetition frequency - switchable to 31.25, 62.5, or 125 KHz), and a AUDIO/CAL knob (audio or calibration dual function - switchable to Ch A or Ch B).
- While 31.25 kHz PRF is used for lower ranges of velocity, 62.5 kHz is used for medium ranges of velocity, and 125 kHz is used for higher range of velocity measurements.
- A speaker which provides audio guidance to the operator for probe placement and optimization is controlled by the VOLUME control knob.
- The AUDIO/CAL knob functions as a switch to select ChA or Ch B speaker audio output and also as a switch to select Ch A or Ch B for calibration mode for the calibration of phasic output.

Channels A and B Each channel has:

- A DIRECTION switch to indicate whether the flow is coming towards (TWD) the probe or moving away (AWY) from the probe (the ZERO position can be used to establish a zero flow baseline at any time)
- Two stereo phone jacks to connect the 10 MHz & the 20 MHz PROBEs
- A switch to select the operation of either 10 or 20 MHz FREQ probe
- A RANGE knob to select the depth at which the sample volume is to be placed (1-10 mm)
- A switch to set the smoothing (FILTER) of the phasic velocity output (back panel) to under-damped (50 Hz), damped (15 Hz), and over-damped (0.25 Hz). Note that mean velocity output is equivalent to over-damped phasic velocity.
- Additionally each channel has a jack to plug in the remote control that will allow for varying depth control while holding the probe for the measurement. Both channels have the exact same configuration.

PDT Back Panel

- The figure below shows the back panel. The back panel has the outputs via BNC connectors for each channel, Power supply receptacle, external ground connection, a USB connection, and RF/DEMOD connections.
- Each channel has INPHASE and QUADRATURE Doppler audio signal outputs, along with PHASIC and MEAN velocity outputs.
- The pulsatility of PHASIC output can be controlled by the FILTER switch on front panel.
- The power supply receptacle is switchable between 110v/220v with appropriate (50-60Hz frequency) and a main switch to control power from the Wall.
- The USB and the RF/DEMOD connectors are for future use.
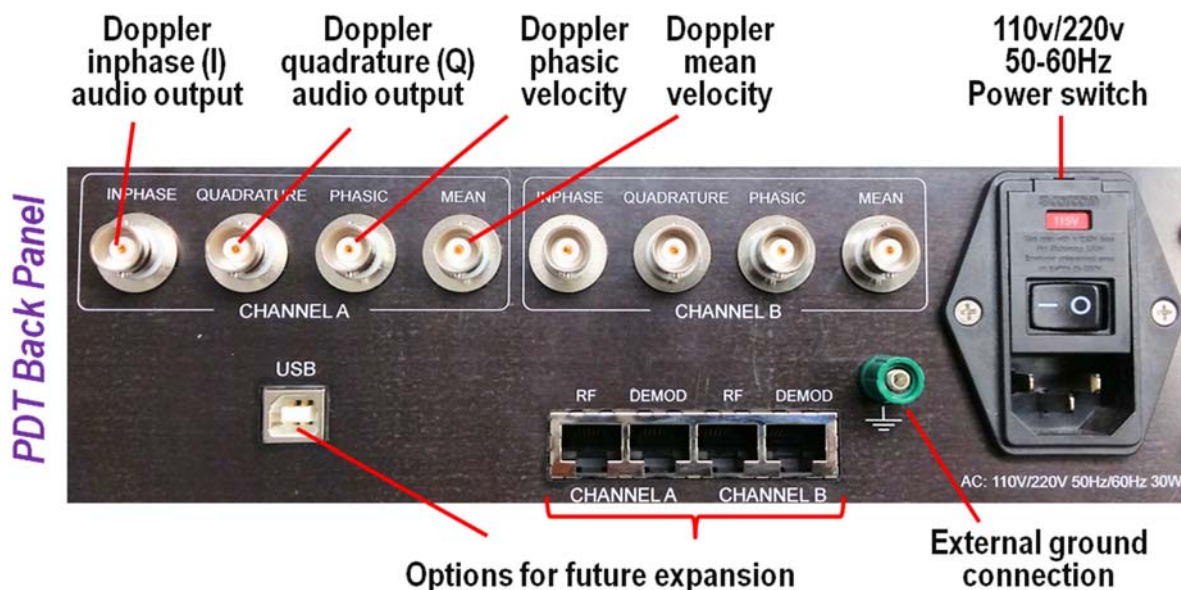
Remote RANGE Control Unit

The remote range control is a small unit with a knob that can be kept close to the location where the animal is placed, to make it easy for the operator to adjust the range depth with one hand while the probe is held in the other hand to measure the signals from arterial sites.

Doppler Signal Digitizer

The Doppler Signal Digitizer (DSD) is a real-time, high speed, high frequency multi-channel USB data acquisition (hardware) system with first two channels dedicated for sampling and processing Doppler inphase and quadrature audio signals, the third channel dedicated for sampling ECG signal and 3 additional channels designated as auxiliary channel that can be used to input physiological signals from other systems.
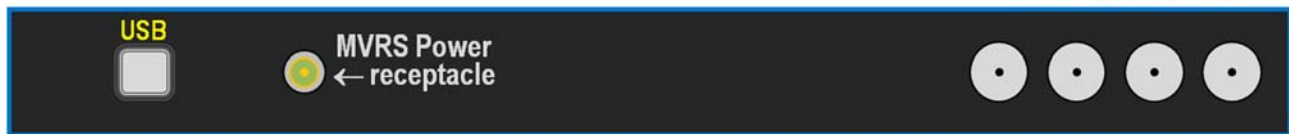
The DSD system is capable of acquiring simultaneously six channels of high resolution signals (16 bits) at high speed (up to 125 kiloSamples/s per channel) and transferring it to a personal computer through a universal serial bus (USB) interface. Typically, Doppler audio signals are sampled at 125 kilo Samples/second (kS/s) and ECG and any other physiological signals are sampled at 4 kS/s in the other four channels. The operation of the DSD system is controlled by the Doppler Workstation which consists of a custom designed GUI software installed on a Windows based laptop. The front and back panels of the DSD system are shown below. Please note that the ECG input is provided by the separate MouseMonitor S system (Please refer to manual of this system for its operation & use).

Doppler Workstation Laptop system with custom software

The Doppler Workstation is a Laptop system configured with the custom designed PC based graphics user interface (GUI; Doppler & physiological data acquisition and analysis software program) and interacts with the DSD system. The acquisition mode on the GUI window will only be active if the laptop is connected via USB with the DSD system, and the DSD system has to be turned on. Detailed description of the software and operation is presented in the Data Acquisition Chapter (CH 3).
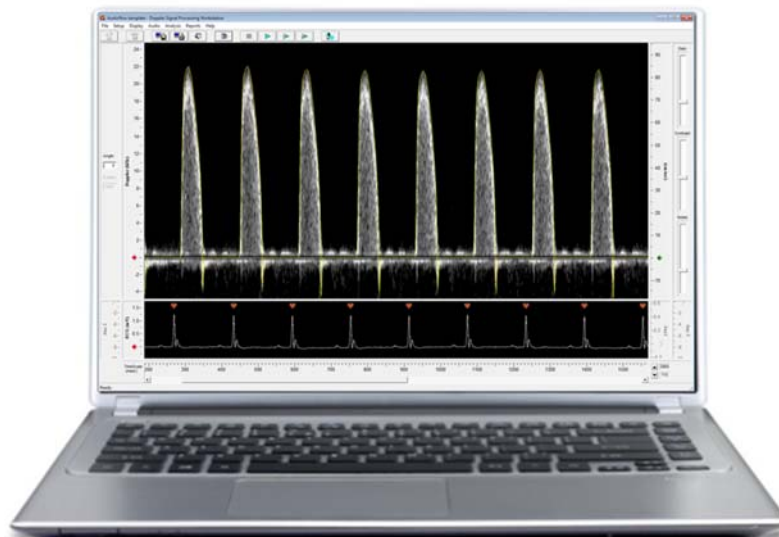
Block diagram of the Doppler Flow Velocity System setup

The following block diagram illustrates the flow of transduced Doppler signals from the animal that are processed to generate the Doppler inphase (I) and quadrature (Q) and along with ECG from MouseMonitor S system and other signals such as blood pressure. All signals are sampled and processed by the high speed DSD system and displayed on the Doppler Workstation via the user interface program.
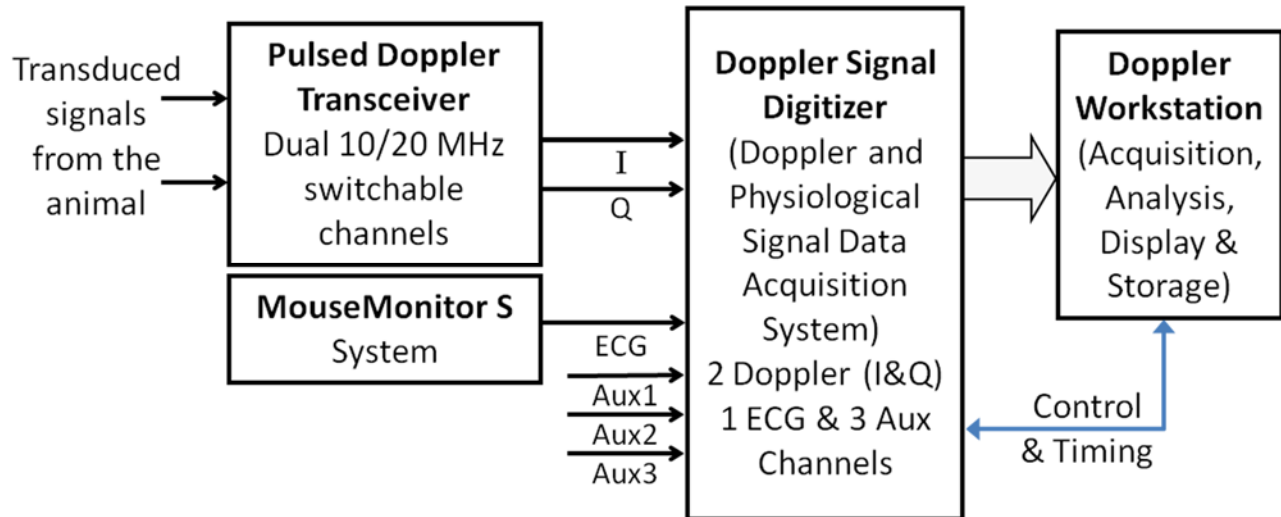
Overall setup of the system hardware

The figure below shows the overall setup of the Doppler Flow Velocity system. The 10 or 20 MHz Doppler probes, or both are connected to the Ch B of Pulsed Doppler Transceiver (PDT). The I & Q of outputs of the Ch B from the PDT system are connected to the CH1 & CH2 of the Doppler Signal Digitizer system. The ECG signal from the MouseMonitor S system is sent to CH3. The additional channels (CH4, CH5, CH6) can be used to simultaneously acquire other physiological signals (such as blood pressure) from the same animal using other systems. The DAQ samples and processes the signals and sends them to the laptop for display and storage. Analysis is performed offline on stored data to extract waveforms and parameters for export.
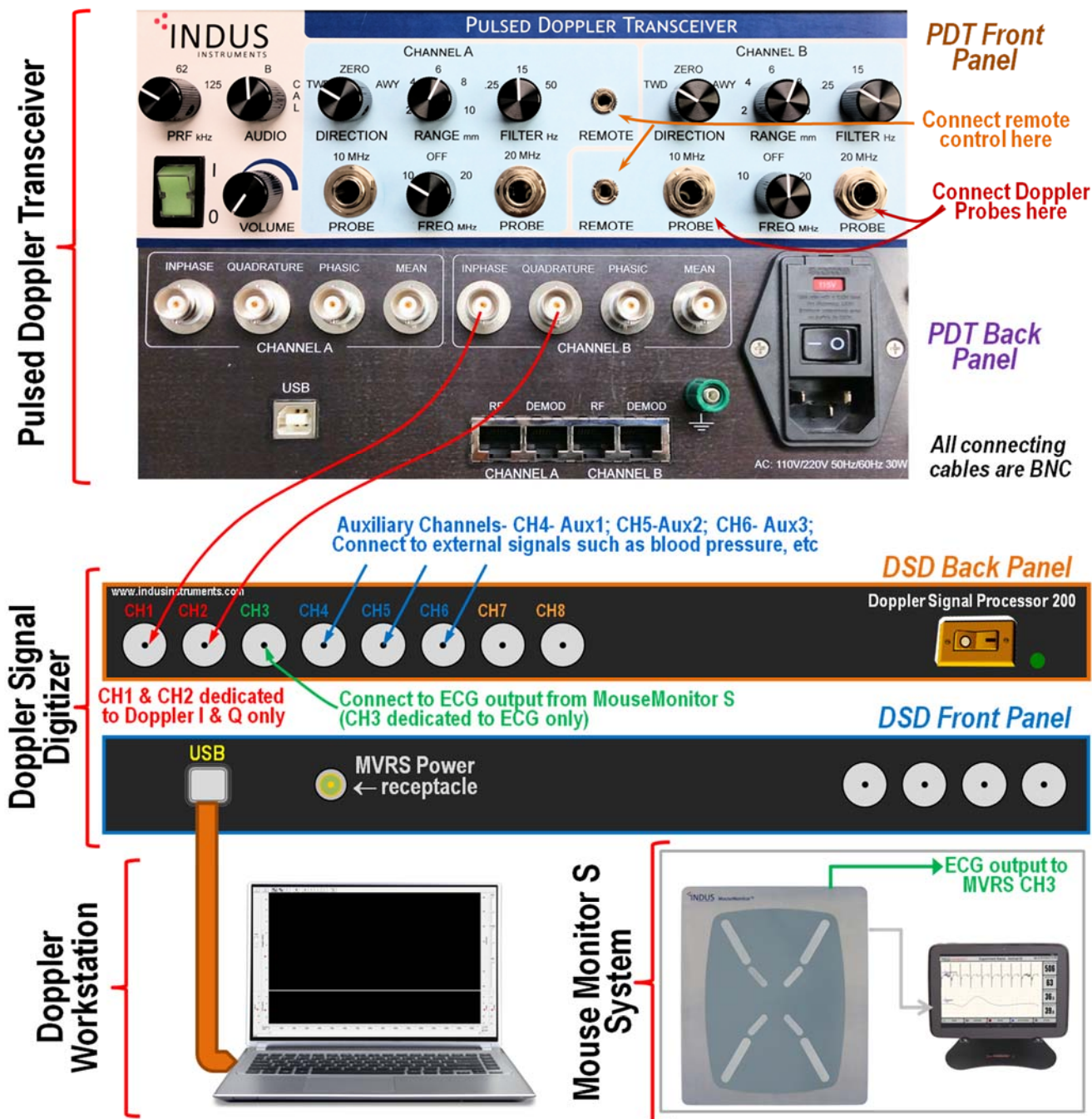
Hardware Specifications

Pulsed Doppler Transceiver Specifications

Capacity:	2 modules (Each switchable between 10 MHz & 20 MHz)	
Power:	110V AC/60Hz or 220V AC/50Hz	
Recorder Outputs:	2 from each Channel (Phasic & Mean)	
Audio Outputs:	2 from each Channel (InPhase & Quadrature)	
Audio Monitor:	Built-in amplifier & speaker selectable from any channel	
External Ground:	For external grounding to chassis if needed	
USB, RF/DEMOD:	For future use	
Ultrasound Frequency	10 MHz	20 MHz
Pulse Repetition Frequency	31.25, 62.5 or 125 kHz	62.5 or 125 kHz
Transmitter Pulse Width	0.4µs	0.4µs
Receiver Pulse Width	0.32µs	0.32µs
Transmitter Output	25V p-p into 50Ω	35V p-p into 50Ω
Variable Range Gate	1-10mm	1-10mm
Audio Bandwidth	≈100Hz to 15kHz	≈200Hz to 25kHz
Velocity Outputs	0.25V/kHz simultaneous phasic & mean	
Audio Outputs	2 in quadrature	
Phasic Output Filter **3-position switch**	Phasic (1 pole@50Hz), Damped (1 pole@15Hz) and Mean (2 poles@0.25Hz)	
Probe Connection	Floating & differential	
Velocity Range	1-100cm/s@0° angle, 2-200cm/s@60° angle	
Electrical Zero	Front panel switches	
Controls	Range adjustment, Polarity switch; Filter switch	

Doppler Signal Digitizer Specifications

Channels	6 (First 2 channels dedicated to Doppler inphase & quadrature,3rd channel dedicated to ECG, 4-6th channels for aux inputs)
Input Range	±10V
Coupling	AC or DC software selectable
Sampling	125kHz per channel, 16bits
Hardware Low Pass Filter	10, 20, 30, 40, 50, 60, 70, 80, 90, 100, 110, 120, 130, 140 or 150kHz
Software High Pass Filter	100, 200, 400, 600, 800, 1000, 1500 or 2000Hz (filter order 2 or 4)
Digital Signal Processor	500 MHz Dual Core Processor
Data link to PC	USB 2.0 (480Mb/s)
Power	100-240V universal AC adapter

MouseMonitor S Specifications (MMS)

Available Numeric Displays

Heart Rate (Leads I, II, & III)-Range:60-999 BPM

R-R Interval (Leads I, II, & III)-Range:60-1000ms

Respiration Rate- Range:15-400BrPM

Core Body Temperature-Range:0-50°C

Pad Temperature-Range:25-42°

SpO$_2$ (Expansion Module)- Range:80-100%

Available Waveform Displays

ECG (Lead I, II, & III)

ECG (Aug. Lead aVL, aVR, & aVF)

Respiration

PhotoPlethysmogram (Exp. Module)

Temperature Probe	
Available Probes	Mouse, Rat, & Neonatal Mouse
Probe Sensor Type	Copper-Constantan Thermocouple
Probe Accuracy	±0.1°C After Calibration

Heated Surgical Platform	
ECG Electrodes	3 Sets, Switchable (Mouse, Rat, or External Electrodes)
Electrode Set 1: Mouse	4 Mouse Limb Electrodes (Non-invasive Surface Electrodes)
Electrode Set 2: Rat	4 Mouse Limb Electrodes (Non-invasive Surface Electrodes)
Electrode Set 3: External	Standard 1.5mm DIN ECG Leads (ANSI/AAMI EC53 & DIN 42-802 compliant)
Heater Type	Responsive Electronic Heater with Multiple Zone Control
Heater Uniformity	<0.5°C Across Active Area
Heater Starup Time	<2 minutes (25°C Initial Condition)
Heater Set Temperature	Adjustable Set Point, 25-42°C by 0.1°C
Power Supply	Universal AC Adapter (100-240V)
Size	10x12 inches
Weight	6.5 pounds

System Software

The Doppler signal processing software was written in Visual C++ and runs on most PCs on MS Window OS. It was custom designed to controls the data acquisition and processing by DAQ and display the processed Doppler signals along with ECG and other physiological signals in real-time. In the offline mode the program can perform semi-automatic analysis of data, export raw and analyzed waveforms and generate parameters based on the markers placed by the user.

The GUI has two panels for display. The upper panel is dedicated to the display of the FFT processed Doppler velocity spectrograms and the lower panel is dedicated ECG and the three auxiliary channels. The software program is written in Visual C++, and is compatible with many different versions of Windows OS including Windows 10.
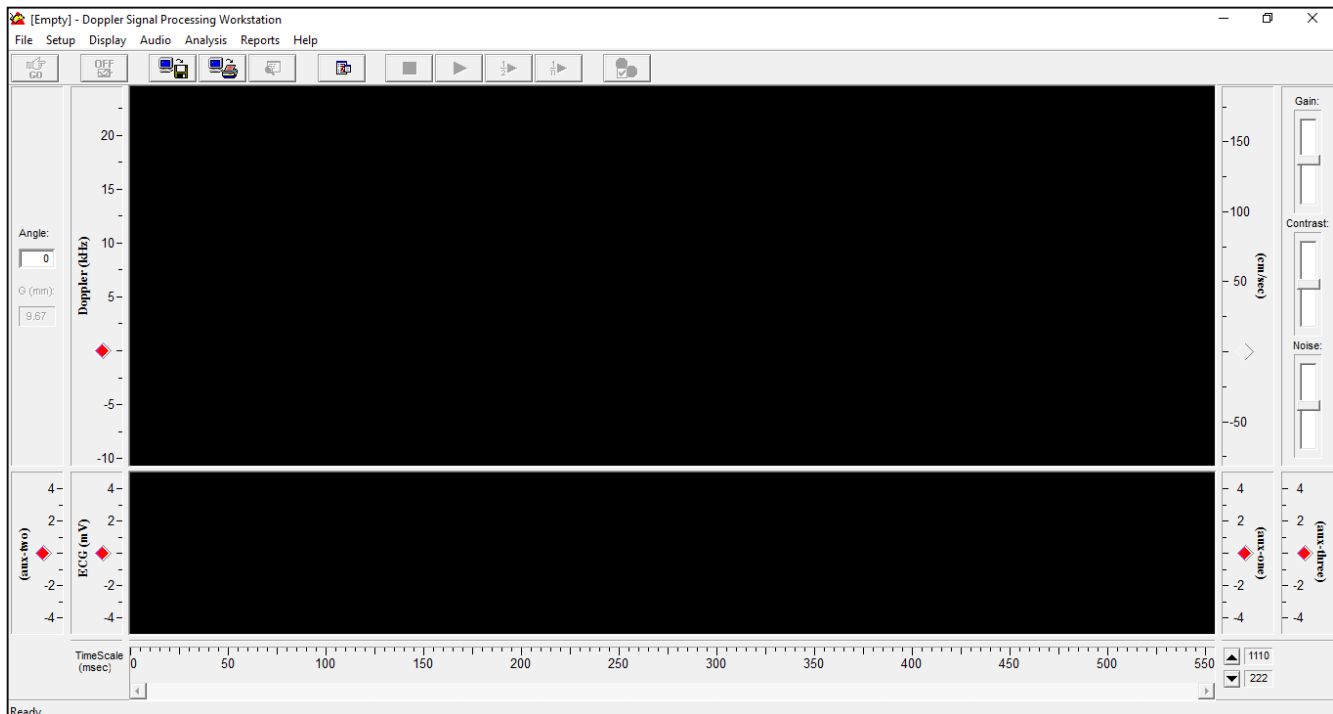
Graphics user interface (GUI) window and description

Shown above is the GUI window of the Doppler system. The upper display panel is dedicated to the processed Doppler spectrogram and the lower display panel is dedicated to ECG signal shared with additional 3 auxiliary inputs that can be turned on/off.

Menus and description

The top menu has the following *drop-down* items:

1. File: *Open, Close, Save, Save As, Save As Next, Set File Info, Export Envelope, Start/Stop Acquisition*

2. Setup: *Load Setup, Save Setup, System Setup, Doppler Setup, ECG Setup, Auxiliary Channel 1 Setup, Auxiliary Channel 2 Setup, Auxiliary Channel 3 Setup, Options, Remote Setup*

3. Display: *Peak Velocity, Analysis Markers, RPeak/Beat Markers, Hide Doppler Spectrogram, Calipers, Audio Cursors, Display All, Hide All, Caliper Display Options, Maximize Spectrogram Pane, Maximize ECG Pane, Restore Maximized Pane*

4. Audio: *Audio Cursor Mode, Playback Normal Speed, Playback Half Speed, Playback 1/5 Speed* (5 is chosen under Audio Options)*, Stop Playback, Audio Options*

5. Analysis: *Open Analysis Control Window, Analysis Mode, Calipers Mode, Analysis Options*

6. Reports: *Quick Report, Quick Report Setup, New Formal Report Format, Open Formal Report Format, General Formal Report, Save Screen Capture, Print Screen Capture, Invert Capture Grayscale*

7. Help: *Keyboard Shortcuts, About DSPW*

The <u>icon menu</u> bar has the following buttons.

1. The GO button ( ) becomes active ( )when the laptop is connected to the DAQ system for data acquisition.

2. The OFF button is 3 way toggle button (:↑ON, :↓ON, :OFF) for ECG R-wave trigger (↑rising edge, ↓falling edge, off).

3. The next two buttons (,) are for saving or printing a screen shot of the GUI window.

4. The next button ( ) is for report generation (rarely used).

5. The next button ( ) is offline analysis button. Clicking this window will pop-up the analysis window to the right side of the screen and has a list of steps that need to be followed depending upon the signal to be analyzed (Described with more details in Data Analysis chapter (Cн 4).

6. The next set of 4 buttons (, , ,) are dedicated for audio playback of recorded signals. The playback time can be varied to reproduce the Doppler sounds at slower heart rates (these buttons are occasionally used).

7. The last button ( ) is for automatic adjustment of gain, contrast, and noise of the Doppler signal. They can also be manual adjusted using the scroll bars ( )on the side for an optimal display.

Other Controls

• There are a few other controls on the GUI that are controlled directly. These include the Doppler frequency scale that can be scaled up/down or its zero can be offset up or down. The maximum scale on the Doppler is limited by the Doppler signal sampling rate.(Ex. if Doppler signal is sampled at 125 kHz, then the maximum display will be 125 kHz regardless of how it is displayed; 0 to 125 kHz, or -25 to 100kHz, -62.5 to 62.5kHz, or -100 to 25kHz, etc)

• Similarly, the ECG and the auxiliary channel scales can be scaled up/down by holding the scale by left click of the mouse and dragging up/down. Their respective zero can be offset up/down by dragging the symbol ( ) with the mouse.

• The full scale of display time can be changed from 110 to 11000 msec (110, 220, 550, 1100, 2200, 5500, and 11000) using the up/down arrow heads on the bottom right of the screen ( ).

• The size of the upper and lower display panels can be adjusted as need by dragging the line between the panels up/down.

• The left panels can hidden by dragging the left inner edge of the display panel to the left and restored by dragging it right. Similarly, the right panels can hidden by dragging the right inner edge of the display panel to the right and restored by dragging it left.

DATA ACQUISITION

Data acquisition involves the following steps that should be done after the initial overall system setup in the laboratory.

Animal Preparation

- Follow the protocol approved for your laboratory for making the noninvasive Doppler and ECG measurements in your lab.
- Anesthetize the animal. If using the gas anesthesia (such as isoflurane) anesthetize the animal in the induction chamber at 3% isoflurane and then transfer it to the anesthesia via nose cone that is taped in place on the MouseMonitor S ECG board. Maintain the anesthesia level at 1-1.5%.
- Other commonly used IP injected anesthetic agents; Rodent cocktail - Ketamine (42.8 mg/ml), Xylazine (8.6 mg/ml), & Acepromazine (1.4 mg/ml); Sodium pentobarbital (4 mg/ml in 20% ETOH). The heart rate of a mouse may vary depending on the type and amount of anesthetic used. The user/researcher should be aware of the effects of the anesthetic they are using on the animals.
- Tape the animal paws to the electrodes in the required configuration (rostral or caudal, prone or supine) with a tiny amount of electrode paste between the paw and the electrode (mouse and similar sized animals on the inner/smaller electrode configuration; rat and similar sized animals on the outer/larger electrode configuration). Make sure the appropriate electrode setting (mouse, rat or external) is chosen on the MMS program on the tablet monitor. (Please refer to the MMS manual for more details). The MMS program will display the selected ECG waveform(s).
- Make sure that one of channels on the low latency cable output is set to ECG (Lead II is standard) and connect the corresponding cable to the ECG on MVRS CH3 (see setup illustration). This will allow for the selected ECG waveform to be sampled and displayed along with the processed Doppler signals on the DAQ system.
- Shave the hair (or use Nair) on the animal at sites where the probe tip will be placed. Use acoustic gel (or water as the probe tips are quite small) to obtain a better acoustic coupling between the tip of the ultrasound probe and the skin surface.
- Have a micro-positioner handy for measurements that require fixed probe position.

Experimental Setup

Make sure that the ECG display is optimal on both the MMS tablet display as well as on the Doppler system. In addition to Doppler flow signals, the MVRS DAQ system can acquire ECG and 3 other auxiliary signals simultaneously. While CH3 on the MVRS DAQ system is designated for ECG, the auxiliary channels can also be used to display additional ECG signals or any other physiological signals from other transducers/systems.

Example setup A

CH1 & CH2 - Doppler I & Q
CH3 - Lead II ECG from MMS
CH4 - None (or any other)
CH5 - None (or any other)
CH6 - None (or any other)

Example setup B

CH1 & CH2 - Doppler I & Q
CH3 - Lead II ECG from MMS
CH4 - Lead I ECG from MMS
CH5 - Lead III ECG from MMS
CH6 - aVR or aVF or aVL from MMS

Example setup C

CH1 & CH2 - Doppler I & Q

CH3 - Lead II ECG from MMS

CH4 - Blood pressure signal

CH5 - None (or other)

CH6 - None (or other)

Example setup D

CH1 & CH2 - Doppler I & Q

CH3 - Lead II ECG from MMS

CH4 - Tissue Doppler signal from Phasic

CH5 - None (or other)

CH6 - None (or other)

Example setup E

CH1 & CH2 - Doppler I & Q

CH3 - Lead II ECG from MMS

CH4 - LV blood pressure signal

CH5 - LV volume signal

CH6 - None (or other)

Example setup F

CH1 & CH2 - Doppler I & Q

CH3 - Lead II ECG from MMS

CH4 - Tissue Doppler signal from Phasic

CH5 - None (or other)

CH6 - None (or other)

Experimental Procedure

- The hand held Doppler probe is positioned appropriately for the type of signal being measured.

- The other end of the probe is connected to the Doppler Analog system. The probe transmits the an ultrasound pulse and waits to receive the echo from the desired depth (set using range gate), before sending out another pulse. The received echo is processed by the Doppler analog system into Doppler audio inphase and quadrature signals which contain the information about the the velocity and direction of the targeted blood flow.

Figure 3.1 Shows experimental setup for acquiring data from a mouse.
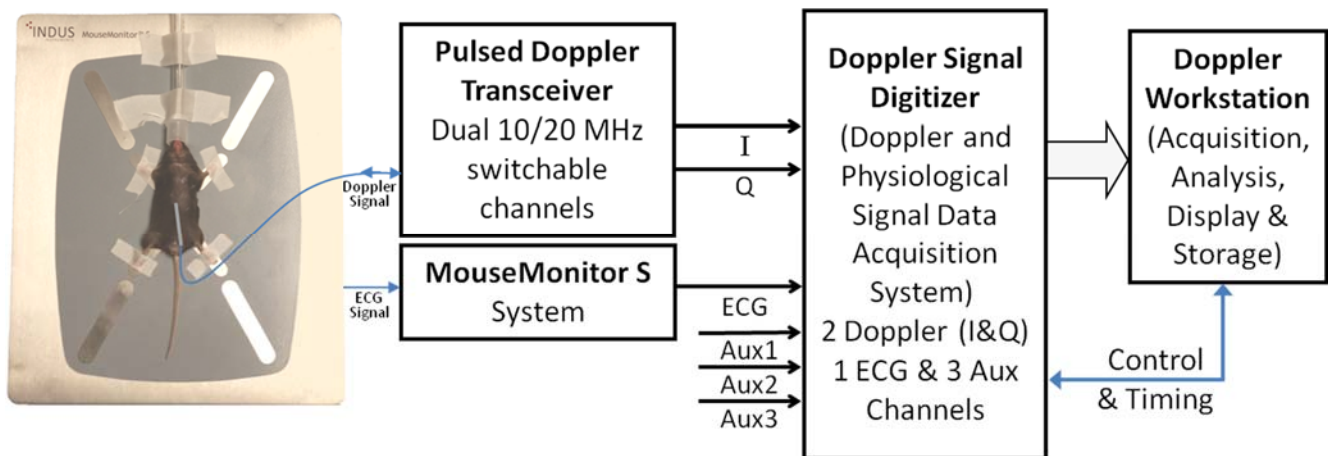
Figure 3.1. Experimental Setup

Doppler Software Settings

- On the laptop desktop screen click on the ( ) Doppler system icon to run the software. The program starts with a user interface window with menus (see fig. 3.2).

    - Menu items: <u>File</u>, <u>Setup</u>, <u>Display</u>, <u>Audio</u>, <u>Analysis</u>, <u>Reports</u>, and <u>Help</u>.

    - Under File menu the standard I/O (Open, Close, Save, etc) options, file information (popup menu), & data acquisition options are available.

    - The Setup menu allows the user to select/set data acquisition parameters.
        - *System*: Crystal frequency and power levels (fig. 3.3a).
        - *Doppler*: Angle (enter *0-90* angle to correct for), Sample Rate (*10, 25, 50, 80, 100, 125* kHz), FFT window (Type: *Rectangle, Triangle, Cosine, Hamming, Hanning, Blackman*; Samples: *128, 256, 512, 1024*; Time Alignment: *Past, Center, Future*; window overlap Time), High pass filter (*1st* & *2nd* order filters at *100, 200, 400, 600, 800, 1000, 1500, 2000* Hz & Low pass filter settings (*None* & from *10000* to *150000* Hz, in steps of 10000), and other display settings (Use Interpolation, Use F/R (Forward/Reverse) not I/Q, and editable Scale Settings), (fig. 3.3b).
        - *ECG*: Trigger (*Polarity, Pretrigger Time, Trigger Level*), General (*Invert, Gain Setting, Sample Rate*), and Scale limits (*Top* & *Bottom* limits) (fig. 3.3c).
        - *M-Mode*: under construction (fig. 3.3d).
        - *Auxiliary Channels*: Auxiliary Channel # (*Source, Gain, Color, Annotations*), Scale limits (*Top* & *Bottom* limits), Record Data (fig. 3.3e).
        - *Options*: Data recording option (*History time*), Window (*Reset Window Pane Arrangement*).
        - *Remote Setup*: Comm Port #

    - The Display menu allows the user to set the view modalities on the screen.

    - The Analysis menu allows you to display analysis window and enable ruler options.

    - The Audio menu allows the user to play a file repeatedly at variable speeds.

    - The Analysis control is a separate window and has several steps to perform analysis on the acquired data offline (see fig. 3.4 for analysis control window).

    - The Reports menu allows the user to specify reports formats, and generate quick reports and detailed long reports, and to save or print a screen capture with the option of inversion of the grayscale image.

- Initial Software Settings - 1. Choosing 10 MHz or 20 MHz in **System** setting, 2. Sampling rate setting (default: 125 kHz), 3. FFT sample size (default: 512 samples), 4. Low pass filter setting (default: 150 kHz), and other processing options (learned during training).

- Press the **GO** ( )button on the UI screen.

- A popup window appears where you enter the subject information, experiment information, file name and directory should be entered here. Then press **OK** (The file is initially set to FileName_00.udf. After each save the file number is automatically incremented up to a maximum

of FileName_99 for a given subject. When the next subject is started make sure the file number is reset to _00 before pressing **OK**. FileName is usually the subject ID given by the user)

- The system will start monitoring. The window scan speed can be modified by using up & down arrow heads ( ) in steps for a comfortable viewing (typical 2sec or 2000msec).

- With the Doppler probe placed at the desired location on the animal the Doppler signal is displayed in the upper window as shown along with the ECG from the MouseMonitor S in the lower window. All signals are displayed in real-time.
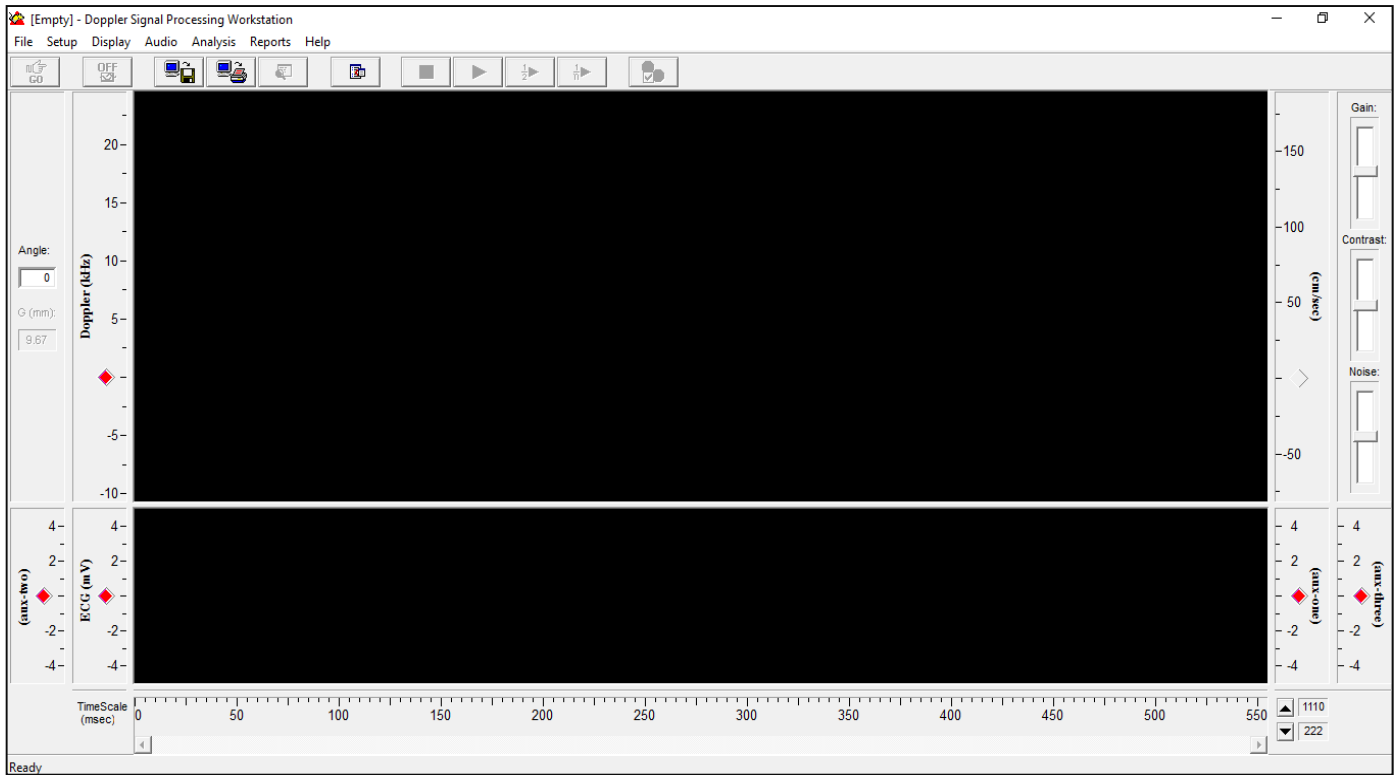
Figure 3.2 User Interface Window with Menus

Figure 3.3a. Popup Window for System Setup
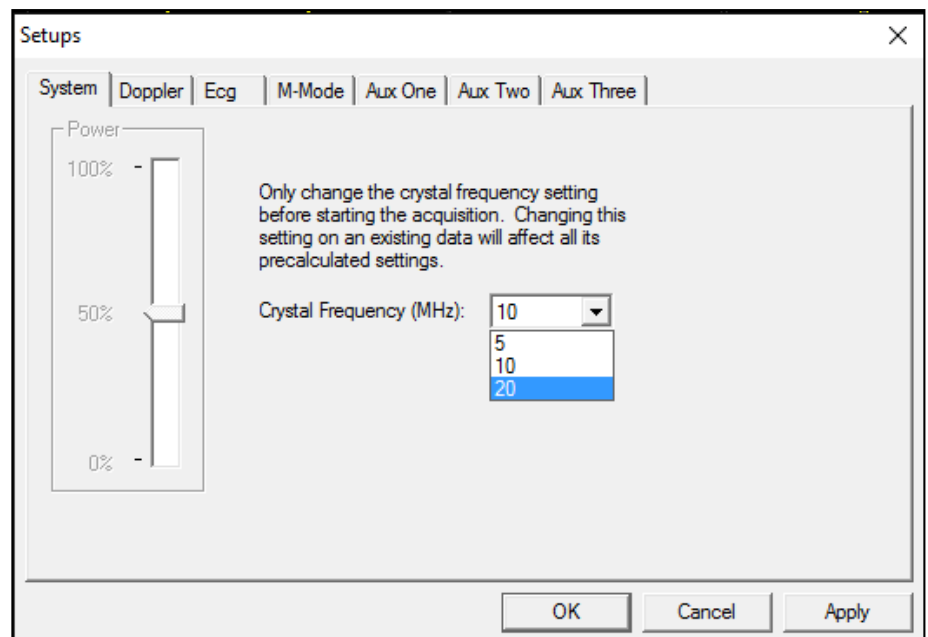
Figure 3.3b. Popup Window for Doppler Setup
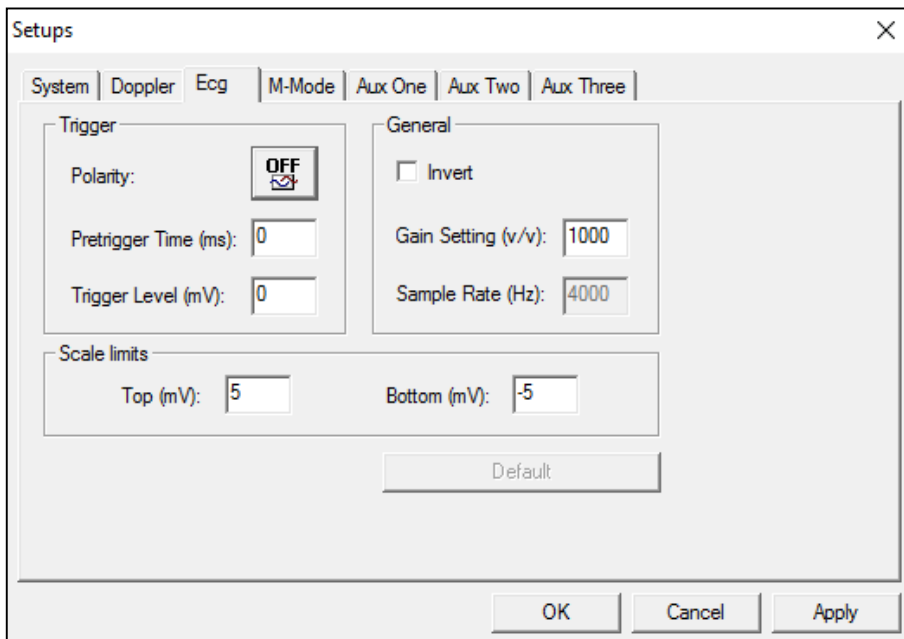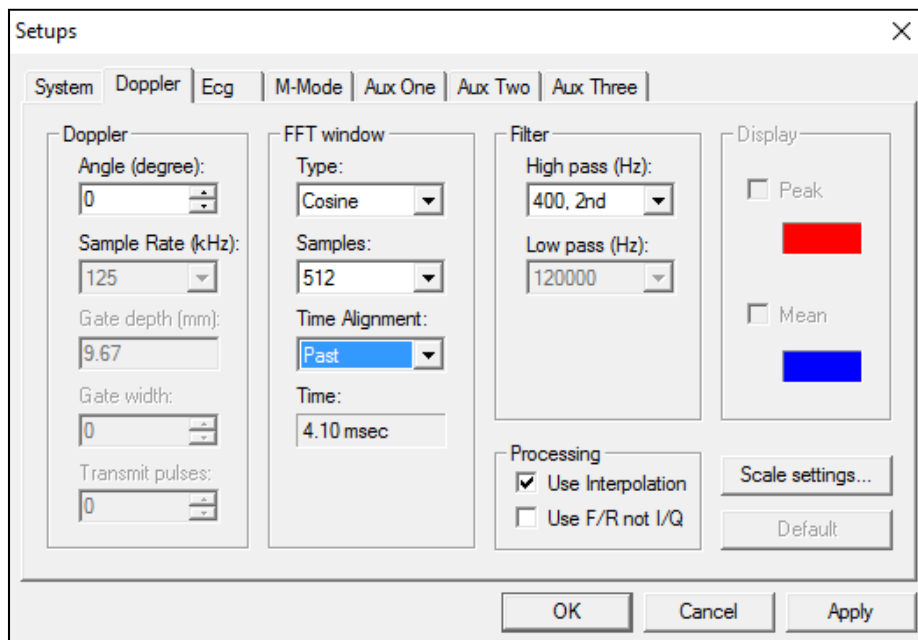
Figure 3.3c. Popup Window for ECG Setup

Figure 3.3d. Popup Window for M-Mode Setup (Inactive Window)

Setups ✕

System | Doppler | Ecg | M-Mode | Aux One | Aux Two | Aux Three |

M-Mode

Depth setting (mm):
15

Transmit Pulses:
0

PRF (kHz):
2.00

Default

OK   Cancel   Apply

Setups ✕

System | Doppler | Ecg | M-Mode | Aux One | Aux Two | Aux Three |

Auxiliary Channel 1

Source:
None

Gain: Color:
1000

Annotation:
Aux1

Scale limits

Top:
5

Bottom:
-5

☑ Record data

Default

OK   Cancel   Apply
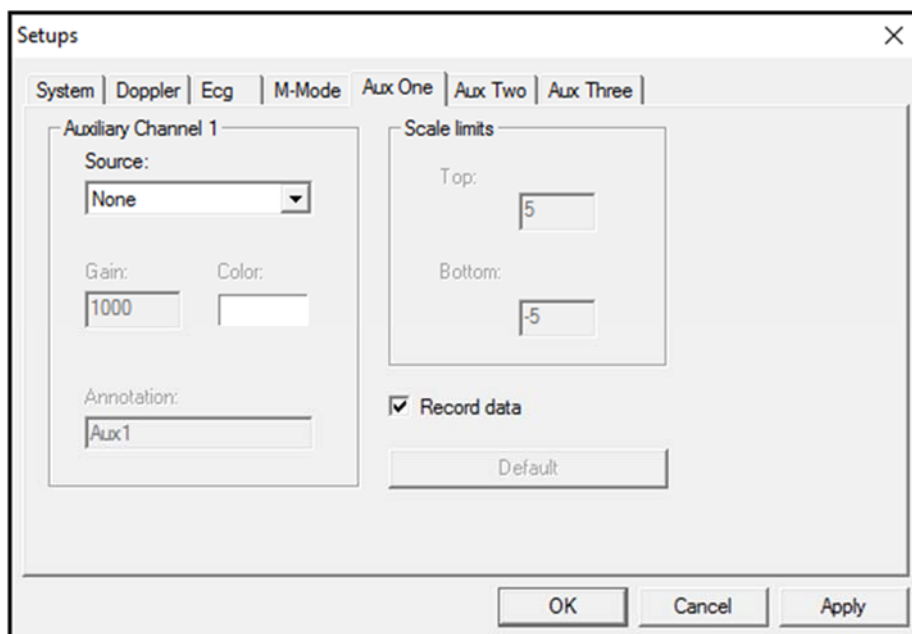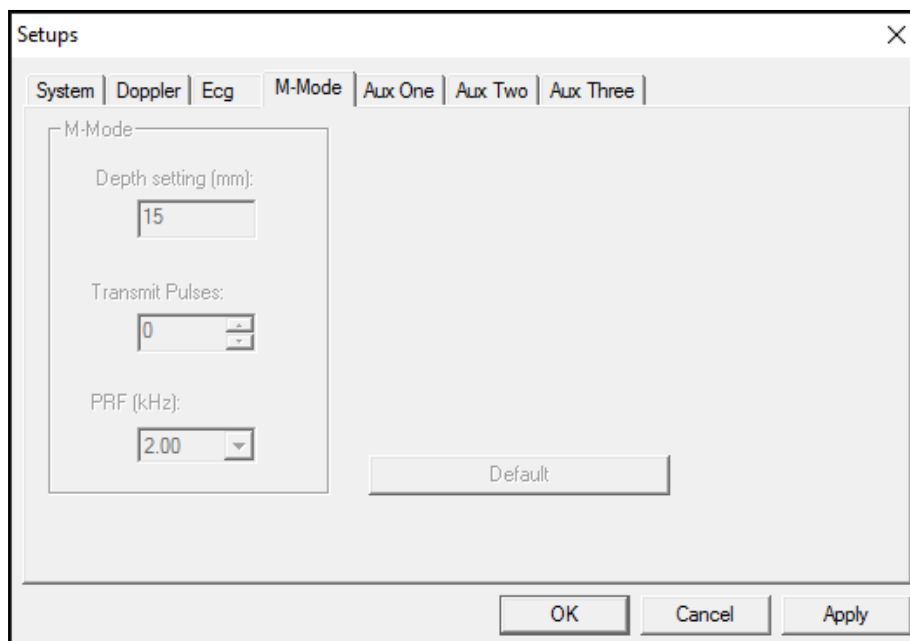
Figure 3.3e. Popup Window for Aux Ch 1 Setup (The Popup Windows are same for Aux Ch2 and Aux Ch3)
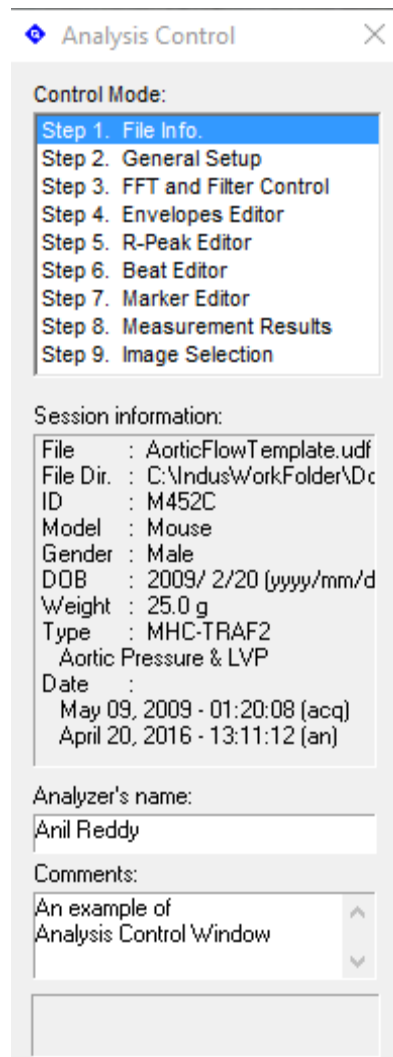
Figure 3.4. Analysis Control Window

Data Collection

a.   After achieving an optimal position of the probe for a blood velocity signal at a given location, the S button on the laptop keyboard (or a foot switch) can be pressed to save an already viewed segment of signal (typically 2 sec, but can be set to as long as 30 sec).

b.   Typically 2-3 recordings are saved for a signal measured at each location. The saved signals can be analyzed offline.

•   Start data acquisition by clicking the **GO** button ( ) or pressing the space bar.

•   Fill in the mouse/animal information in the popup menu.

•   Position and hold the ultrasound probe in the required orientation for the respective signal to be collected.

•   The remote can be operated with the left hand if the user is holding the probe in the right hand.

•   The display sweep rate can be set for comfortable viewing.

•   After achieving an optimal probe position and viewing satisfactory data can be saved in 2 or 3 second segments. This segment consists all signals that are connected at the front end.

DATA ANALYSIS

Cardiovascular Signals/Waveforms and Parameter Algorithms

This section describes various cardiovascular/physiological signals that are acquired noninvasively and processed to obtain parameters. Flow velocity signals from aortic root, mitral inlet, left main coronary artery, thoracic aorta (aortic arch), abdominal aorta, left and right carotid arteries, left and right renal arteries, left and right mid-cerebral arteries, left and right femoral arteries, caudal artery are described. Also described are ECG and other auxiliary signals. Parameters are extracted offline from the above recorded signals. These parameters represent noninvasive indices of cardiac (systolic and diastolic) and cardiovascular function in a mouse. The signals are captured in segments (2-3sec is standard; maximum is 30sec) during real-time display and stored for offline analysis.

Overview of Offline Signal Analysis

The following parameters extracted offline from the above signals 1-6:

1. ECG acquired simultaneously with signals in 1-6.
    a. R-R interval (ms)
    b. Heart rate (beats/min)

2. Aortic outflow velocity signal.
    a. Pre-ejection time (ms)
    b. Peak velocity (cm/s) [or Peak height, kHz]
    c. Peak acceleration (cm/s^2)
    d. Stroke distance (cm) [area under velocity curve]
    e. Ejection time (ms)
    f. Rise time (ms) [Time from onset to peak velocity]
    g. Mean velocity (cm/s) (over Cardiac cycle or R-R interval)
    h. Mean acceleration (cm/s^2) (over Rise time)

3. Mitral inflow velocity signal.
    I.   *Early (E) filling part of the signal*
    a. Peak velocity of E (cm/s)
    b. Stroke distance of E (cm)
    c. Duration of E (ms)
    d. Acceleration time of E (ms)
    e. Deceleration time of E (ms)
    f. E-Peak½t (ms) (time from E-peak velocity to ½ E-peak velocity)
    g. Linear deceleration time of E (ms)
    h. Linear deceleration rate of E (cm/s^2)

    II. *Atrial (A) filling part of the signal*
    a. Peak velocity of A (cm/s)
    b. Stroke distance of A (cm)
    c. Duration of A (ms)

III. *E-A ratios*
a.   E:A peak velocity ratio
b.   Total area (cm)
c.   A area/Total area
d.   Peak E/Total area (/min)

IV. *Isovolumic time durations*
a.   Isovolumic contraction time (ms)
b.   Isovolumic relaxation time (ms)

4. Flow velocity signals from thoracic aorta & abdominal aorta.
a.   Thoracic aorta pulse transit time (ms) (time from R-peak to the appearance of flow velocity pulse at the thoracic aorta)
b.   Abdominal aorta pulse transit time (ms) (time from R-peak to the appearance of flow velocity pulse at abdominal aorta)

Calculation of Pulse Wave Velocity (PWV)
a.   Separation distance between 2 flow sampling points (cm)
b.   Calculation of PWV (cm/s^2)

5. Peripheral flow velocity signals- Cerebral, Carotid, Thoracic & Abdominal Aorta, Renal, Femoral, Caudal (tail).
a.   Peak systolic blood flow velocity (cm/s^2)
b.   Lowest diastolic blood flow velocity (cm/s^2)
c.   Time averaged mean blood flow velocity (cm/s^2)
d.   Pulsatility Index, PI
e.   Resistivity Index, RI

6. Coronary flow velocity signals from left main coronary artery
a. Peak diastolic coronary flow velocity
b. Area under diastolic coronary flow velocity waveform
c. Peak systolic coronary flow velocity
d. Area under systolic coronary flow velocity waveform

Signals, Beats, and Markers

1. **ECG acquired with cardiac/arterial signals**

The ECG waveform is recorded with standardized Lead II configuration (other lead configurations are also available with MMS system). ECG waveform is displayed along with the Doppler spectra of the flow velocity signals and other cardiovascular signals for timing purposes, and to measure R-R intervals, which will be used to calculate the heart rate. Please note that some of the parameters of the Doppler signals can be extracted only in the presence of ECG signal.

1.a) R-R interval (ms)

This parameter represents the time between two consecutive heartbeats. The peaks of R-waves of the ECG are detected and the time between two consecutive R-peaks, called R-R time interval is measured. A mean value of all R-R intervals in one ECG signal record is obtained. Detection of *x* R-peaks results in a value average over (*x-1*) R-R intervals.
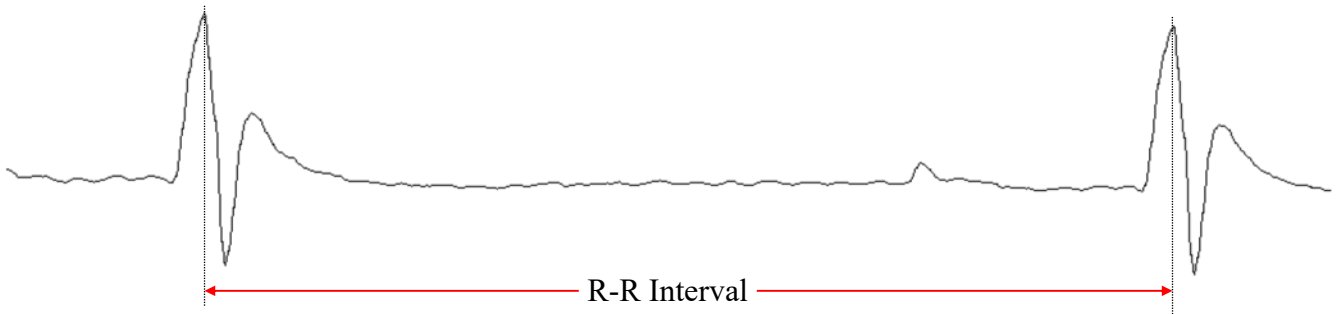
Algorithm:

- Detect R-peak in the ECG signal record.

- Measure R-R interval time.

    t_{R1} is the time between the consecutive R-peaks

- Compute average of R-R intervals.

    R-R interval = $(\Sigma t_{Rn})/n$ where n - number of intervals

1.b) Heart rate (beats/min)

This parameter represents the rate at which the heart beats. It uses the R-R intervals to calculate the average heart rate during the outflow. In mice heart rates can ranges from 500 to 600 beats/min. This rate could be affected by anesthetic used, disease, or transgenic modifications which make the heart rate range from as low as 200 beats/min to as high as 800 beats/min.
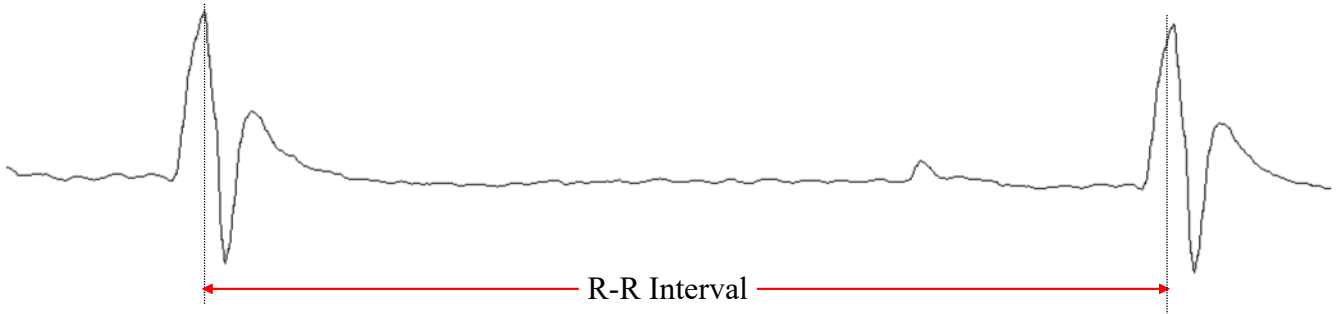
Algorithm:

- Use the calculated mean R-R interval (in sec) and convert it to number of beats (intervals) per minute.

  Heart Rate = 60/R-R interval

2A. Aortic (systolic or outflow) flow velocity signal

This signal represents the ascending aortic flow velocity resulting from left ventricular ejection. It occurs during the systolic phase of the cardiac cycle and is presented in the form of Doppler spectrogram in real-time. A ?mm 10 MHz pulsed Doppler probe with a 9-10mm range gate depth is used to obtain optimum values of ascending aortic flow velocity signal. To obtain this signal the probe tip is placed just lateral to the xiphoid and is directed towards the right ear. The probe is inclined between 0°-10° to the horizontal. Aortic outflow is also referred to as left ventricular ejection, systolic flow, or simply, outflow. Typical peak aortic flow velocity with the 10 MHz Doppler is 75-105 cm/sec (10-14 kHz) with the assumption that the probe is inclined at 0°. A 5° angle of the probe/sound beam with the axis of flow results in ≈1.5-% decrease in peak flow velocity estimate. A decrease in the aortic outflow velocity indicates low cardiac output or poor LV systolic function. An increase in aortic outflow indicates higher cardiac output or enhanced LV systolic function.
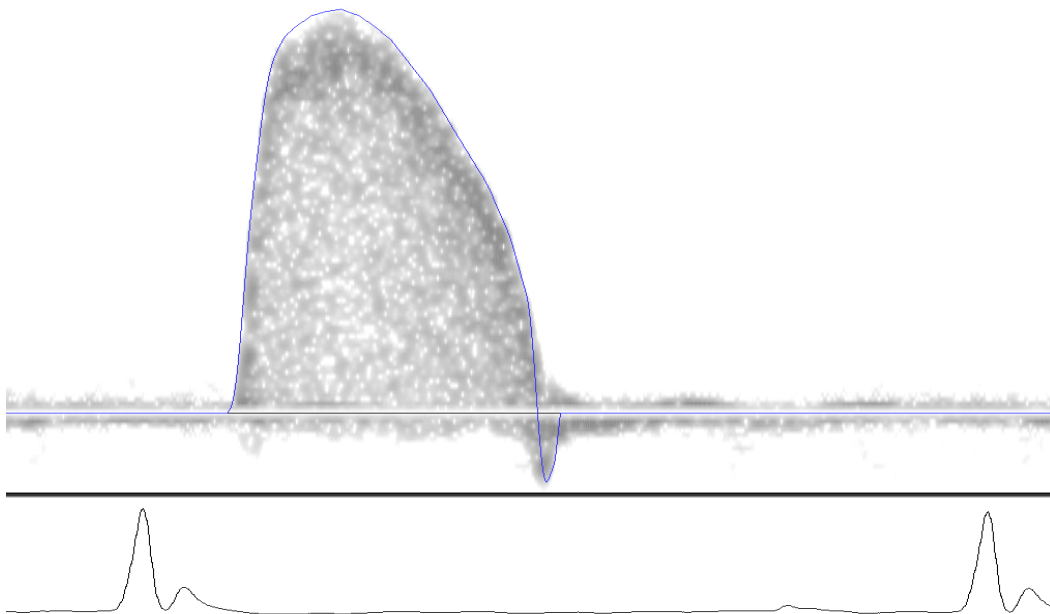
2A.a) Pre-ejection time (ms)

      This parameter represents the time from the R-wave trigger to the onset of aortic outflow velocity. Here the key point to remember is how the R-wave trigger is defined. Ideally its the R-peak, but practically one would like to be able to move a few points in either direction from the R-peak to determine proper flow timings. Also, care should be taken to account for the time shift of the spectrogram due to FFT window timing. In mice this time ranges from 5 to 10 msec.

Pre-ejection time (ms)
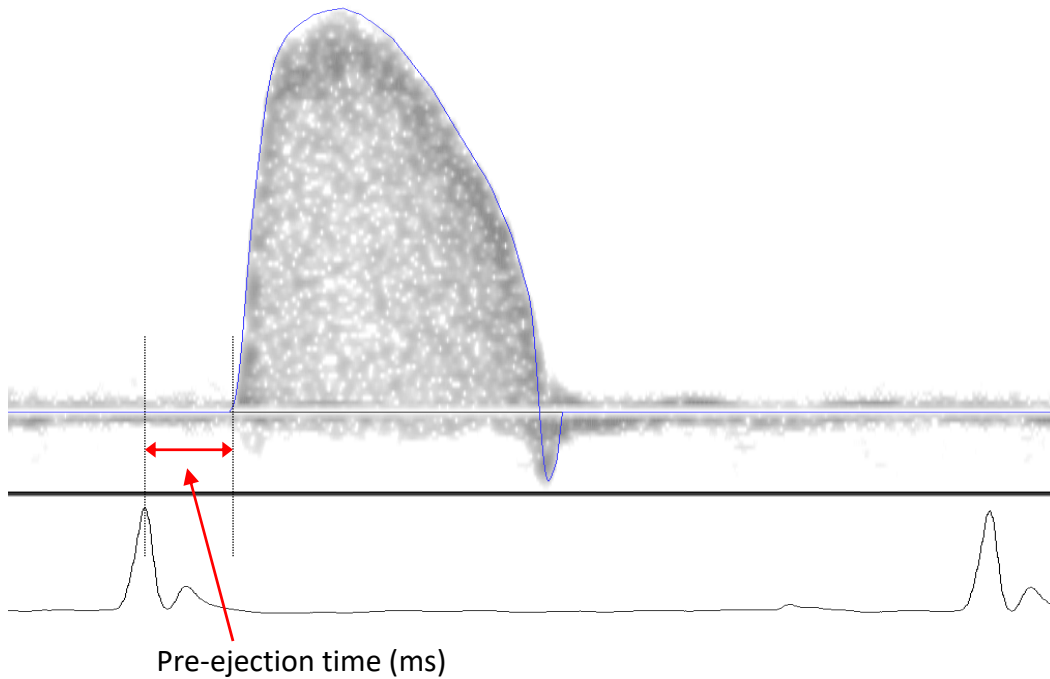
Algorithm:

- If t_{R1}, t_{R2}, ..., t_{Rn}, represent the times of occurrence of R-waves,

  and t_{S1}, t_{S2}, ..., t_{Sn}, represent the onset times aortic outflow velocity, then

  $$t_{PE1} = (t_{S1} - t_{R1})$$

  where t_{PE1} is the pre-ejection time of 1st flow curve in the segment.

- Compute the average of all pre-ejection times.

  $$\text{Pre-ejection time} = (1/n) \, \Sigma t_{PEn}$$

2A.b) Peak velocity (cm/s)

This parameter represents the peak velocity of the aortic outflow. The peak value is also represented by height in frequency, because each vertical data line in the flow represents a range of frequencies that are proportional to the velocity of the blood (erythrocytes). In mice the peak usually occurs about 50 to 75 milliseconds after the occurrence R-wave and has velocity ranging from 75 to 105 cm/s. It is important that the Doppler probe is held steady, otherwise, there may be a downward trend in peak flows. Repeated measurements with effort to hold probe steady may be needed. Peak aortic velocity is the most useful measure of systolic function in our studies. It is relatively unaltered by heart rate and decreases after experimental myocardial infarction. It increases modestly by inotropic interventions like isoproterenol infusion.
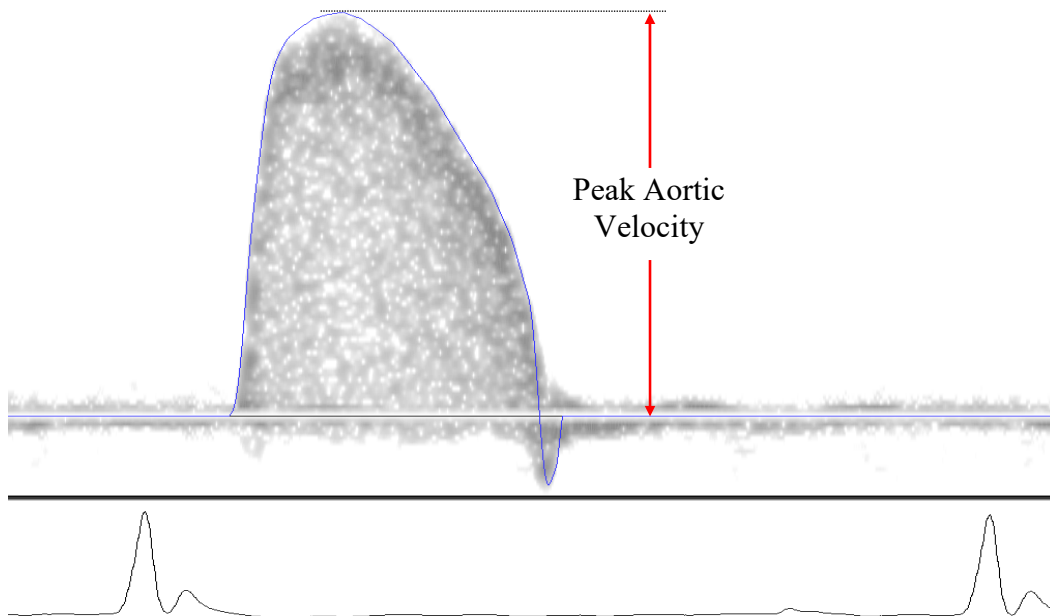
Algorithm:

- After the application of appropriate noise-contrast-gain parameters the velocity peaks of the outflow signal are measured.

    p_{V1} is the peak velocity of the 1ˢᵗ flow curve in the signal record.

- Compute the average of all velocity peaks.

    If p_{V1}, p_{V2}, ..., p_{Vn} represent the peak velocities of LV outflows, then

    Peak velocity = $(1/n) \sum p_{Vn}$

2A.c) Stroke distance (cm) (area under each flow velocity curve)

This parameter represents the positive area under the aortic outflow velocity curve from onset till end (area under the envelope of flow velocity curve). This parameter can be calculated by finding the area under each flow velocity curve in an R-R interval.

Area Under Peak
Aortic Velocity
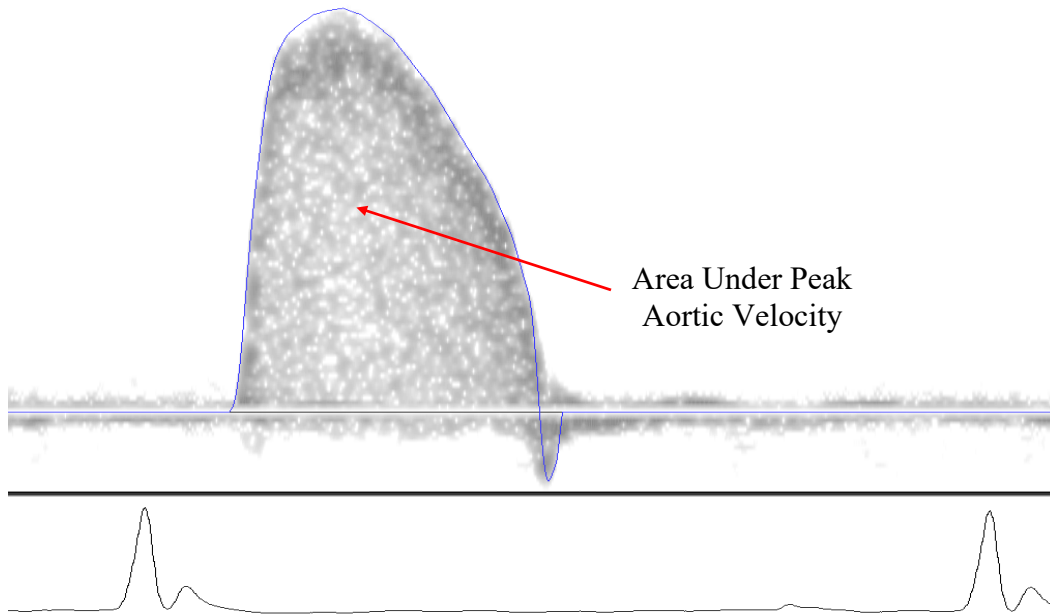
Algorithm:

- Use envelope detection to detect the peak frequency of each spectrum record of the aortic flow velocity waveform (use a known threshold to minimize low level noise).
- Once the peaks representing the envelope are detected, then the area under the curve is calculated (using trapezoidal or Simpson's rule).

    s_1 is the area under the aortic outflow waveform in the 1st cardiac cycle of the signal.

- Compute average of all individual aortic outflow wave stroke distances.

    Stroke Distance = $(1/n) \Sigma(s_n)$

2A.d) Ejection time (ms)

This parameter represents the amount of time taken from the onset to the end of aortic outflow velocity curve. Abnormalities such as LV infarction or other diseases that affect LV may prolong the duration of ejection time.
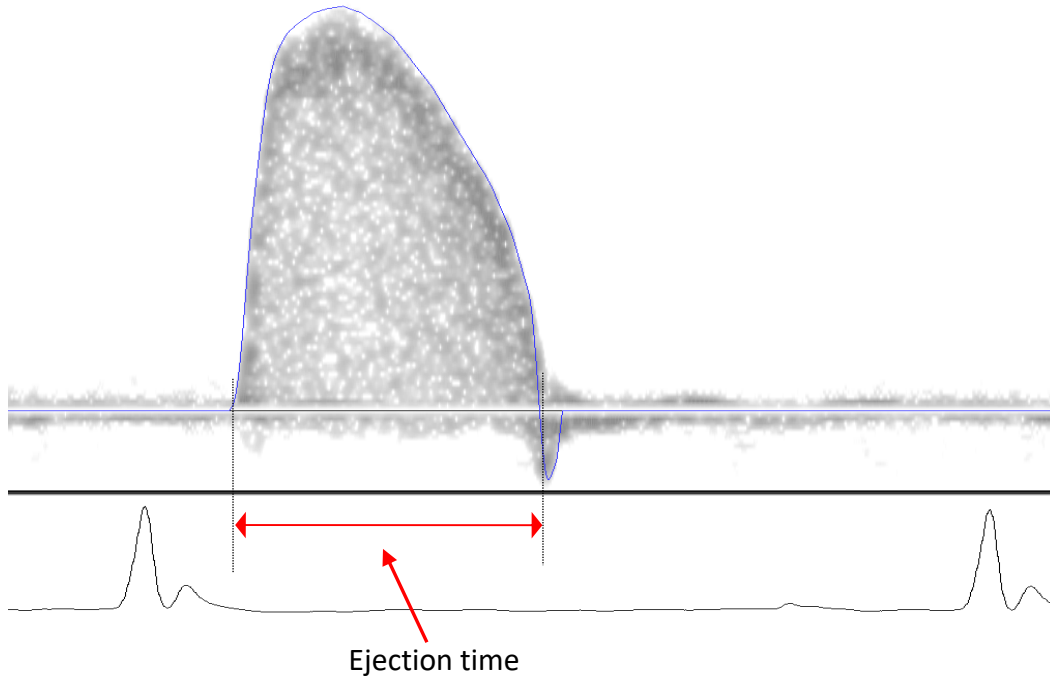
Ejection time

Algorithm:

- Computes time from the opening to closing of aortic valve (LV ejection).

  t_{ET1} is the ejection time of the LV in the 1st cardiac cycle of the signal.

- Computes average of LV ejection time in all cardiac cycles.

  Ejection time = $(1/n)\ \Sigma t_{ETn}$

2A.e) Rise Time (ms) (from onset to peak height)

This parameter represents the time from onset of aortic outflow velocity to the time where peak velocity of the flow is observed. LV infarction or other LV diseases may prolong the duration of RiseTime (time-to-peak-height).
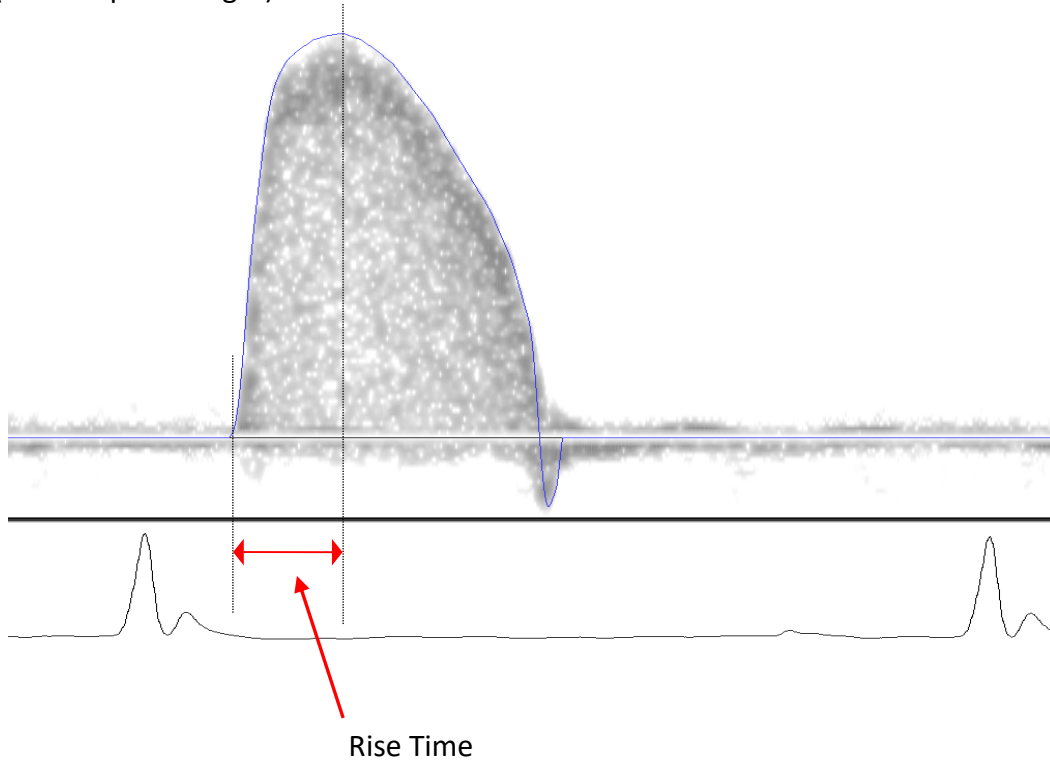
Rise Time

Algorithm:

- Computes time from onset of LV ejection to peak LV flow velocity

    t_{RT1} is the time to reach peak flow in the 1st curve in the signal record.

- Computes the average of time-to-peak height values.

    Rise Time = $(1/n)\ \Sigma t_{RTn}$

2A.f) Mean velocity (cm/s)

This parameter represents the average aortic blood flow velocity during each cardiac cycle.
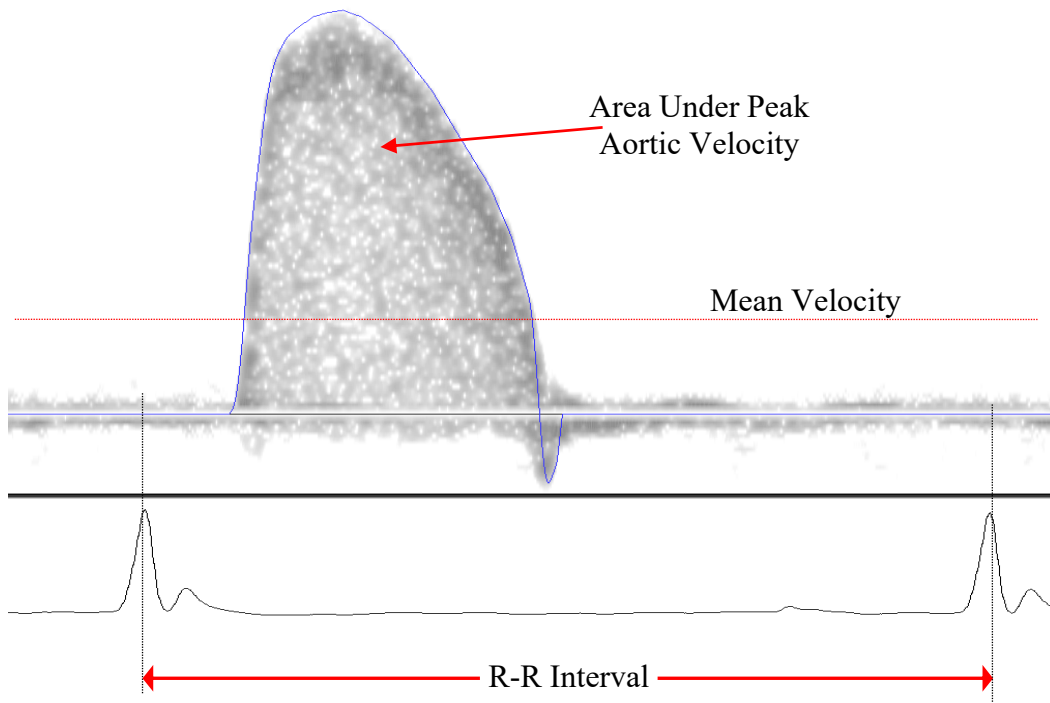
Algorithm:

- Compute average velocities using: Area/R-R interval for each flow curve.

    v_{M1}= Area/R-R interval, where Area is stroke distance

- Compute the mean of the average flow velocity of all curves.

    Mean velocity = $(1/n) \Sigma v_{Mn}$

2A.g) Mean acceleration (cm/s²)

This parameter represents the mean acceleration of the LV flow and is calculated by dividing peak aortic flow velocity over Rise time. This is probably the most sensitive measure of systolic function, and the variability even within a second of recording can be problematic for statistical use.

Peak Aortic Velocity
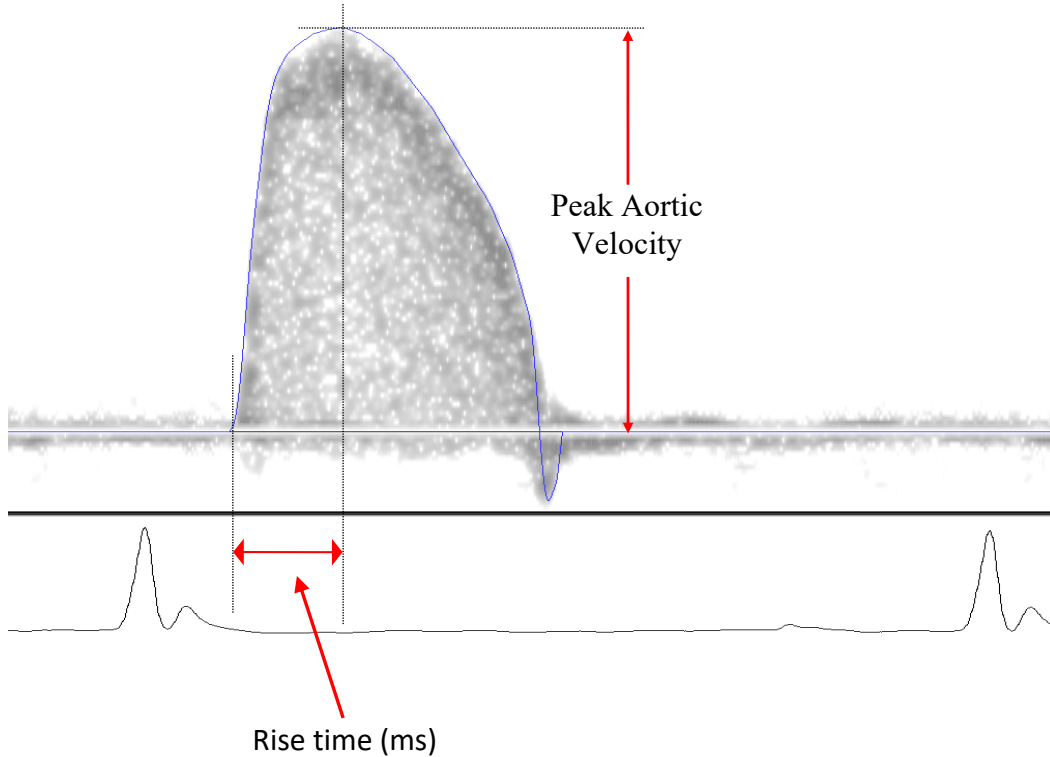
Rise time (ms)

Algorithm:

- Compute the mean acceleration of each aortic outflow velocity.

    a_{M1} = m * Peak Velocity/ Rise Time   m=0.001*7.5

- Compute the mean of the accelerations of the LV flows.

    Mean acceleration = $(1/n) \Sigma a_{Mn}$

3A. Mitral (inflow) velocity signal

      This Doppler spectrogram signal represents the mitral flow velocity from the left atrium into the left ventricle during diastole. A 10 MHz pulsed Doppler probe with a range gate depth set between 6-8 mm is used to obtain an optimal inflow velocity signal. The probe is placed just lateral to the xiphoid and is pointed to the left ear and the range is adjusted to place the sample volume at the mitral valve orifice. The mitral flow velocity signal is biphasic. One is an early (E) peak that occurs during rapid filling phase, and is usually longer in time and larger in magnitude. The other, a shorter in time and smaller in magnitude (A) peak, which occurs with atrial contraction and is known as atrial filling phase. The amplitude of A curve may depend on depends on the R-R interval. If R-R interval is shorter, the amplitude of A is larger. The duration of E-A curve can be different for different animals, and may sometimes be different in the same animals. Thus it may be necessary to acquire several segments to obtain average values. The E-curve is measured with respect to the R-wave preceding it (E-curve) and the A-curve is measured with respect to the R-wave following it (A-curve) (see figure).

Epeak Wave

Apeak Wave
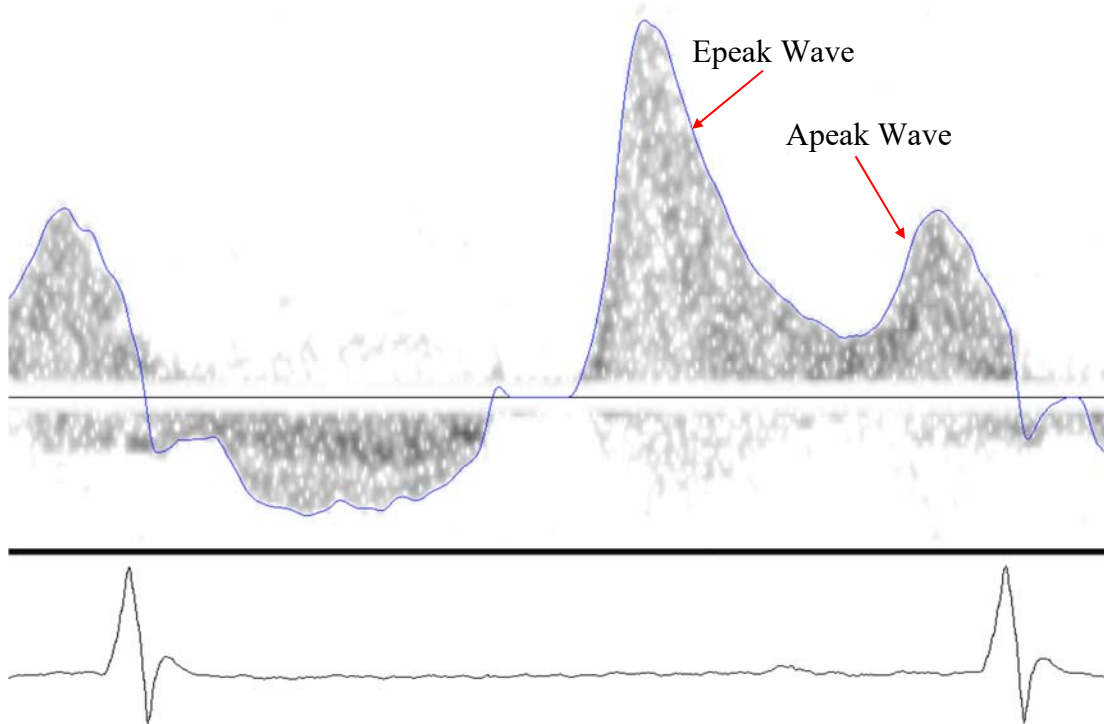
3A.I. a) Early (E) filling curve: Peak velocity of E (cm/s)

This parameter represents the peak velocity of the E curve. The peak value is also represented by height in frequency, because each vertical data line in the flow represents a range of frequencies that are proportional to the velocity of the blood erythrocytes.

This parameter is relatively unaltered by heart rate and decreases with impaired relaxation (aging) and increases with augmented relaxation (hyperthyroidism). In animals with elevated LA pressures, peak E height may paradoxically increase (pseudo-normalization).
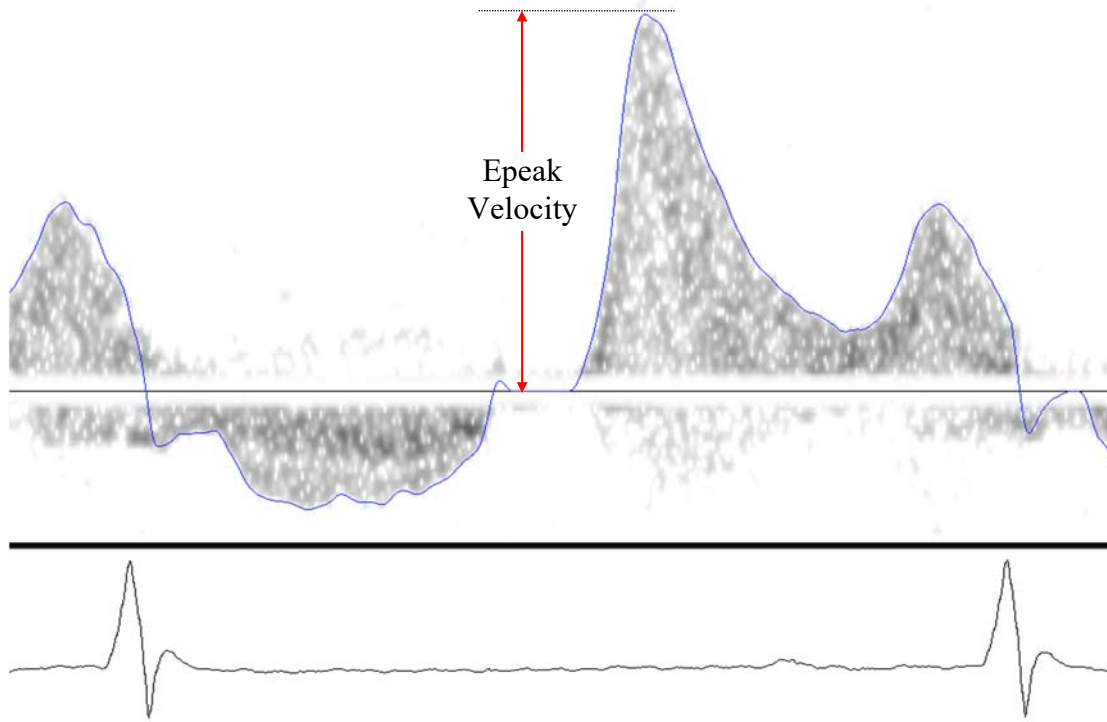
Algorithm:

- After the application of appropriate noise-contrast-gain parameters the velocity peaks of the outflow signal are measured.

    p_{VE1} is the peak velocity of the 1st flow curve in the signal record.

- Compute the average of all velocity peaks.

    If $p_{VE1}, p_{VE2}, ..., p_{VEn}$ are the peak velocities of E curve, then

    Peak E velocity = $(1/n) \Sigma p_{VEn}$

3A.I.b) Stroke distance of E (cm) [area under E curve]

This parameter represents the positive area under the E curve from onset till end (area under the envelope of E-flow velocity curve). This parameter can be calculated by finding the area under the each E-flow curve of an R-R interval. Care must be taken when the fusion of (E and A) curves occurs. This situation occurs when the heart rate goes up.
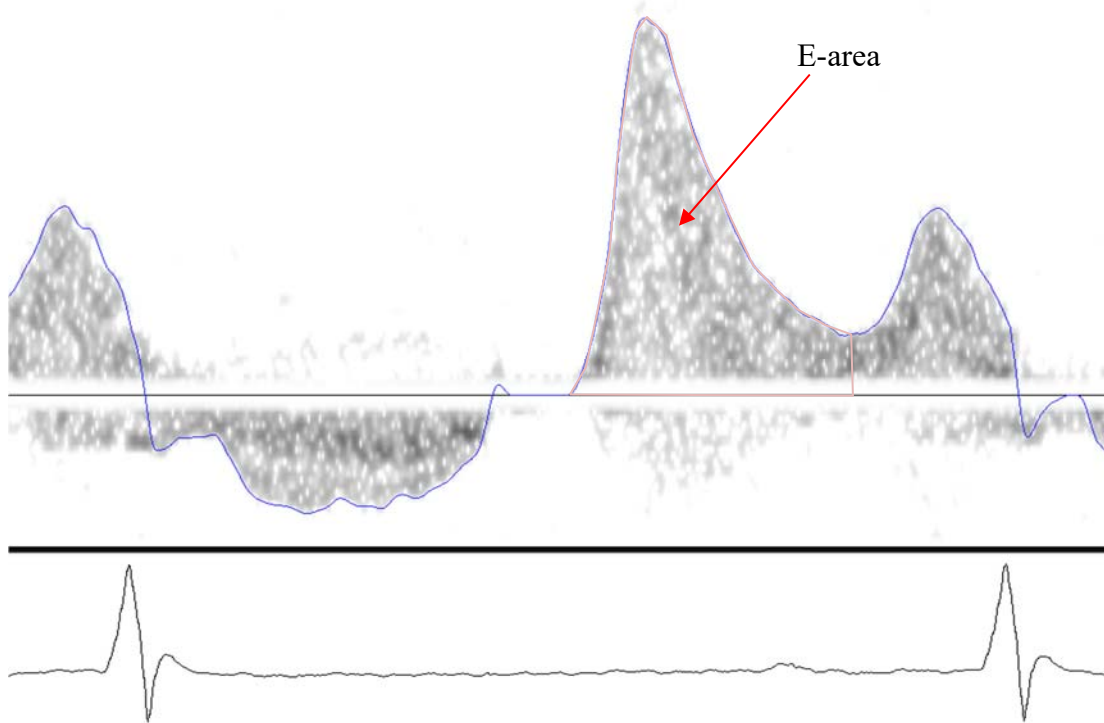
E-area

Algorithm:

- Use envelope detection techniques or another method to pick the peak frequency of each spectrum record from the flow curve (use a known threshold to minimize low level noise).
- Once the peaks representing the envelope are detected, then the area under the curve is calculated (using trapezoidal or Simpson's rule).

    A_{E1} is the area under 1st E curve in the segment

- Compute average of all E curve stroke distances.

    Stroke distance of E = $(1/n) \Sigma A_{En}$

3A.I.c) Duration of E (ms)

This parameter represents the amount of time taken from the onset to the end of E flow velocity signal.
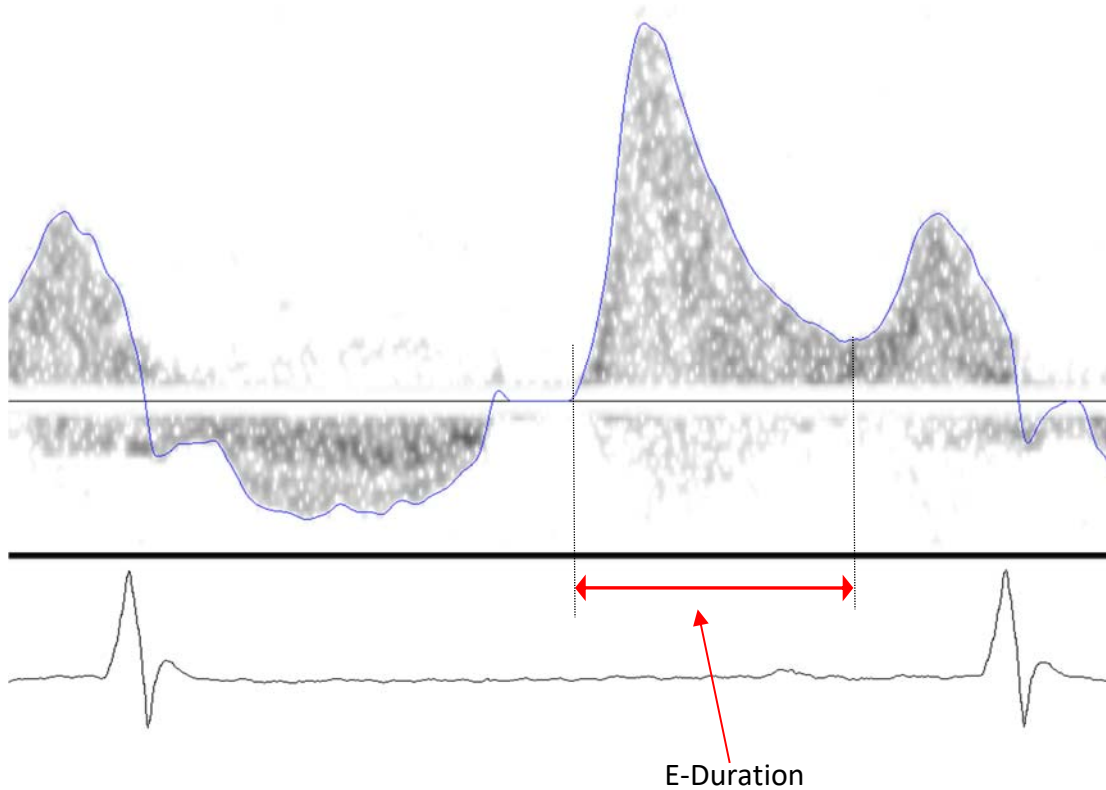
E-Duration

Algorithm:

- Compute time from onset till the end of the E flow velocity curve.

    t_{E1} is the time duration of 1st E curve in the segment

- Compute average of all E flow times.

    Duration of E = $(1/n) \Sigma(t_{En})$

3A.I.d) Acceleration time of E (ms)

This parameter represents the acceleration time, which is the time from onset of E flow to the peak value of E flow.

Acceleration time of E
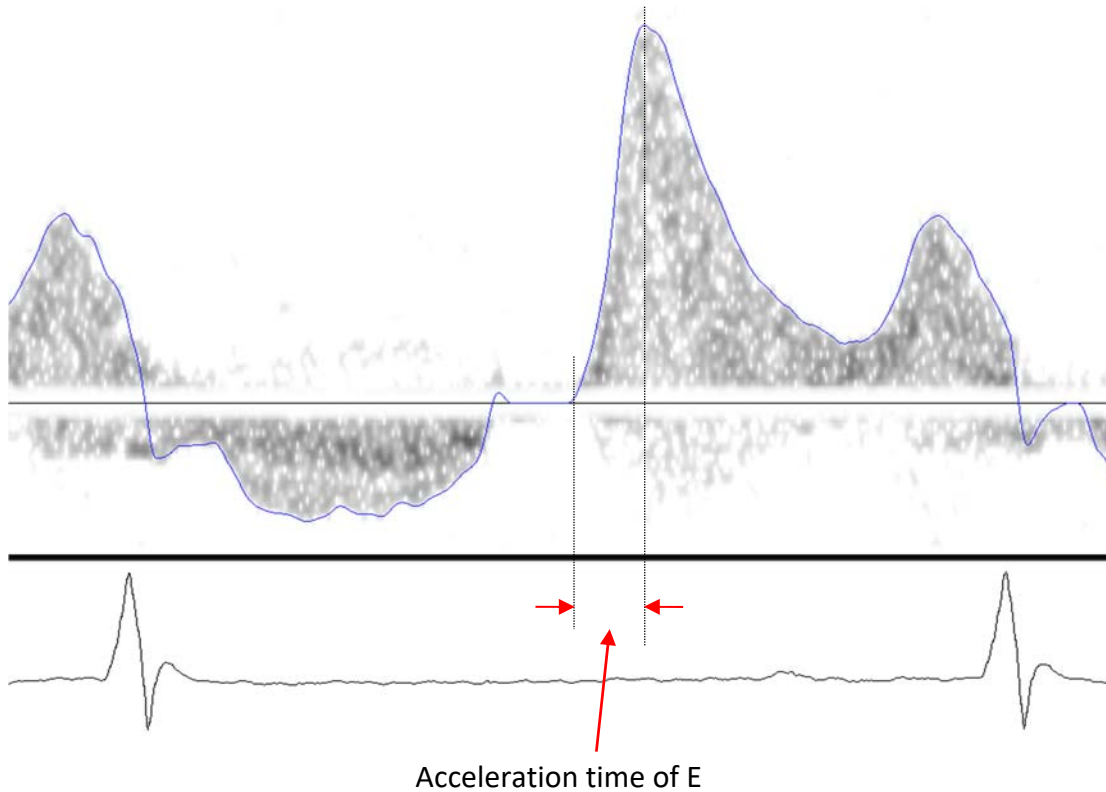
Algorithm:

- Compute the difference between the time at peak velocity and the time at onset of the E-flow velocity.

  t_{AE1} is the acceleration time of 1st E curve in the segment

- Compute the average of the times of the curves.

  Acceleration time of E = $(1/n) \Sigma t_{AEn}$

3A.I.e) Deceleration time of E (ms)

This parameter represents the total period of time of E flow velocity during which the velocity drops from peak value to the end of E (The velocity is usually minimum at the end of E).

Deceleration time of E
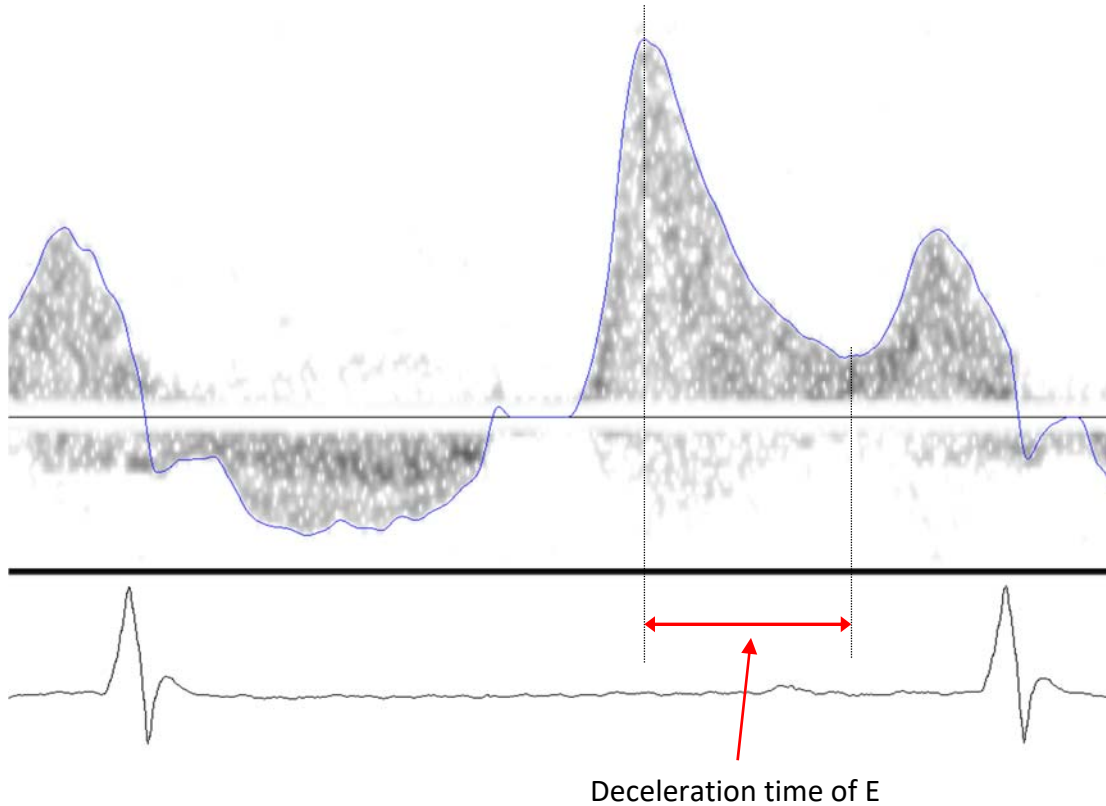
Algorithm:

- Compute the difference between the time of peak E velocity and time of the end of E flow.

    t_{DE1} is the deceleration time of the 1st E curve in the segment

- Compute the average of all the deceleration times.

    Deceleration time of E = $(1/n) \Sigma t_{DEn}$

3A.I.g) T½P (Time from Epeak to half Epeak) (ms)

This parameter represents the amount of time it takes for the peak E flow velocity to reduce by half and involves assumptions of the Bernoulli equation. Note that this time is ½ of linear deceleration time.

Time from Epeak to ½ Epeak
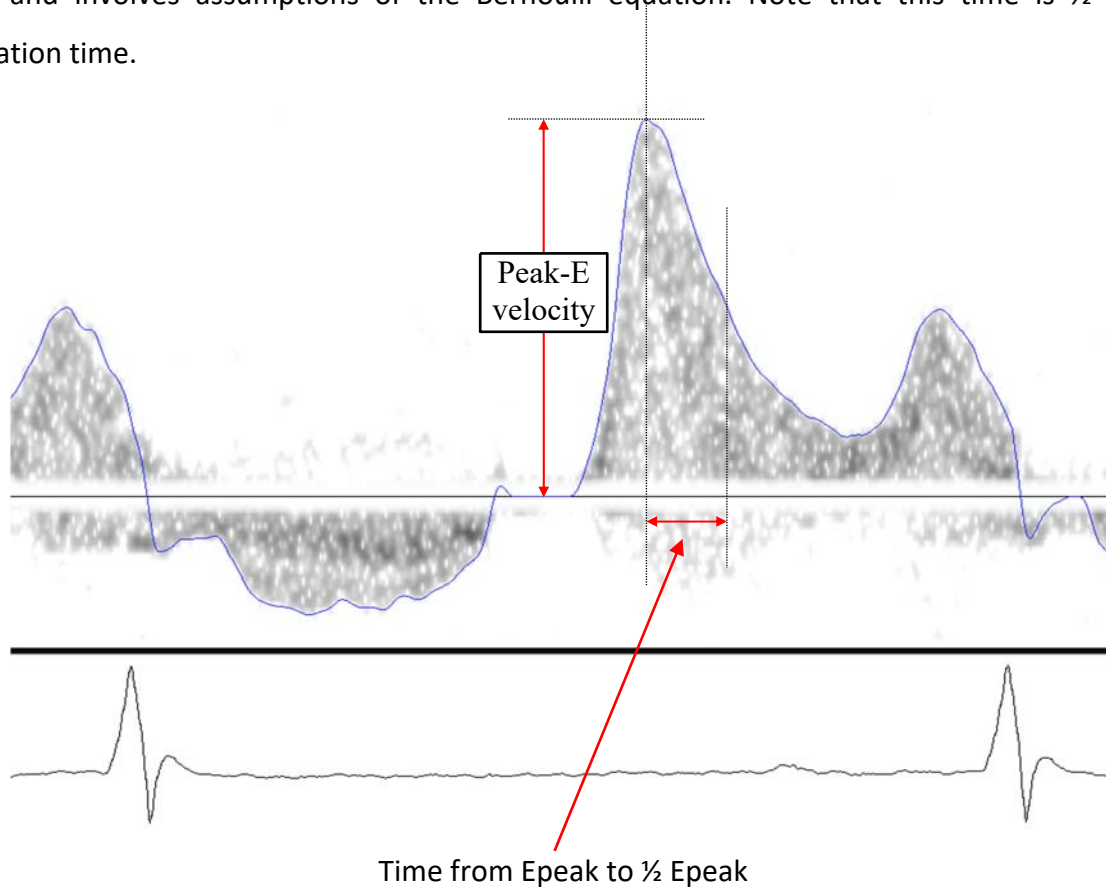
Algorithm:

- Find the time at which the flow is at its peak (t_{PE1}).
- Find the time at which flow drop to half of peak on the descending side of the flow curve ($t_{PE½1}$).
- Calculate the difference between the two times:

    $t_{PHE1} = (t_{PE1} - t_{PE½1})$

- Calculate the mean time to half peak.

    Time from peak to half peak of E = $(1/n) \sum t_{PHEn}$

3A.I.f) Linear deceleration time (ms)

This parameter represents the amount of time during which the deceleration of the E flow is linear. Linear deceleration time may be useful in interpreting the presence of pseudo-normalization in that the interval will be shorter than expected.

Linear deceleration time
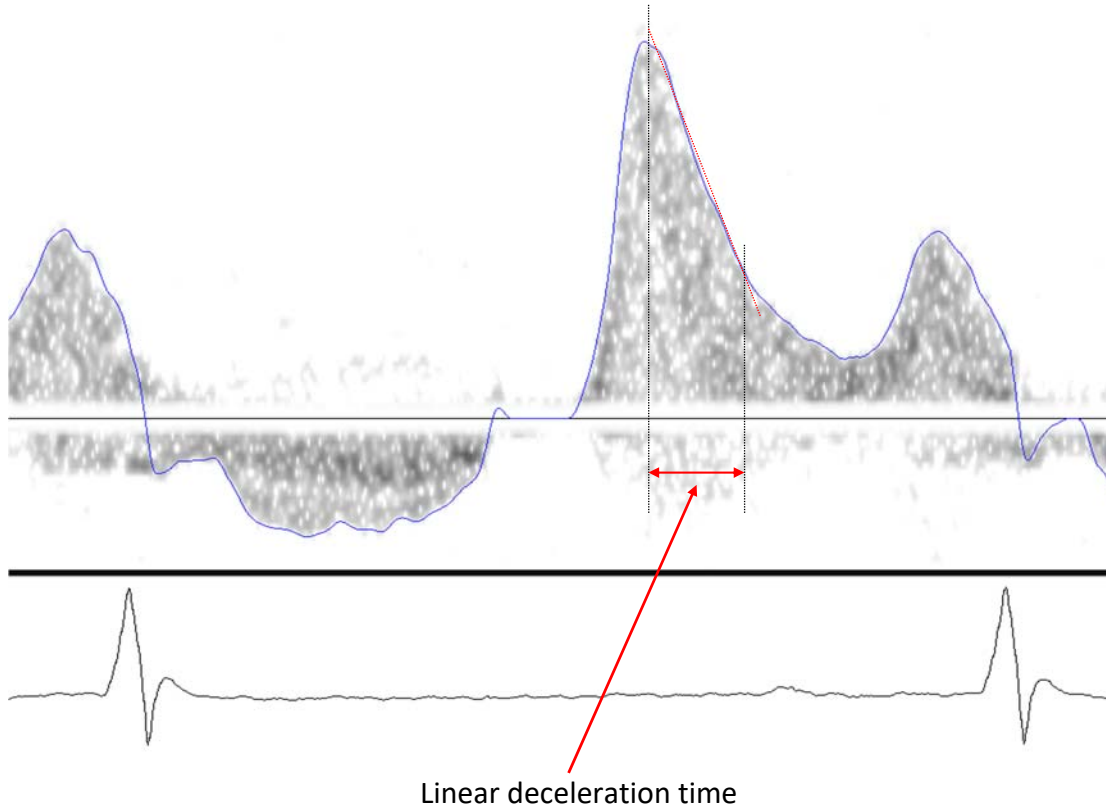
Algorithm:

- Find the time at which the flow is at its peak (t_{PE1}).

- Then find the time along the decreasing flow curve before which the flow is fairly linear (t_{LE1}).

- Calculate the time difference to obtain linear deceleration time.

    $t_{LDE1} = (t_{PE1} - t_{LE1})$

- Compute the average of all the linear deceleration times.

    Linear deceleration time of E = $(1/n) \Sigma t_{LDEn}$

3A.I.f) Mean Deceleration rate (cm/s^2)

This parameter is the obtained by dividing the peak E height by the linear deceleration time. This parameter is paradoxically elevated in pseudo-normalization.

Epeak velocity

Linear deceleration time
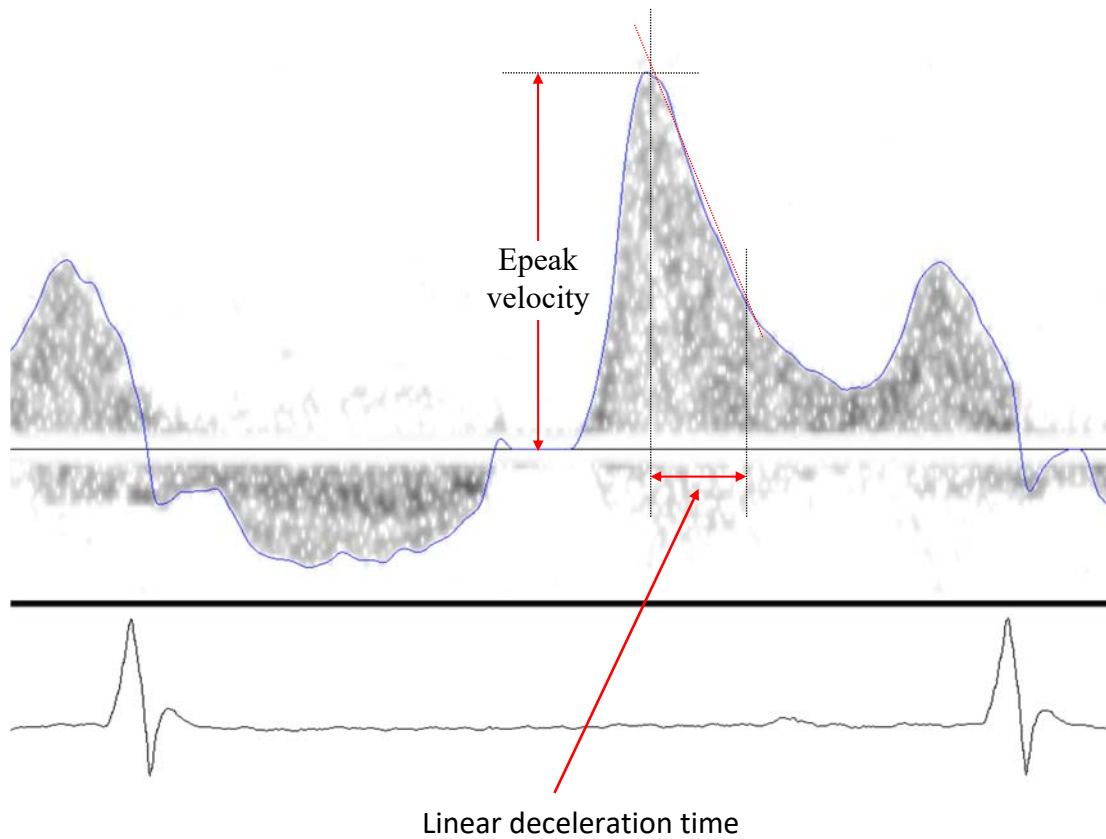
Algorithm:

- Measure the peak velocity (p_{VE1})of E curve.

- Measure the linear deceleration time (t_{LD1})of the E curve.

- Calculate the mean deceleration (d_{ME1}) rate of the E curve.

    $d_{ME1} = p_{VE1}/ t_{LD1}$

- Compute the average of several mean deceleration rates of E in a given signal record.

    Mean deceleration rate of E = $(1/n) \Sigma d_{MEn}$

3A.II.a) Atrial (A-filling curve): Peak velocity of A (Hz or cm/s)

This parameter represents the peak velocity of the atrial (A) curve. The Apeak filling is dependent on the heart rate and will increase with increasing heart rate. The peak value is also represented by height in frequency, because each vertical data line in the flow represents a range of frequencies that are proportional to the velocity of the blood erythrocytes. It is the average of all peaks in the time segment.
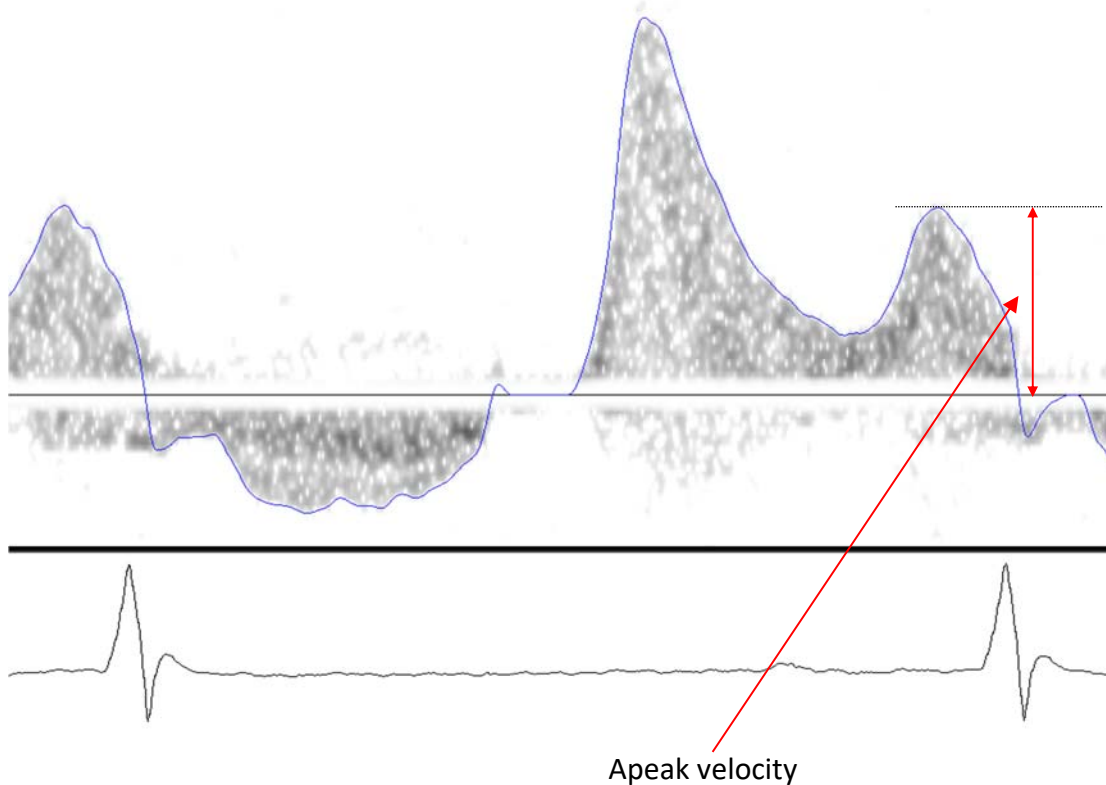
Apeak velocity

Algorithm:

- Measure the peak velocity (v_{PAn})of each A curve from the spectrogram.
- Compute the average of all A-peak velocities.

Peak velocity of A = $(1/n) \Sigma\ v_{PAn}$

3A.II.b) Stroke distance of A (cm), (area under A curve)

This parameter represents the positive area under the (A) flow curve from start till end. The area increases with increasing heart rate. This value is averaged over the number of curves in a given time segment.
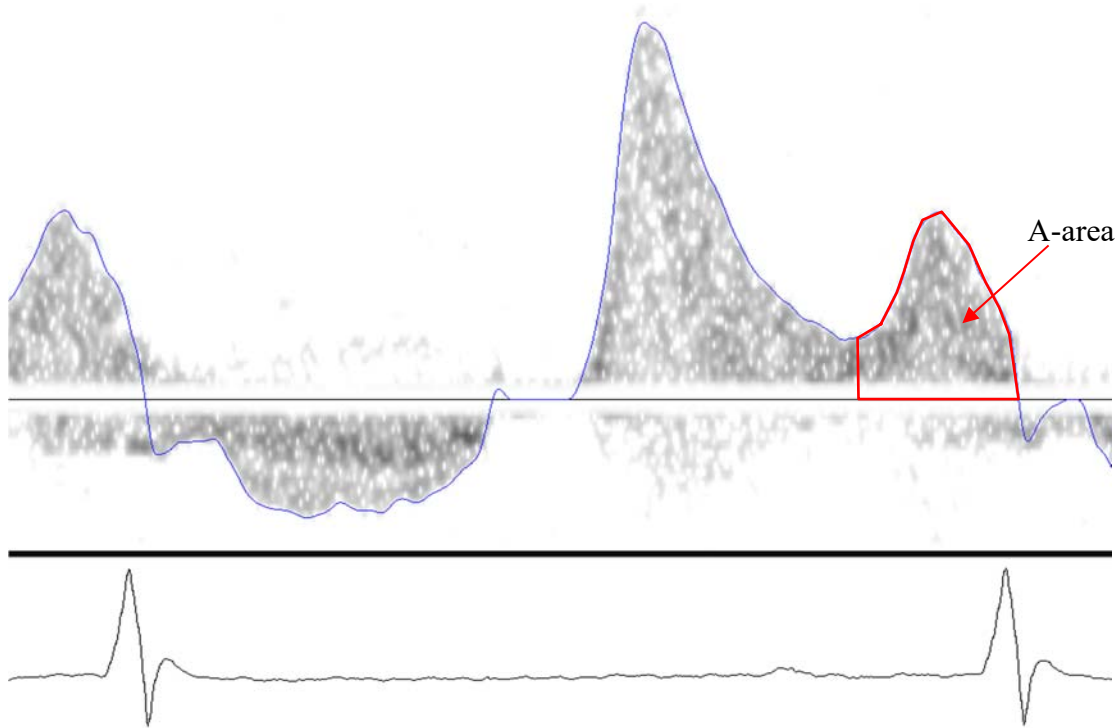
A-area

Algorithm:

- Use envelope detection techniques or another method to pick the peak frequency of each spectrogram of the flow velocity curve (use a known threshold to minimize low level noise).

- Once the peaks representing the envelope are detected, then the area under the curve is calculated (using trapezoidal or Simpson's rule).

  A_{A1} is the area under 1st A curve in the segment

- Compute average of all A curve stroke distances in a give E-A flow velocity signal record.

  Stroke distance of A = $(1/n) \sum A_{An}$

3A.II.c) Duration of A (ms)

This parameter represents the amount of time taken from the start to end of (A) flow curve.

The parameter calculated is the average of the flow times of all A curves in a given time segment.
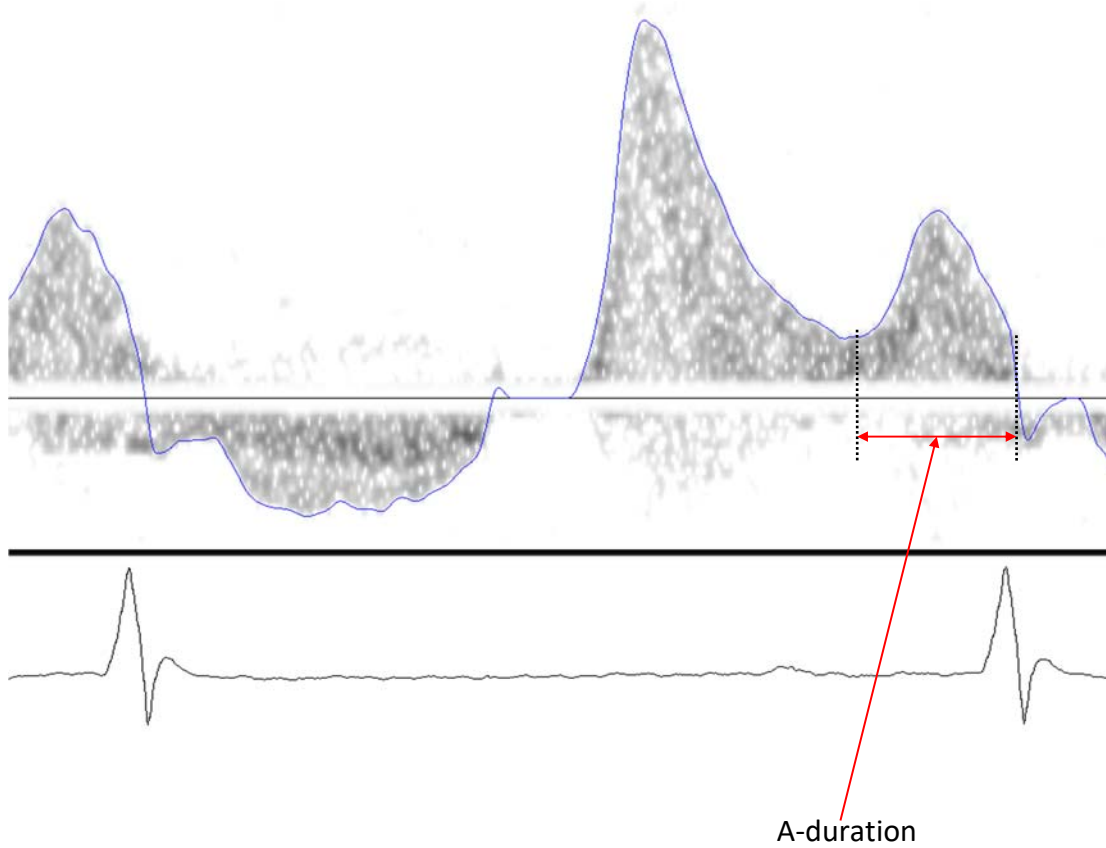
A-duration

Algorithm:

- Compute time from start till the end of the (A) flow (t_{A1}).

- Compute average of all (A) flow duration times.

  Time duration of A = $(1/n) \Sigma(t_{An})$

3B. E-A Relations

The E-A relationships reflect the characteristics of the diastolic function and are frequently used in evaluating the diastolic function in mice. For the most part, the (A) filling can be thought of as a compensatory mechanism for inadequate E filling. The relationships provide information on tachycardia (fast) or bradycardia (slow) rates of the heart, and cardiac output, thus indicating diastolic abnormalities.
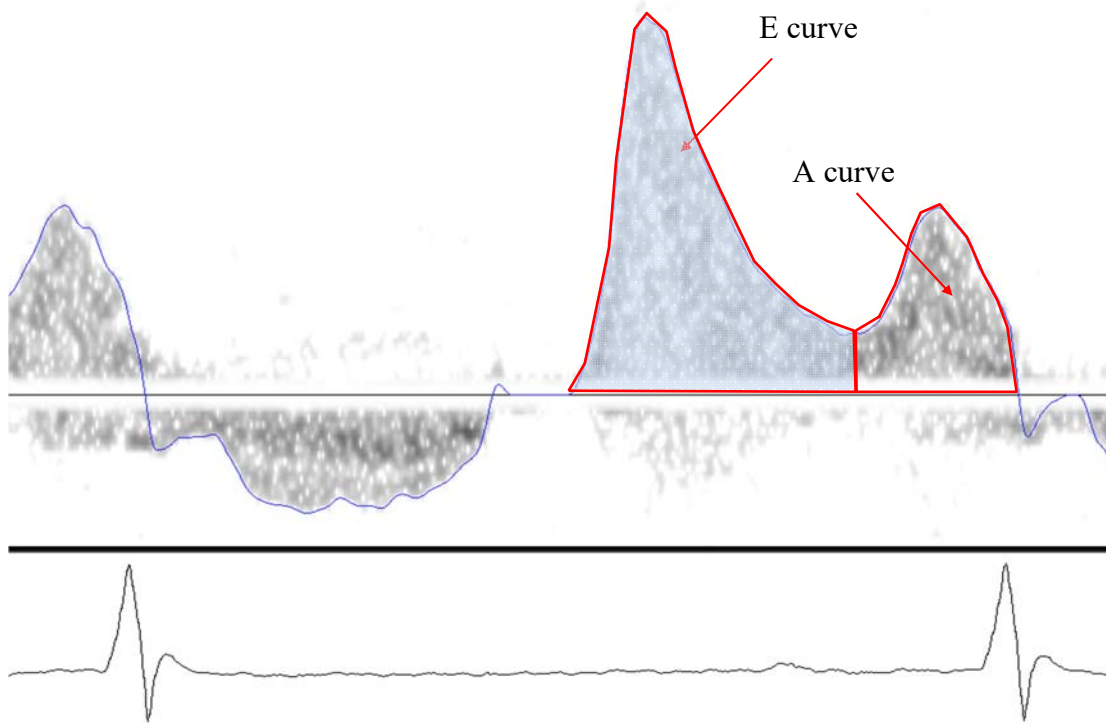
3B.a) E-A peak velocity ratio

The E-A ratio of the peak velocities is a good indicator of the heart rate (and perhaps aging). Typically in the young mouse E/A is greater than 4.0 with heart rates approximately 300 beats/min. Even in normal young mice at heart rates about 500 beats/min (just before E-A fuse) the E/A ratio is greater than 2.0. This is an overall excellent measure of diastolic function.
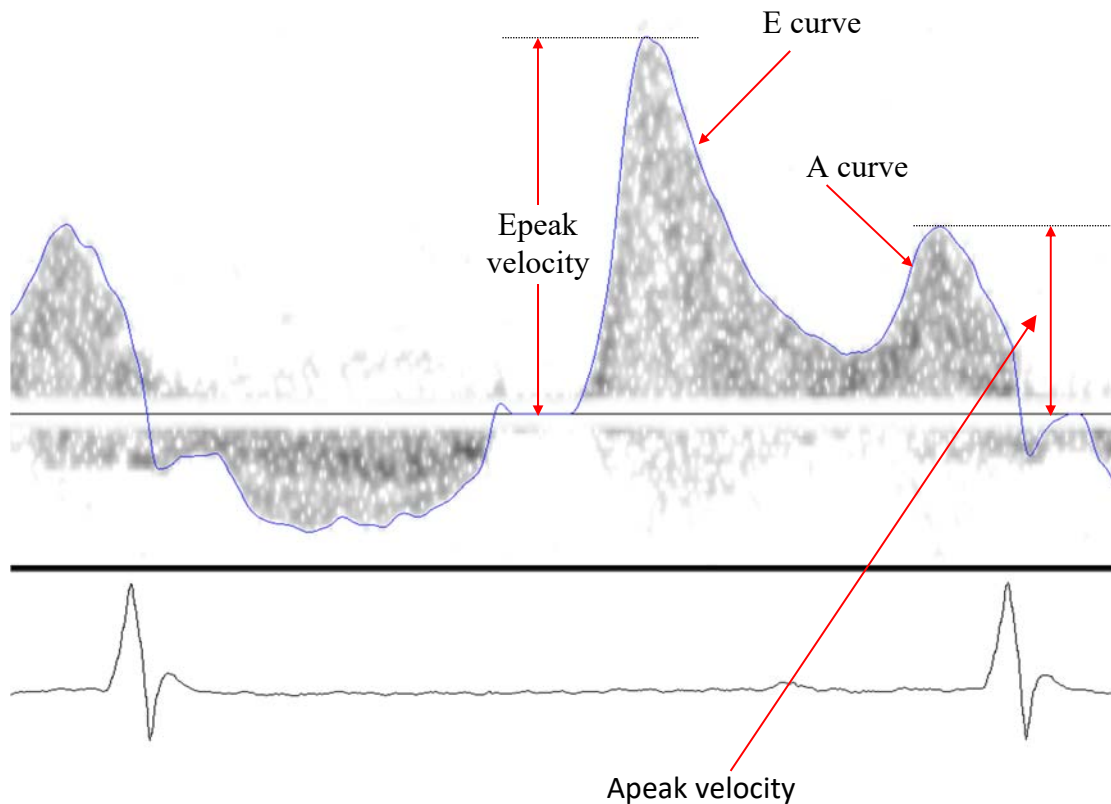
Algorithm:

- Use the measured values of peak-E velocity and peak-A velocity in each E-A flow velocity curve and calculate the ratio.

$$r_{VEA1} = v_{PE1}/v_{PA1}$$

- Calculate the mean of the velocity ratios of E-A sets calculated in a given E-A flow velocity signal record.

$$\text{E-A velocity ratio} = (1/n) \; \Sigma \; r_{VEAn}$$

3B.b) E-A area ratio

The E-A ratio of the areas is also an indicator of heart rate. The E/A area ratio gives roughly the same information as the E/A peak ratio.
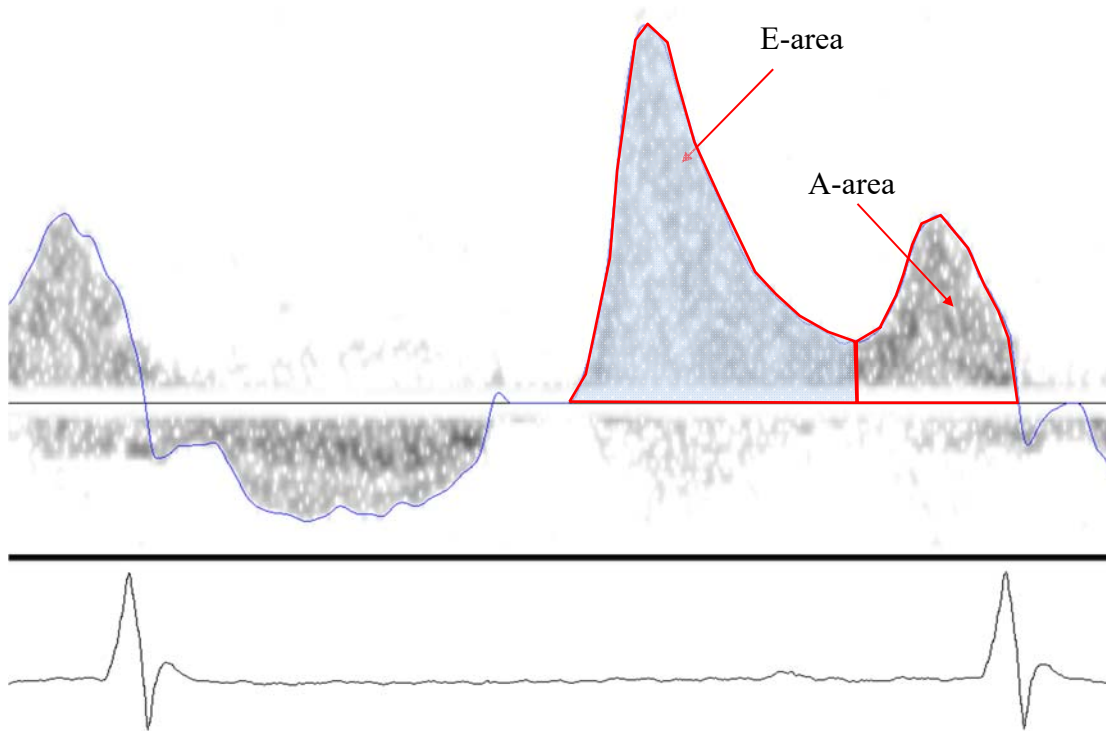
Algorithm:

- Use the calculated values of the E-area and A-area to calculate the ratio in each flow pattern.

    $r_{AEA1} = A_{E1}/A_{A1}$

- Then take the mean of the area ratios of the E-A sets calculated in a given E-A flow velocity signal record.

    E-A area ratio = $(1/n) \, \Sigma \, r_{AEAn}$

3B.c) Total area (under E & A)

This parameter represents the area (cm - of stroke distance) during the entire inflow period. This parameter is the equivalent of the inflow volume which can be calculated if the mitral valve cross-sectional area is known.

E-area + A-area
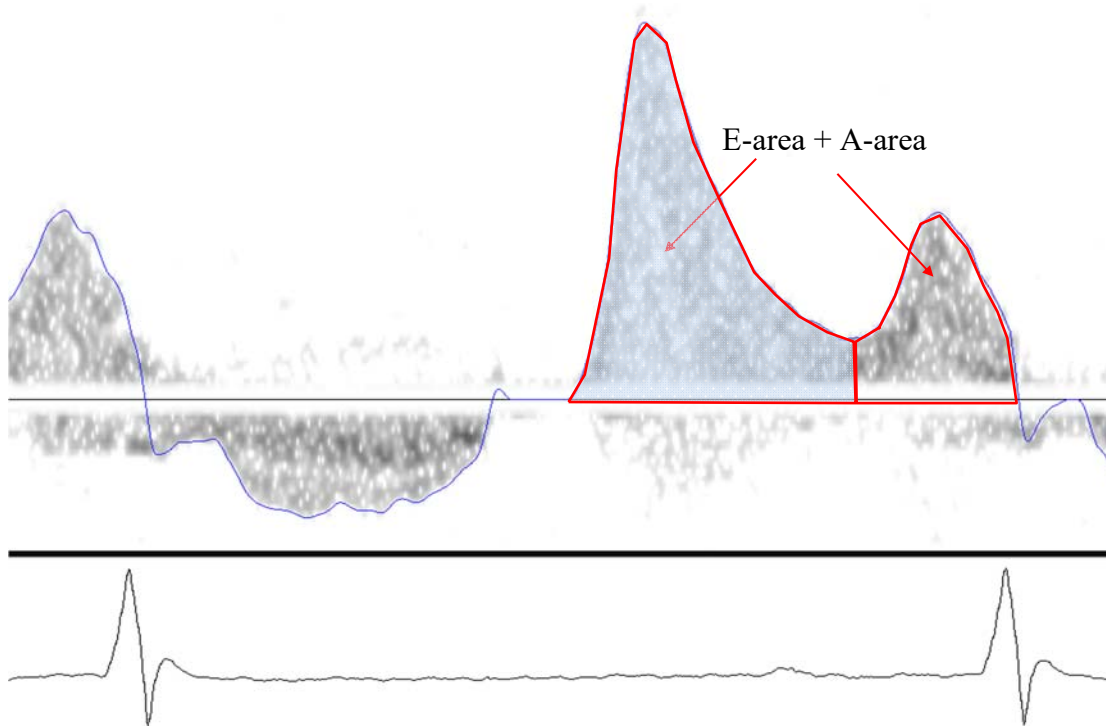
Algorithm:

- Use the computed areas under E & A curves to obtain the total area.

    $T_{AEA1} = A_{E1} + A_{A1}$

- Then take the mean of the total areas of the E-A sets calculated in a time segment.

    Total E-A area = $(1/n) \sum T_{AEAn}$

3B.d) A area/Total area = Atrial filling fraction (AFF).

This parameter represents the ratio of the area of (A) curve to the total (E+A) area. The atrial component often is increased to compensate for inadequate early filling. Although dependent on the heart rate the AFF is quite sensitive to impaired diastolic function.
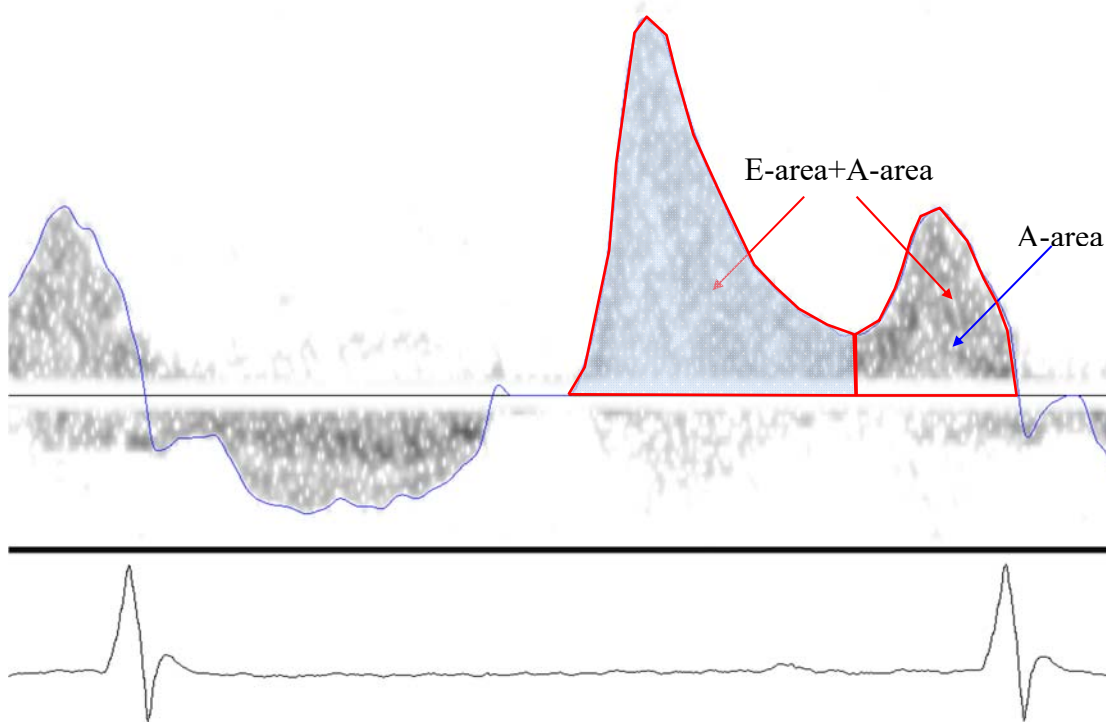
Algorithm:

- Use the computed areas under E & A curves to obtain the total area.

    $T_{AEA1} = A_{E1} + A_{A1}$

    $F_{AffEA1} = A_{A1}/T_{AEA1}$

- Then take the mean of the total areas of the E-A sets calculated in a time segment.

    Atrial filling fraction of E-A = $(1/n) \Sigma F_{AffEAn}$

3B.e) Peak E/Total area (stroke volume/s)

One problem with our techniques is that the location of the sample volume is not known. This ratio is independent of location within the LV inflow tract and gives same information as peak E (get ref) from our paper.
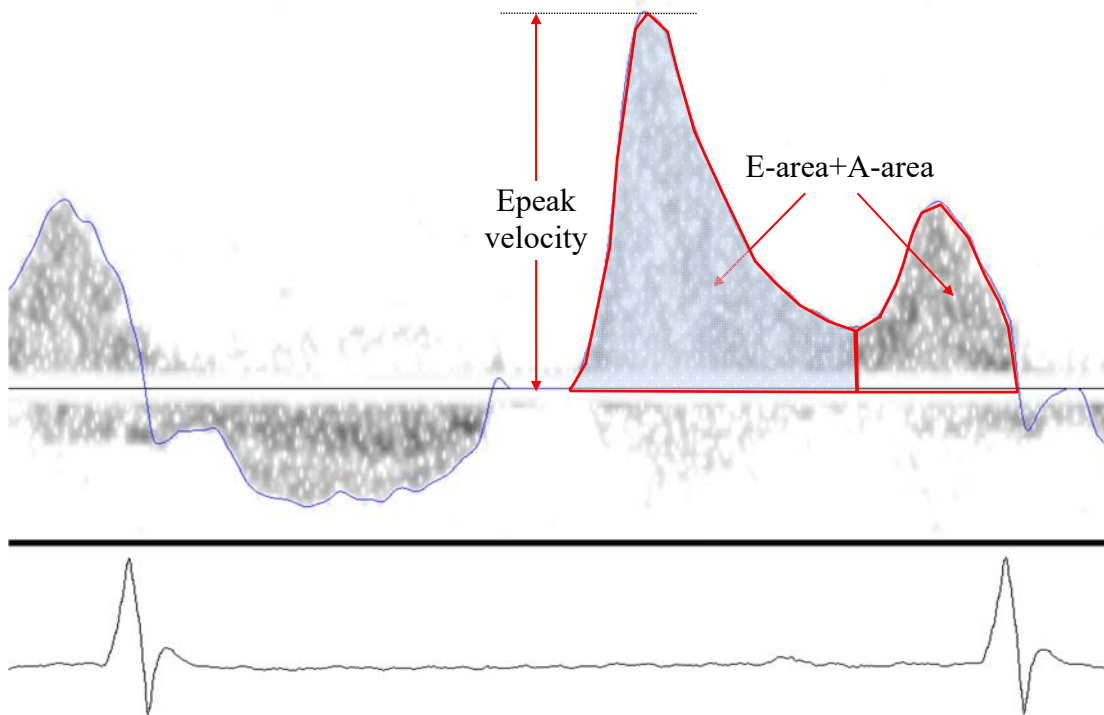
Algorithm:

- Use the computed areas under E & A curves to obtain the total area.
- Use the computed peak-E velocity and calculate the ratio.

    $r_{VTAEA1} = v_{PE1}/T_{AEA1}$

- Then take the mean of the ratios of the E-A sets calculated in a time segment.

    EAPTA_ratio_inflow = $(1/n) \Sigma\ r_{VTAEAn}$

3C.a) IVRT (isovolumic relaxation time) (ms)

This parameter represents the time interval from aortic valve closing to mitral valve opening. The parameter is different between the start of the E inflow and the end of outflow. With the probe positioned in the mitral area, slight movement medially will catch outflow (negative direction) and inflow. For calculation of this parameter, often the movement is not necessary and the aortic will be seen anyway. IVRT can be an excellent measure of relaxation. It is increased by age, poor relaxation and elevated aortic pressure. It is decreased by increase in heart rate and elevated left atrial pressure (see pseudo-normalization).
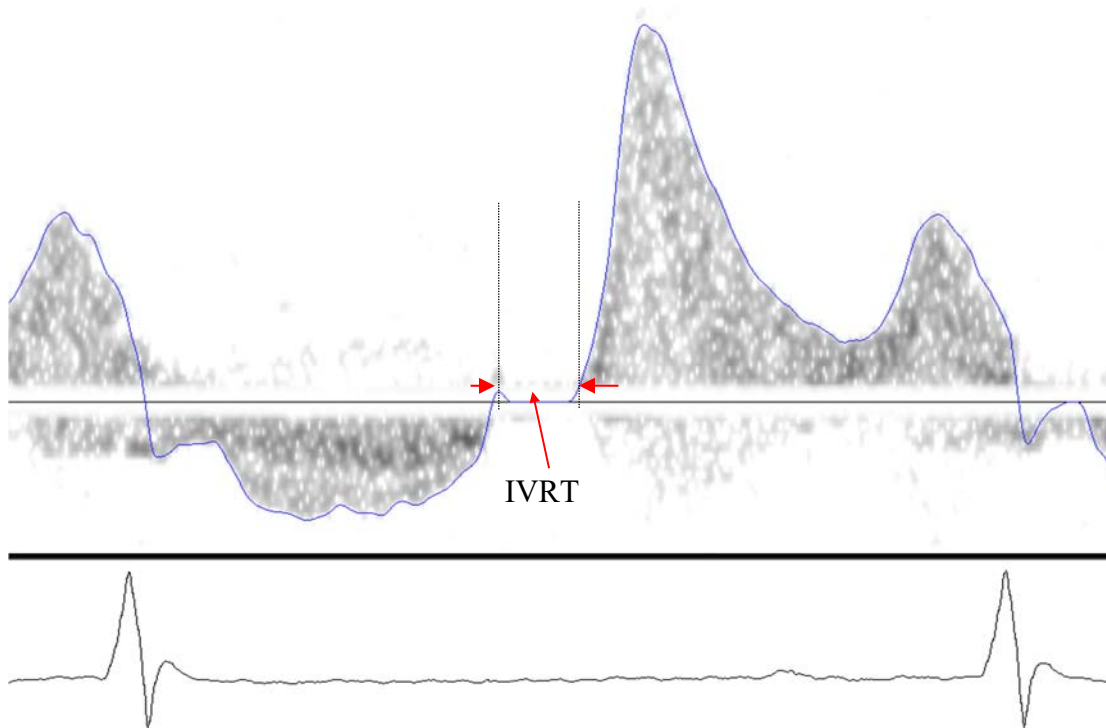
Algorithm:

- Compute the time from the end of outflow to the start of inflow.
- Compute the average of all IVRT.

$$ivrt\_time\_inflow = (1/n) \ \Sigma(t_{mitsn} - t_{miten})$$

3C.b) IVCT (isovolumic contraction time) (ms)

This parameter represents the time interval from the mitral valve closing to aortic valve opening. The parameter is different between the end of (A) inflow and the start of outflow. With the probe positioned in the mitral area, slight movement medially will catch outflow (negative direction) and inflow. For calculation of this parameter, often the movement is not necessary and the aortic will be seen anyway. IVCT can be an excellent measure of contraction.
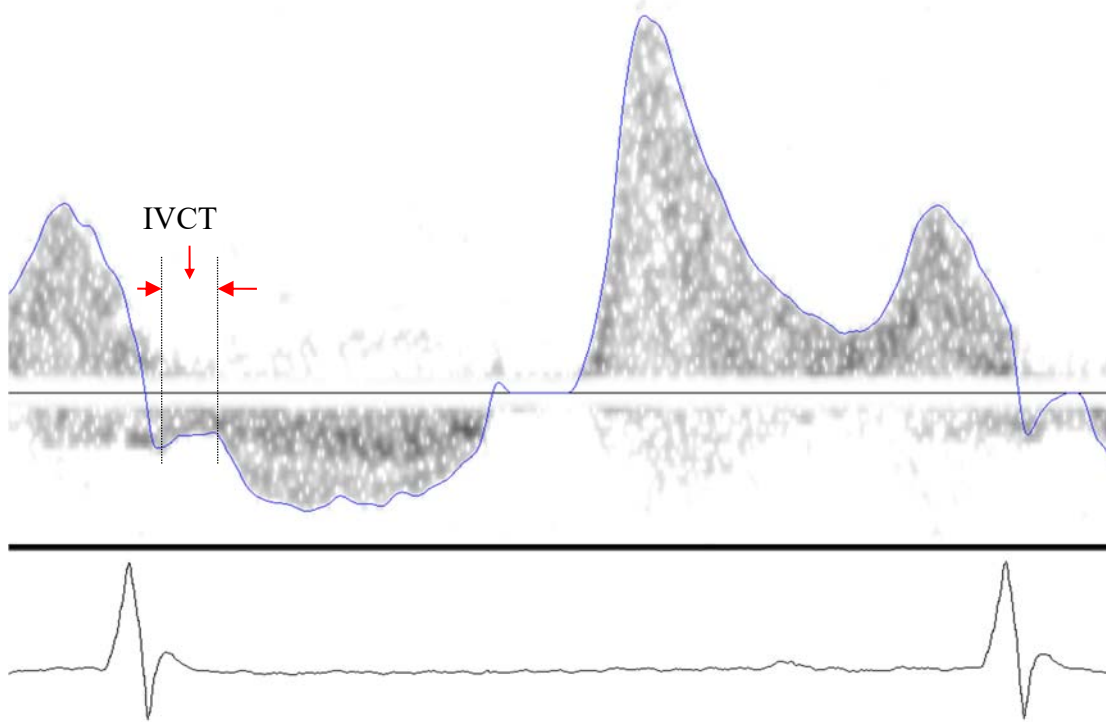
Algorithm:

- Compute the time from the end of inflow to the start of outflow.
- Compute the average of all IVCT.

$$\text{ivct\_time\_inflow} = (1/n) \, \Sigma(t_{miten} - t_{aotsn})$$

4A. Aortic arch & abdominal arterial flow signals

Doppler flow signals from aortic arch and abdominal arteries are used to estimate the propagation velocity of the pulse wave generated by the pumping of the blood into the aorta. The propagation velocity computed as pulse wave velocity (PWV) is an indicator of arterial wall compliance. Diseases such as atherosclerosis and hypertension, and conditions developed from drugs can alter the compliance or stiffness of the arterial wall, which is reflected in the PWV measurements.

4A.a) Time interval from R-peak to onset of blood flow velocity at aortic arch [also called Thoracic aorta] (msec).

Pre-ejection time interval (ms)
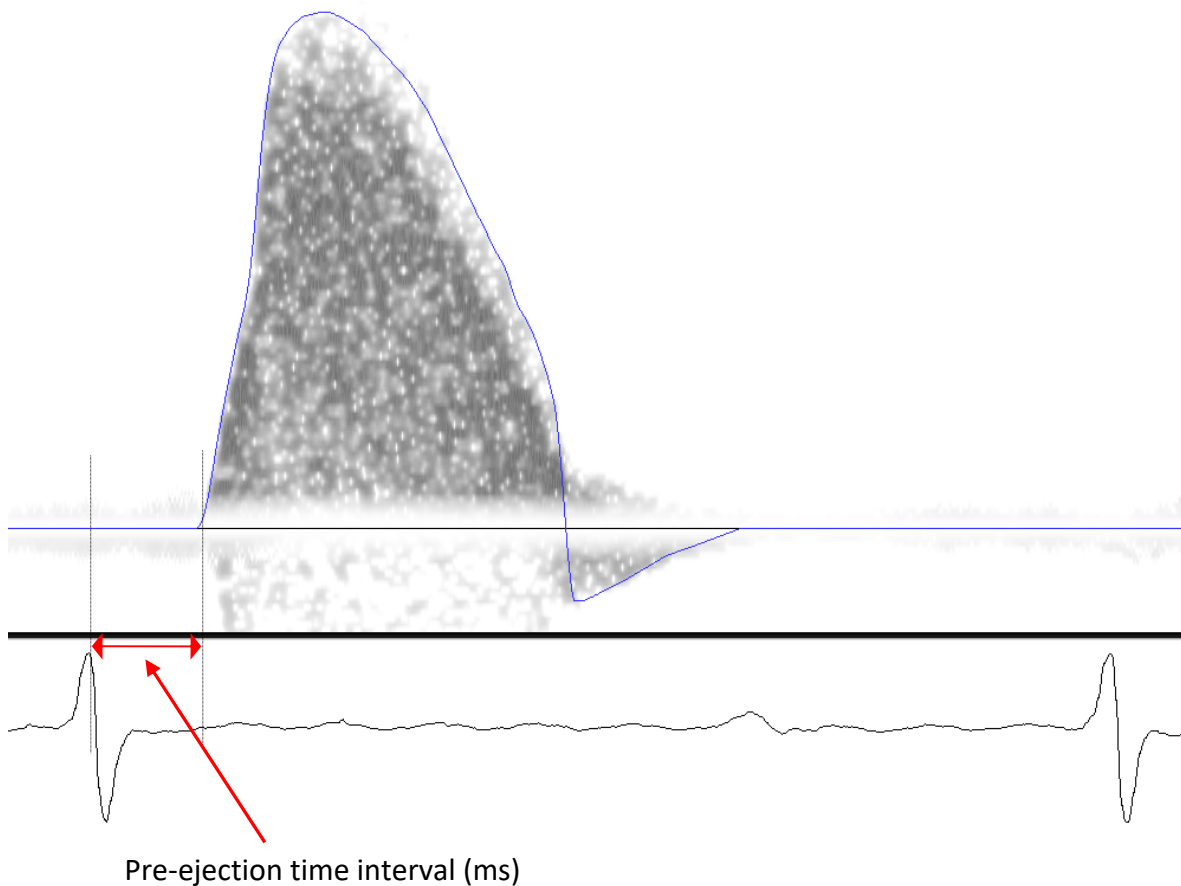
Algorithm:

- If t_{aatr1}, t_{aatr2}, ..., t_{aatrn}, represent the time points of R-waves and t_{aats1}, t_{aats2}, ..., t_{aatsn} represents the time points of flow onset at aortic arch then,

$$t_{aati1} = (t_{aats1} - t_{aatr1})$$

where t_{aati1} is the time interval of 1st flow curve in the segment

- Compute the average of all time intervals.

Pre-ejection time_interval_aorticarchflow = $(1/n) \Sigma t_{aatin}$

4A.b). Time interval from R-peak to the onset of abdominal arterial flow (msec)

Pre-ejection time interval (ms)
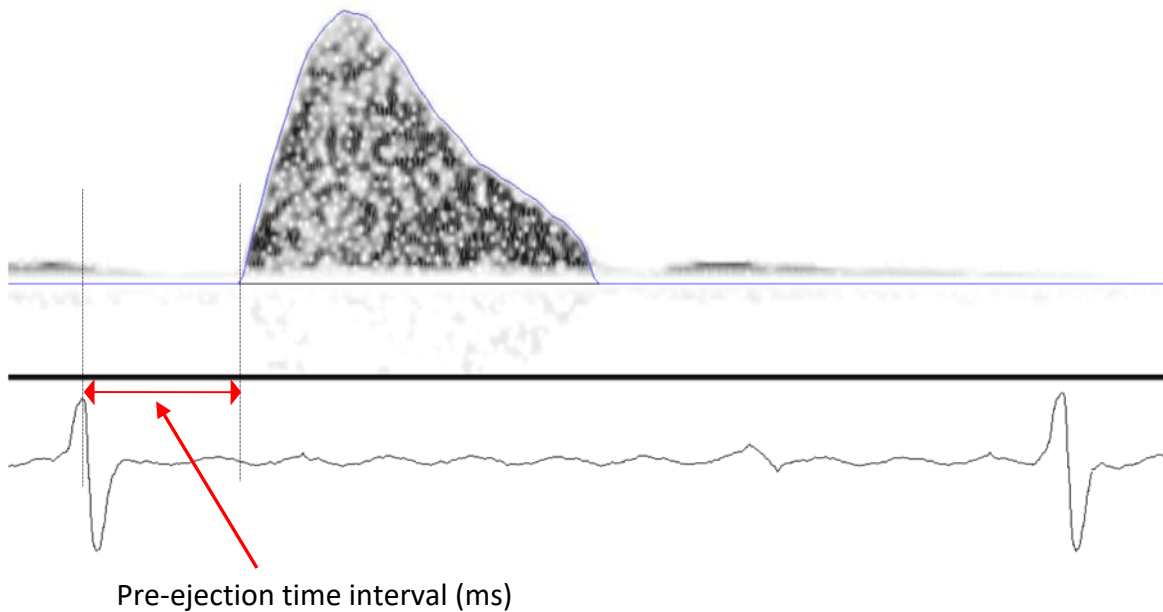
Algorithm:

- If t_{abtr1}, t_{abtr2},....., t_{abtrn}, represent the time points of R-peaks and t_{abts1}, t_{abts2}, ..., t_{abtsn} represents the time points of flow onset abdominal artery then,

$$t_{abti1} = (t_{abts1} - t_{abtr1})$$

Where t_{abti1} is the time interval of 1st flow curve in the segment

- Compute the average of all time intervals.

$$\text{Pre-ejection time\_interval\_abd.arteryflow} = (1/n) \, \Sigma t_{abtin}$$

4**B.a)** **Separation distance (SPD):** The distance from the point where aortic arch flow is measured to point downstream where abdominal arterial flow is measured ($\cong$ 4 cm in mice).

4B.b) **Pulse transit time (PTT):** The difference between the time intervals of aortic arch flow and abdominal arterial flow gives the pulse transit time.

PTT = t_{abti1} - t_{aati1}

t_{abti1} - time interval from R-peak to onset of abdominal artery flow

t_{aati1} - time interval from R-peak to onset of aortic arch flow

4B.c) **Pulse wave velocity (PWV)**: Pulse wave velocity is obtained by dividing the separation distance by pulse transit time.

PWV = SPD/PTT

5A. Peripheral flow velocity signals - Carotid Artery

The carotid arteries supply blood to the head.
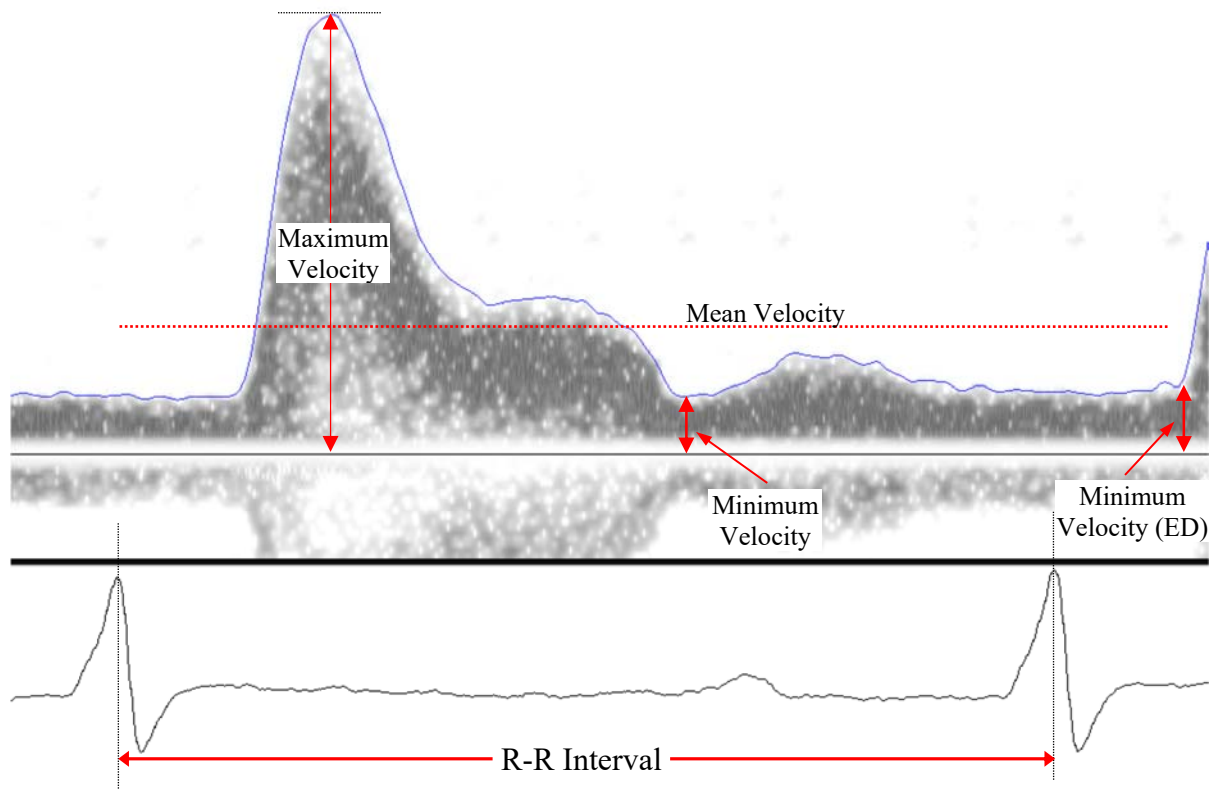
Measurements made on the above signal are:

Heart rate, HR (beats/min) = 60/(R-R interval in sec).

Maximum velocity, V_{max} (cm/sec), (peak systolic blood flow velocity).

Minimum velocity, V_{min} (cm/sec), (lowest diastolic blood flow velocity)

Minimum velocity (ED), V_{minED} (cm/sec), (lowest diastolic blood flow velocity)

Mean velocity, V_{mean} (cm/sec), (time averaged mean blood flow velocity).

Pulsatility Index, PI = $(V_{max} - V_{min})/V_{mean}$.

Resistivity Index, RI = $(V_{max} - V_{minED})/V_{max}$.

5B. Peripheral flow velocity signals -Renal Artery

The renal arteries carry blood to the
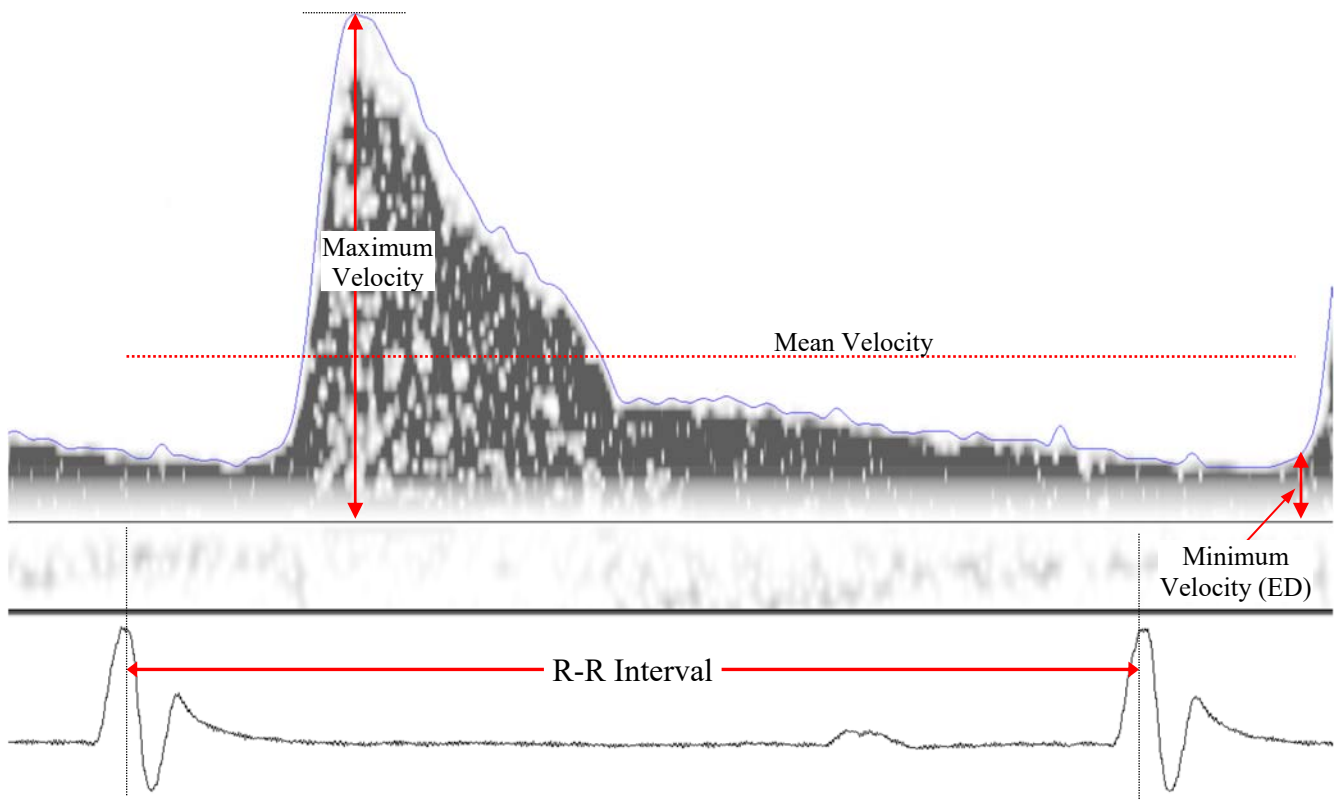
Measurements made on the above signal & typical values are:

1. Heart rate, HR = 60/(R-R interval in sec) = xxxx (beats/min).

2. Maximum velocity, V_{max} (peak systolic blood flow velocity) = xxxx (cm/sec).

3. Minimum velocity, V_{minED} (lowest diastolic blood flow velocity) = xxxx (cm/sec).

4. Mean velocity, V_{mean} (time averaged mean blood flow velocity) = xxxx (cm/sec).

5. Pulsatility Index, PI = $(V_{max} - V_{minED})/V_{mean}$ =.

6. Resistivity Index, RI = $(V_{max} - V_{minED})/V_{max}$ =.

5**C. Peripheral blood flow velocity signals -** Femoral Artery
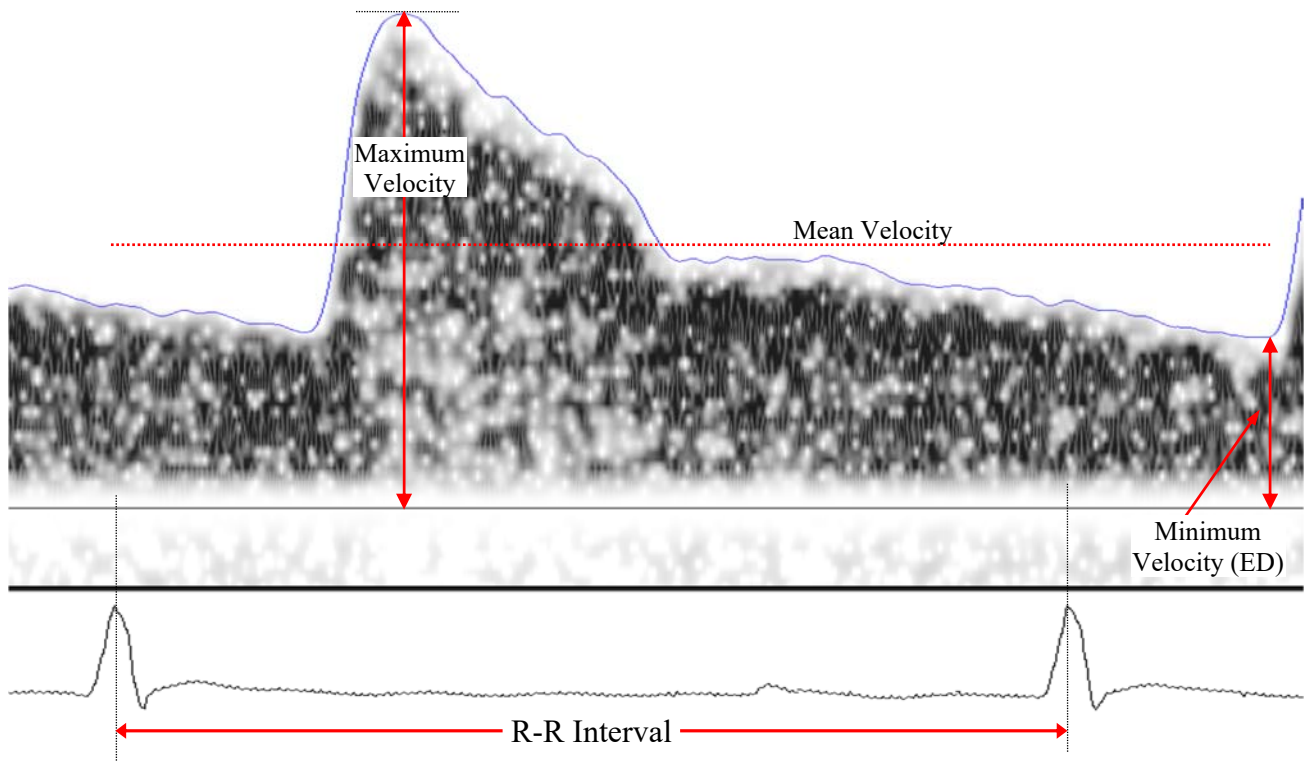
Measurements made on the above signal & typical values are:

1. Heart rate, HR = 60/(R-R interval in sec) = xxxx (beats/min).

2. Maximum velocity, V_{max} (peak systolic blood flow velocity) = xxxx (cm/sec).

3. Minimum velocity, V_{minED} (lowest diastolic blood flow velocity) = xxxx (cm/sec).

4. Mean velocity, V_{mean} (time averaged mean blood flow velocity) = xxxx (cm/sec).

5. Pulsatility Index, PI = $(V_{max} - V_{minED})/V_{mean}$ =.

6. Resistivity Index, RI = $(V_{max} - V_{minED})/V_{max}$ =.

5D. Peripheral blood flow velocity signals - Caudal (tail) Artery
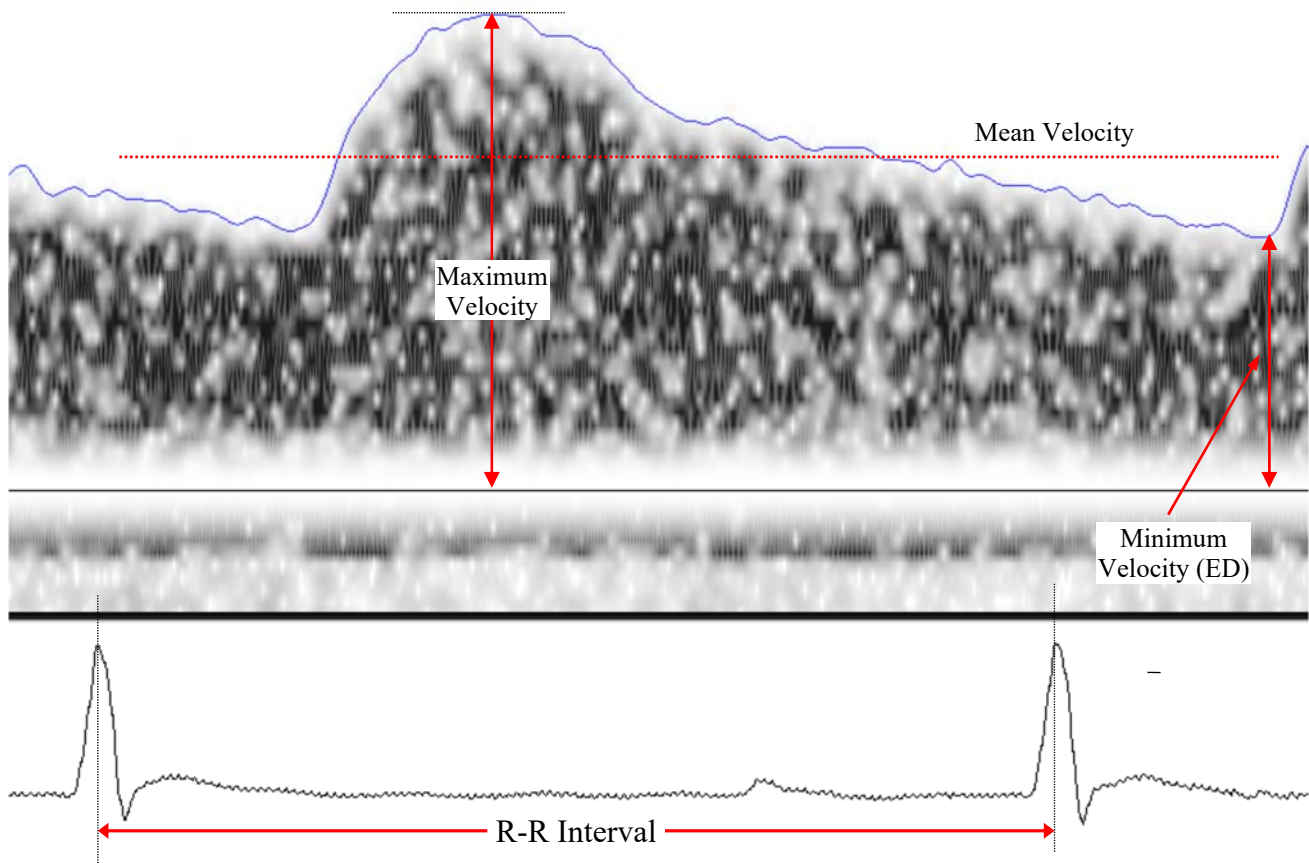
Measurements made on the above signal & typical values are:

1. Heart rate, HR = 60/(R-R interval in sec) = xxxx (beats/min).

2. Maximum velocity, V_{max} (peak systolic blood flow velocity) = xxxx (cm/sec).

3. Minimum velocity, V_{minED} (lowest diastolic blood flow velocity) = xxxx (cm/sec).

4. Mean velocity, V_{mean} (time averaged mean blood flow velocity) = xxxx (cm/sec).

5. Pulsatility Index, PI = $(V_{max} - V_{minED})/V_{mean}$ =.

6. Resistivity Index, RI = $(V_{max} - V_{minED})/V_{max}$ =.

6A. Coronary artery (left main) flow velocity signals

       Coronary blood flow is often normal at rest even in the presence of severe coronary artery disease. Therefore to determine the existence of coronary artery disease, a coronary vasodilator such as adenosine is administered to increase blood flow. The ratio of maximum hyperemic flow to resting baseline flow is used as an index of coronary vascular reserve. In the presence of coronary lesions coronary vascular reserve is reduced because of a reduction in hyperemic flow. Coronary vascular reserve is also reduced by other cardiac pathologies because of an increase in baseline flow.

       The administration of a specific and maximal coronary vasodilator such as adenosine however, is much more difficult and problematic in mice where the veins are more difficult to cannulate and the tolerated doses and volumes are much smaller. Alternatively, one of the most widely used anesthetic agents (isoflurane gas) is also a potent coronary vasodilator when administered at higher concentrations.
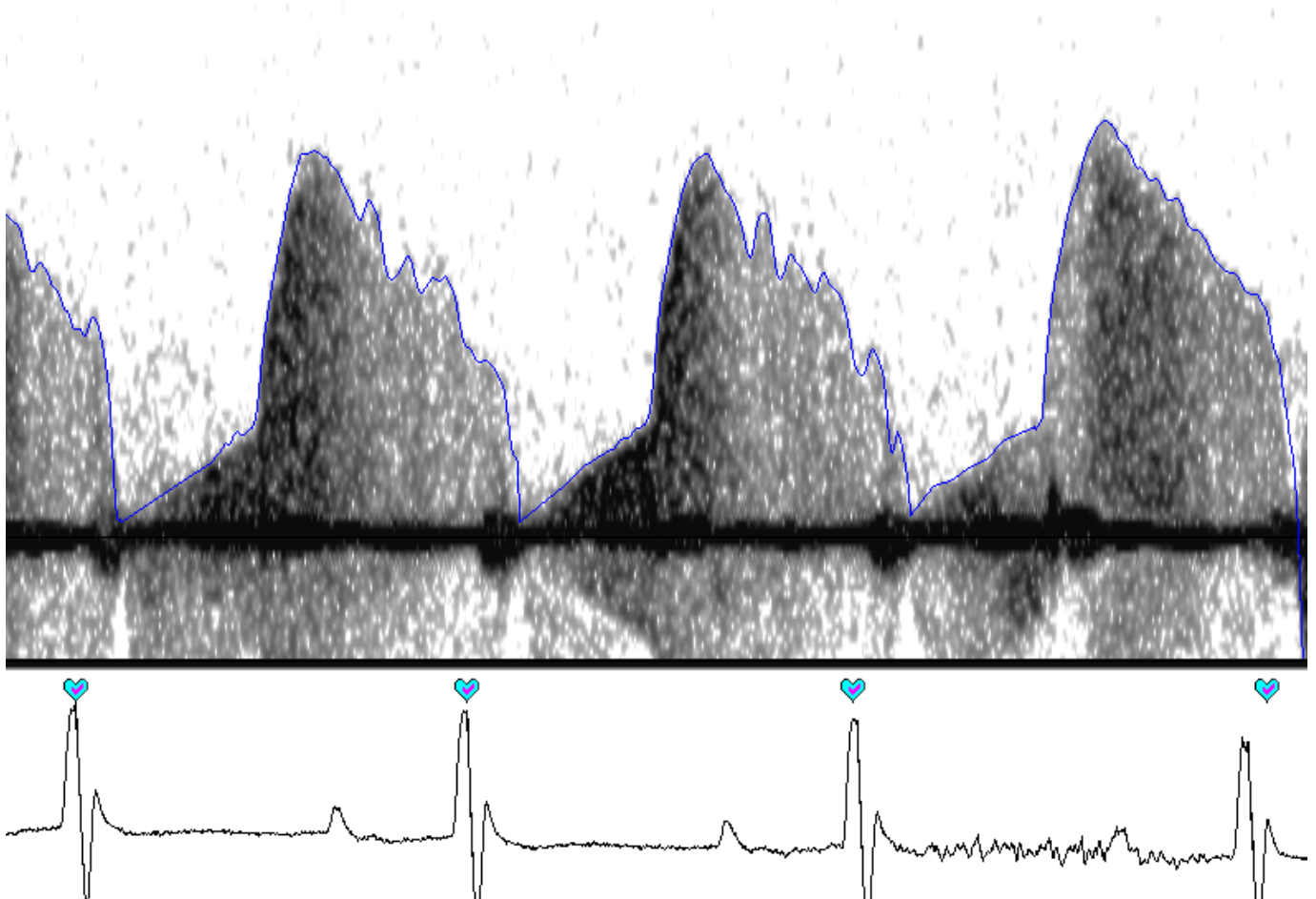
Data Analysis Work Flow

Data analysis in the ultrasound data acquisition software is controlled from the Analysis window (see figure below). The analysis steps are shown at the top portion of this window, and they will always be visible as long as the window is there. This window will directly interact with data structure of the file whose contents are displayed in the main window.

Overview of off-line analysis

There are nine steps that are available for analysis.

1. File Information. This step shows the user the information about the animal (ID, species, gender, age weight, type/strain), file name and directory, comments, data of acquisition and date of analysis. All the information can also be edited (via *Set File info* menu under *File* menu) after acquisition of the signal except the date of acquisition. Additionally, the analyzer's name and comments (see fig.4a) can be made in this window.

2. General Setup. Here the user can identify what kind of data are going to be analyzed and what kinds of parameters are intended to be analyzed (fig. 4b).

3. Filter & FFT. The high pass filter and FFT options are set in this step (fig. 4c).

4. Envelopes. Compute & display the envelope of Doppler spectrogram (fig. 4d).

5. R-Peak Selection. Allows for automatic selection of R-peaks. Can add, move or delete R-peaks manually (fig. 4e).

6. Beat Selection. Perform automatic and/or manual selection of beats (fig. 4f).

7. Markers. Automatic (not yet implemented) & manual placement of markers on the signal that will be used in the calculation of parameters (fig. 4g).

8. Measurements. This step will compute the parameters in accordance with the information provided given from the above steps and display the results in the results window (fig. 4h).

9. Image Selection This step allows the user to capture segments of the processed signal image displayed on the screen (fig. 4i).

Figure 4a

Figure 4b

Figure 4c

Figure 4a

◆ Analysis Control ✕

Control Mode:

Step 1. File Info.
Step 2. General Setup
Step 3. FFT and Filter Control
Step 4. Envelopes Editor
Step 5. R-Peak Editor
Step 6. Beat Editor
Step 7. Marker Editor
Step 8. Measurement Results
Step 9. Image Selection

Session information:

File   : AorticFlowTemplate.udf
File Dir. : C:\IndusWorkFolder\Do
ID   : M452C
Model   : Mouse
Gender   : Male
DOB   : 2009/ 2/20 (yyyy/mm/d
Weight   : 25.0 g
Type   : MHC-TRAF2
   Aortic Pressure & LVP
Date   :
   May 09, 2009 - 01:20:08 (acq)
   April 20, 2016 - 13:11:12 (an)

Analyzer's name:

Anil Reddy

Comments:

An example of
Analysis Control Window

Figure 4b

◆ Analysis Control ✕

Control Mode:

Step 1. File Info.
Step 2. General Setup
Step 3. FFT and Filter Control
Step 4. Envelopes Editor
Step 5. R-Peak Editor
Step 6. Beat Editor
Step 7. Marker Editor
Step 8. Measurement Results
Step 9. Image Selection

Type

Data: | Doppler ▼ |

Signal: | Aortic Outflow ▼ |

Animal: | Mouse ▼ |

Edit Measurement Name

Measurement names: | default ▼ |

Full Name	Abbr...	^
☑ Heart Rate	HR	
☑ R-R Interval	RR	
☑ Pre-ejection ...	PET	
☑ Peak Velocity	PV	
☑ Stroke Distance	SD	
☑ Ejection Time	ET	∨

Clear All   Set All

Figure 4c

◆ Analysis Control ✕

Control Mode:

Step 1. File Info.
Step 2. General Setup
Step 3. FFT and Filter Control
Step 4. Envelopes Editor
Step 5. R-Peak Editor
Step 6. Beat Editor
Step 7. Marker Editor
Step 8. Measurement Results
Step 9. Image Selection

Doppler

High pass filter:

| 400, 2nd ▼ |

FFT window type:

| cosine ▼ |

FFT window samples:

| 512 ▼ |

Time Alignment:

| Past ▼ |

FFT window time:

| 4.10 msec |

Figure 4d

◆ Analysis Control	✕

Control Mode:

| Step 1. File Info. |
| Step 2. General Setup |
| Step 3. FFT and Filter Control |
| **Step 4. Envelopes Editor** |
| Step 5. R-Peak Editor |
| Step 6. Beat Editor |
| Step 7. Marker Editor |
| Step 8. Measurement Results |
| Step 9. Image Selection |

☑ Display envelope plot

Peak

Auto adjust display

Auto Calculate

Fix plot

Figure 4e

◆ Analysis Control	✕

Control Mode:

| Step 1. File Info. |
| Step 2. General Setup |
| Step 3. FFT and Filter Control |
| Step 4. Envelopes Editor |
| **Step 5. R-Peak Editor** |
| Step 6. Beat Editor |
| Step 7. Marker Editor |
| Step 8. Measurement Results |
| Step 9. Image Selection |

☑ Display beat & r-peak markers

RPeak

☐ Invert ECG

Auto Calculate

Editor

R-Peak registered: 18

Undo last action

Figure 4f

◆ Analysis Control	✕

Control Mode:

| Step 1. File Info. |
| Step 2. General Setup |
| Step 3. FFT and Filter Control |
| Step 4. Envelopes Editor |
| Step 5. R-Peak Editor |
| **Step 6. Beat Editor** |
| Step 7. Marker Editor |
| Step 8. Measurement Results |
| Step 9. Image Selection |

☑ Display beat & r-peak markers

Editor

Selected beat(s): 18

Select all beat(s)

Undo last action

Figure 4g

Figure 4h

Figure 4i

Figure 4g

◆ Analysis Control   ✕

Control Mode:

- Step 1. File Info.
- Step 2. General Setup
- Step 3. FFT and Filter Control
- Step 4. Envelopes Editor
- Step 5. R-Peak Editor
- Step 6. Beat Editor
- **Step 7. Marker Editor**
- Step 8. Measurement Results
- Step 9. Image Selection

☑ Display analysis markers

Options

Edit marker names

Marker names : default ▾

Current Marker Selected

Full Name:

Flow velocity start

Type: FVS ▾

☑ Cross hair on mouse click/drag

Figure 4h

◆ Analysis Control   ✕

Control Mode:

- Step 1. File Info.
- Step 2. General Setup
- Step 3. FFT and Filter Control
- Step 4. Envelopes Editor
- Step 5. R-Peak Editor
- Step 6. Beat Editor
- Step 7. Marker Editor
- **Step 8. Measurement Results**
- Step 9. Image Selection

Calculate

● Avg.   ○ Min.   ○ Max.

Listed by: default full name ▾

Name	Avg
Heart Rate	373.82
R-R Interval	160.51
Pre-ejection Time	16.25
Peak Velocity	83.60
Stroke Distance	3.73
Ejection Time	60.38
Rise Time	20.75
Mean Velocity	23.17
Mean Acceleration	4039.32

Copy Results to Clipboard

Figure 4i

◆ Analysis Control   ✕

Control Mode:

- Step 1. File Info.
- Step 2. General Setup
- Step 3. FFT and Filter Control
- Step 4. Envelopes Editor
- Step 5. R-Peak Editor
- Step 6. Beat Editor
- Step 7. Marker Editor
- Step 8. Measurement Results
- **Step 9. Image Selection**

Number of image captured: ____

Capture   Recap.   Delete

Prev.   ____   Next

Bound in msec

Start at: 99

Length: 715

☑ Invert

Include to image

☑ Spect.   ☑ Ecg   ☐ Mmode

Parameters

1. **ECG accompanying flow velocity signals:**

    - R-R interval (ms)
    - Heart rate (beats/min)

2. **Aortic flow velocity signal:**

    - Pre-ejection time (ms)
    - Mean velocity (cm/s)
    - Ejection time (ms)
    - Peak acceleration (cm/s^2)
    - Time to peak (ms)
    - Mean acceleration (cm/s^2)
    - Peak velocity (cm/s)
    - Stroke distance (cm)

3. **Mitral flow velocity signal:** ***Early (E) filling signal:***

    - E-peak velocity (cm/s)
    - Stroke distance of E (cm)
    - E-duration (ms)
    - Acceleration time of E (ms)
    - E-deceleration time (ms)
    - E-peak to ½ E-Peak time (ms)
    - E-linear deceleration time (ms)
    - E-Linear deceleration rate (cm/s^2)

    Atrial (A) filling signal:

    - A-peak velocity (cm/s)
    - Stroke distance of A (cm)
    - A-duration (ms)

    E-A Relations:

    - E/A peak velocity ratio
    - Total (E-wave+A-wave) area (cm)
    - A area/Total area
    - Peak E/Total area

    Outflow-Inflow (Aortic-Mitral) Relations:

    - Isovolumic Relaxation time, IVRT (ms)
    - Isovolumic Contraction time, IVCT (ms)

4. **Pulse wave velocity:** ***Thoracic & abdominal aorta flow velocity signals:***

    - Separation distance between the 2 signal sampling locations (cm).
    - Pre-ejection times from the flow velocity signal (ms).
    - Calculate PWV (cm/s) = separation distance (cm)/pulse transit time (s).

5. Peripheral flow velocity signals:

- Peak flow velocity (cm/s)
- Stroke distance (cm)
- Minimum flow velocity (cm/s)
- Mean velocity (ms)
- Pulsatility Index
- Resistivity Index

6. Coronary flow velocity: *Left main coronary flow velocity signal:*

- Peak diastolic velocity (cm/s)
- Peak systolic velocity (cm/s)
- Area under diastolic wave (cm)
- Area under systolic wave (cm)
- Peak dias/sys velocity ratio
- Peak dias/sys area ratio
- Coronary flow reserve = Baseline peak dias/Hyperemic peak dias velocity

ECG Beats

Detection (💚) & Selection (❤️) of R-peaks of ECG that accompanies each flow velocity signal
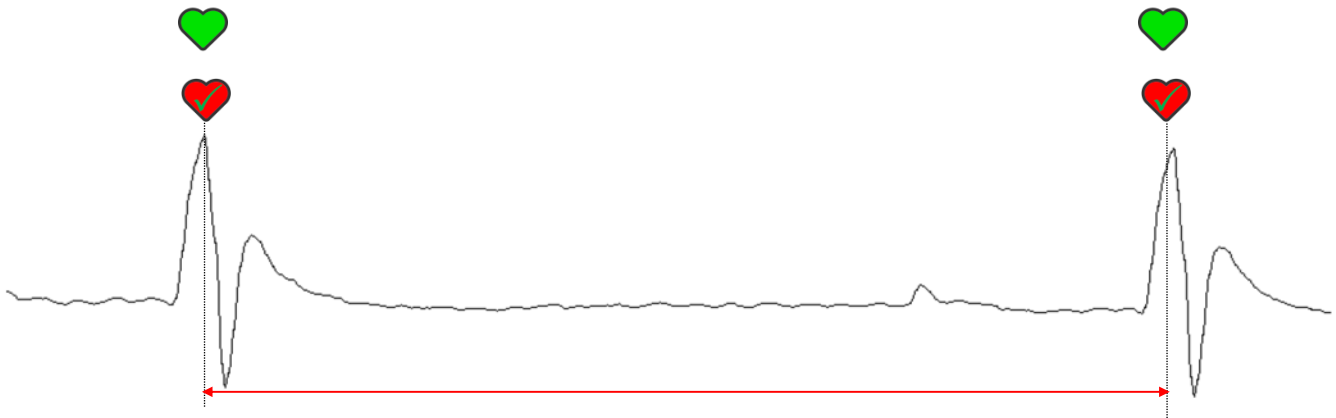
Detection of ECG R-peaks is done before any analysis markers are placed (because some of the markers may not give values without the detection and selection of R-peaks). When the Auto Calculate button, R-peaks are automatically detected and green heart markers appear at each R-peak. When the Select all Beats is button is pressed the green hearts turn red with a green check mark inside. This calculate the R-R intervals, averages them and calculates a heart rate.

The detection of the R-peaks along with placement of markers in the Doppler window is required to determine some of the timing parameters and some of velocity, acceleration, deceleration, and area under the curve parameters.

Beats and Markers

Markers for Aortic Outflow Velocity Parameters
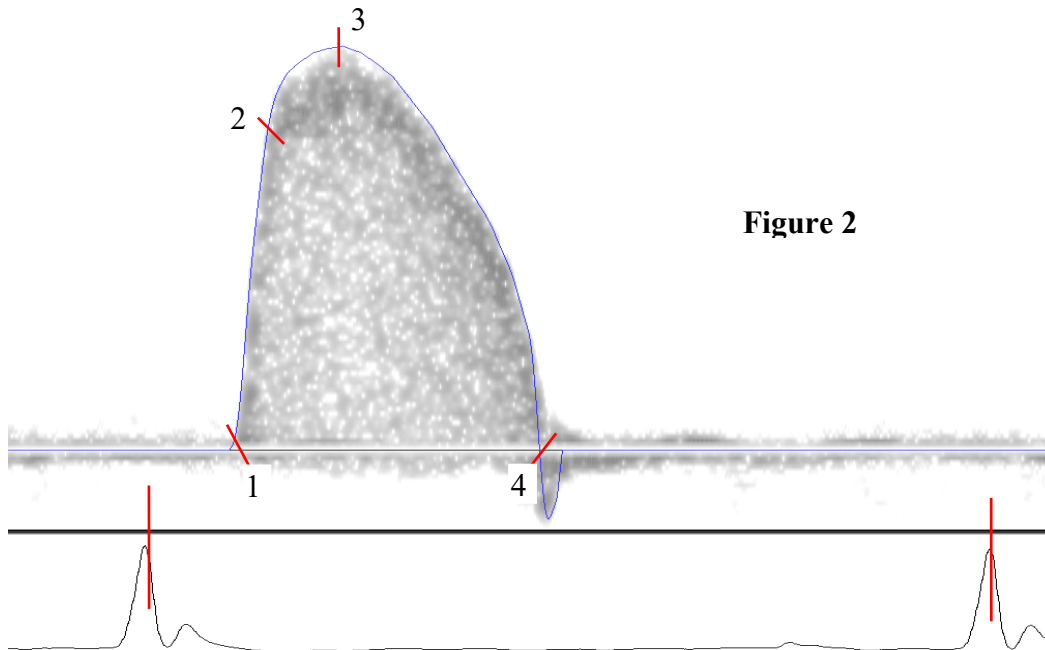
Figure 2

1. **FVS** <u>Flow Velocity Start</u>: (FVS) This represents the start of the pumping of the left ventricle. The velocity signal of aortic flow starts with zero velocity. The delay in the FVS onset with respect to time may indicate problems with the electrical conduction system of the heart. This marker can be used to mark the start of other flow velocity signals except mitral signal.

2. **LAE** <u>Linear Acceleration End</u>: (LAE) This marker represents the end (or slowing down) of the aortic flow velocity signal, that is, it marks the end of linear acceleration of the aortic signal. A low peak velocity of the outflow could cause problems in measuring LAE point.

3. **PFV** <u>Peak Flow Velocity</u>: (PFV) This marker represents the maximum velocity of the aortic flow signal. Delays in the occurrence of peak aortic velocity could be caused by left ventricular infarction. This marker can be used to find the peak velocity of other flow velocity signals except mitral signal.

4. **FVE** <u>Flow Velocity End</u>: (FVE) This represents the end of the aortic flow with the aortic valves closing shut as the pressure in the aorta exceeds the ventricular pressure. This marker can be used to mark the end of velocity of other flow velocity signals except mitral signal.

Markers for Mitral Inflow Velocity Parameters

Figure 3
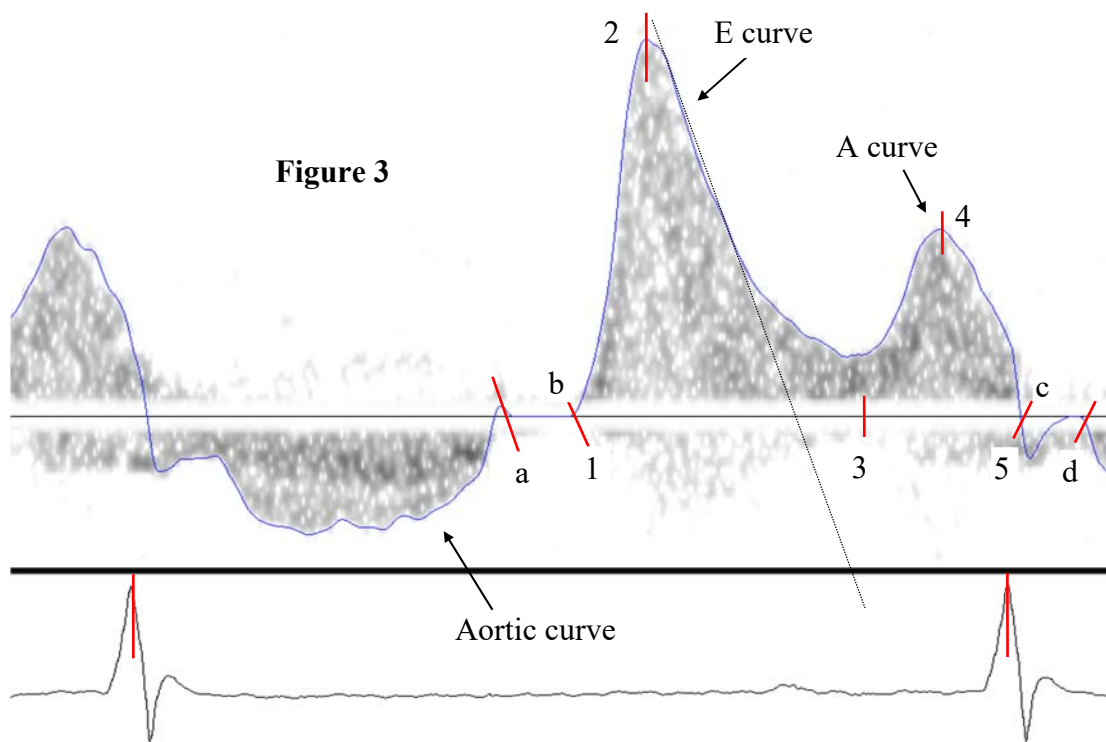
Early (E) Filling Flow Velocity

1(&b). ES (&IVRTE) Early flow velocity Start: (ES & IVRTS)This represents the start of the early filling flow from the left atrium into left ventricle. When the ventricles are relaxing they cause a negative pressure to occur in them thus forcing the mitral valves to open, thus resulting in early (E) mitral flow of blood. The E flow is related to the R peak occurring before it. This time also represents the end of isovolumic relaxation of the left ventricle.

2. EPV Early flow Peak Velocity: (EPV) This represents the point where the early filling occurs at maximum velocity. Decreased EPV may be an indication of impaired relaxation (aging) and increases with augmented relaxation (hyperthyroidism). This is also the point from where (linear) deceleration of the E-flow starts.

3. EEAS Early flow velocity End (& atrial flow velocity start): (EEAS) This represents the end of early filling of the ventricle and start of A flow. Velocity becomes diminished during later part of the E-flow.

Atrial (A) Filling Flow Velocity

3. EEAS Atrial flow velocity Start (& early flow velocity end): (EEAS) This represents the end of E-flow and start of the atrial filling after the occurrence of the P-wave of the ECG. If the heart rate is high

(above 500 beats/min) the E-flow fuses with A-flow curve and makes it difficult to locate this marker.

4. APV <u>Atrial flow Peak Velocity</u>: (APV) This represents the peak velocity of the atrial flow into the ventricle. The high heart rate (above 500 beats/min) may sometimes cause the peak-A to merge with E-flow making it difficult to find peak-A velocity. Also, the peak-A velocity appears to increases as A-flow fuses with E-flow.

5(&c). AE (&IVCTS) <u>Atrial flow velocity End</u>: (AE & IVCTE)This represents the end of the atrial flow and the start of isovolumic contraction of the left ventricle.

a. IVRTS <u>Isovolumic Relaxation Time Start</u>: (IVRTS)The marker **a** represents the starting time of the relaxation of the ventricles after pumping the blood out of the heart. Marker **b** (see marker **1**) represents the end of ventricular relaxation at which time the mitral valves open and blood starts to flow into the left ventricle.

d. IVCTE <u>Isovolumic Contraction Time End</u>: (IVCTE) The marker **c** (see marker **5**) represents the starting time of the contraction of the ventricles before the pumping the blood out of the heart. The marker **d** represent the end of ventricular contraction at which time the aortic valves open and blood ejects into the aorta.

Peripheral flow velocity signals (Carotid arterial flow velocity signal):
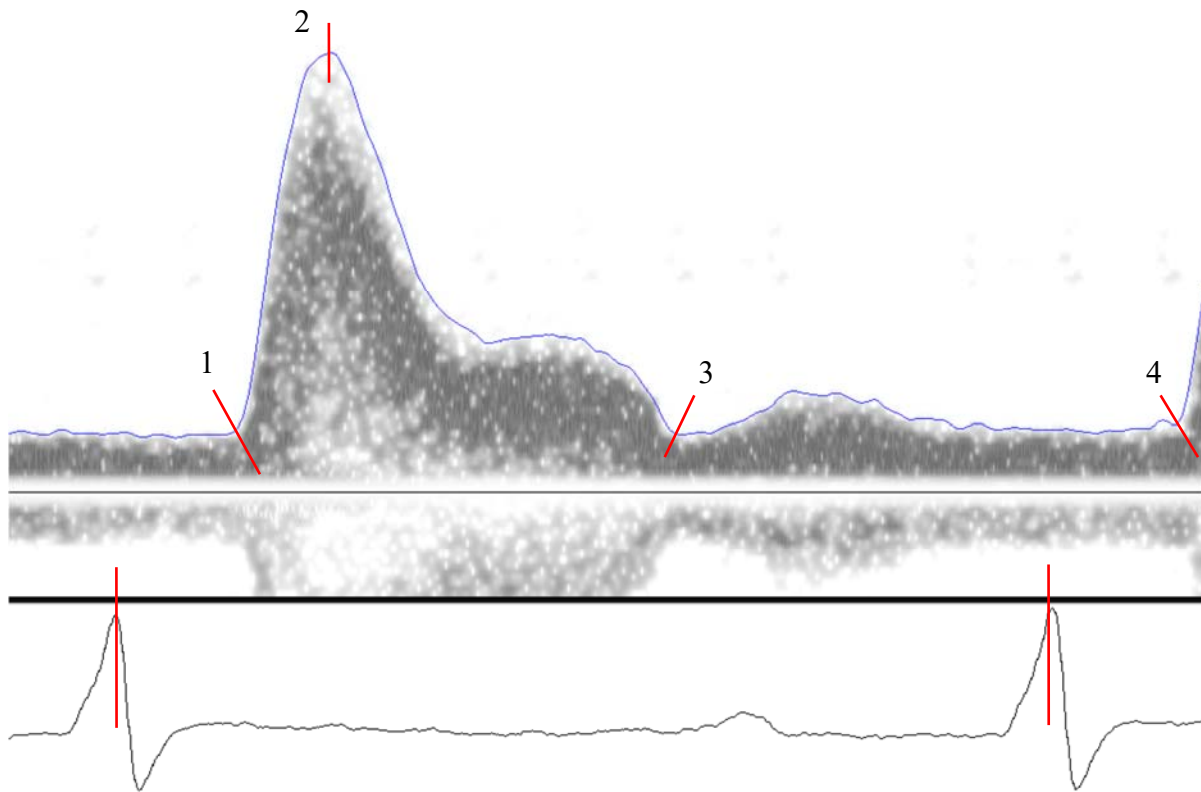
1 (&4). FVS <u>Flow Velocity Start (of peripheral artery):</u> (FVS) This represents the time of start of the peripheral arterial flow velocity signal. This marker re as Start of next cardiac cycle as well End of previous cardiac cycle. This applies only under the Peripheral Flow option.

2. PFV <u>Peak Flow Velocity (maximum peripheral flow velocity):</u> (PFV) This represents the velocity where the peripheral arterial flow velocity is maximum.

3. MFV <u>Minimum Flow Velocity (of peripheral artery):</u> (MFV) This represents the velocity where the peripheral arterial flow velocity is minimum.

4. FVS <u>Flow Velocity End (of peripheral artery):</u> (FVS) **See 1 above**.

Pulse wave velocity (Thoracic aorta flow velocity signal):
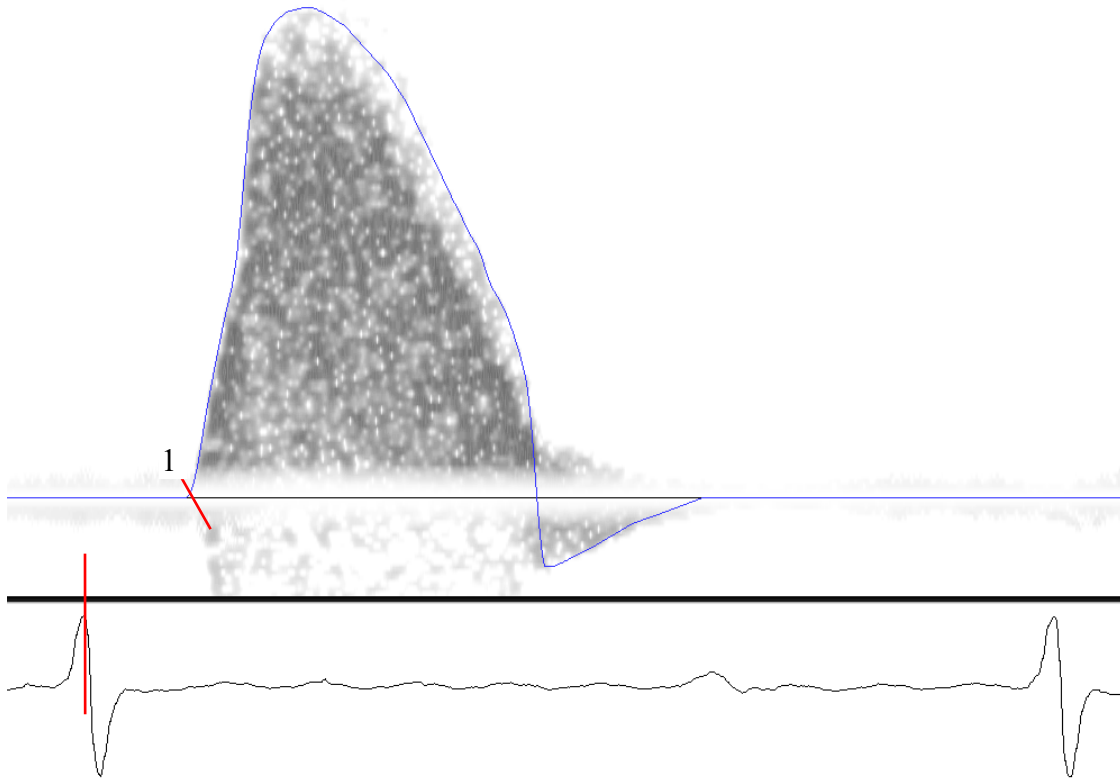
1. FVS Flow Velocity Start (of thoracic aorta): (FVS) This represents the start of the flow velocity pulse at the aortic arch of the thoracic aorta. The velocity signal starts at zero velocity.

Pulse wave velocity (Abdominal aorta flow velocity signal):
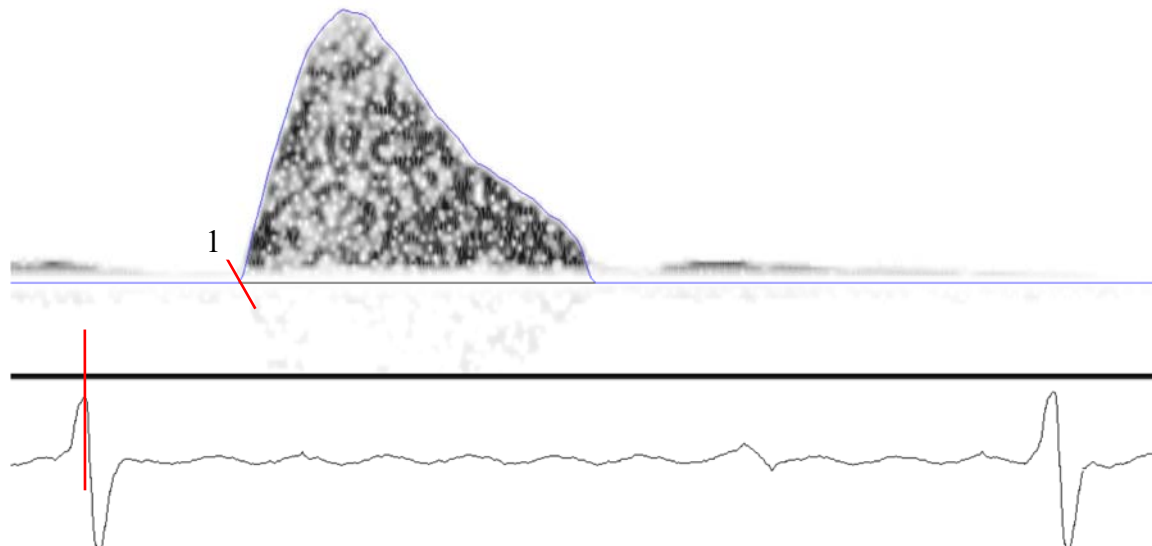
1. FVS Flow Velocity Start (of abdominal aorta): (FVS) This represents the start of the flow velocity pulse at the abdominal aorta. The velocity signal starts at zero velocity.

Marker names and what they represent.

Aortic outflow markers

1. **FVS**   Flow velocity start [outflow linear acceleration start]

2. **LAE**   Linear acceleration end [outflow linear acceleration end]

3. **PFV**   Peak flow velocity [outflow peak velocity]

4. **FVE**   Flow velocity end [outflow end]

Mitral inflow markers

1. **ES** (*IVRTE*)   Early-flow start (also Isovolumic relaxation time end)

2. **EPV**   Early-flow peak velocity

3. **EEAS**   Early-flow end Atrial-flow start

4. **APV**   Atrial-flow peak velocity

5. **AE** (*IVCTS*)   Atrial-flow end (also Isovolumic contraction time start)

6. **IVRTS**   Isovolumic relaxation time start

7. **IVCTE**   Isovolumic contraction time end

Peripheral flow signal markers

1. **FVS**   Start time of peripheral flow signal

2. **PFV**   Peak velocity of a peripheral flow signal

3. **MFV**   Minimum velocity of a peripheral flow signal

4. **FVE**   End time of peripheral flow signal

Pulse-wave velocity signal markers

1. **FVS**   Thoracic aorta-flow start

1. **FVS**   Abdominal aorta-flow start

Formulas for Measurements (parameters) in Terms of the Markers

ECG signal accompanying flow velocity signals:

- R-R interval (ms) = R-Peak2_t - R-Peak1_t

- Heart rate (beats/min) = 60.0/(R-R interval in sec)

1. Aortic flow signal:

- Pre-ejection time (ms) = FVS_t - R-Peak_t

- Ejection time (ms) = FVE_t - FVS_t

- Time to peak (ms) = PFV_t - FVS_t

- Peak velocity (cm/s) = PFV_v

- Stroke distance (cm) = Area (FVS_t to FVE_t)

- Ejection mean velocity (cm/s) = Stroke distance/ (Ejection time in sec)

- Mean velocity (cm/s) = Stroke distance/(R-R interval in sec)

- Peak acceleration (cm/s^2) = (LAE_v-FVS_v)/(LAE_t-FVS_t)

- Mean acceleration (cm/s^2) = Peak velocity/(Time to peak in sec)

R-Peak_t represents the R-peak time before the onset of a given flow velocity curve.

2. Mitral flow signal: *Early (E) filling curve*:

- Peak velocity of E (cm/s) = EPV_v

- Stroke distance of E (cm) = Area (ES_t to EEAS_t)

- Duration of E (ms) = EEAS_t - ES_t

- Acceleration time of E (ms) = EPV_t - ES_t

- Deceleration time of E (ms) = EEAS_t - EPV_t

- E peak to ½ E peak time (ms) = Time (EPV_v to ½* EPV_v)

- Linear deceleration time (ms) = 2 * Time (EPV_v to ½* EPV_v)

- Linear deceleration rate (cm/s^2) = EPV_v/(Linear deceleration time in sec)

Atrial (A) filling curve:

- Peak velocity of A (cm/s) = APV_v

- Stroke distance (cm) = Area (EEAS_t to AE_t)

- Duration of A (ms) = AE_t - EEAS_t

E-A relations:

- E-A peak velocity ratio   = Peak velocity of E/Peak velocity of A

Isovolumic contraction and relaxation times:

- Isovolumic contraction time (ms)   = IVCTE_t - AE_t

- Isovolumic relaxation time (ms)   = ES_t - IVRTS_t

3. Pulse-wave velocity signals

- Pre-ejection time of thoracic aorta flow velocity (ms)   = FVS_t - R-Peak_t

- Pre-ejection time of abdominal aortic flow velocity (ms)   = FVS_t - R-Peak_t

4. Peripheral flow velocity signals

- Maximum flow velocity (cm/s)   = PFV_v

- Minimum flow velocity (cm/s)   = MFV_v [needs new marker]

- Mean flow velocity (cm/s)   = Area (FVS_t to FVE_t)/(R-R interval in sec)

- Pulsatility Index, PI   = (PFV_v - MFV_v)/Mean flow velocity

- Resistivity Index, RI   = (PFV_v-MFV_v)/PFV_v

<u>Analysis Procedures</u>

Analysis Procedure For aortic outflow velocity signal of a mouse and for the same signal with analysis control window (fig. 4a).

1. Open a data file from file menu.

2. Select data type (Doppler or M-mode).

3. If Doppler, select signal type (Aortic, Mitral, Pulse Wave, or Peripheral).

4. Select parameters to be calculated for the chosen signal.

5. Adjust Soft Filter (HPF) & FFT settings as desired.

6. Calculate the envelope. Edit the envelope if necessary. Adjust Gain-Noise-Contrast controls if necessary and re-calculate envelop.

7. Can detect R-peaks automatically & manually edit R-peak positions.

8. Can select the desired R-peaks to choose the R-R time interval immediately following the selected R-peak. Only the beats in the selected R-R intervals will be available for analysis.

9. Depending on the type of signal the necessary markers are placed to enable the parameter calculations.

   The calculated parameters are displayed in the result window. Check for the correctness of parameters displayed in Results window.

10. If parameters not OK, repeat the above steps as necessary.

    If parameters are satisfactory, then send parameters to clipboard for transfer to spreadsheet for statistical analysis.

11. Also, can select report generation (single/dual format).

12. Select the type of report that needs to be generated (graph, text, etc.).

13. Print a hard copy of report or save to a new file (different from data file).

14. Save the data file to the existing file or to a new (name) data file.

    Steps 13-14 are described in detail in Report Generation chapter.

Figure 4a: Analysis of Aortic Outflow Signal
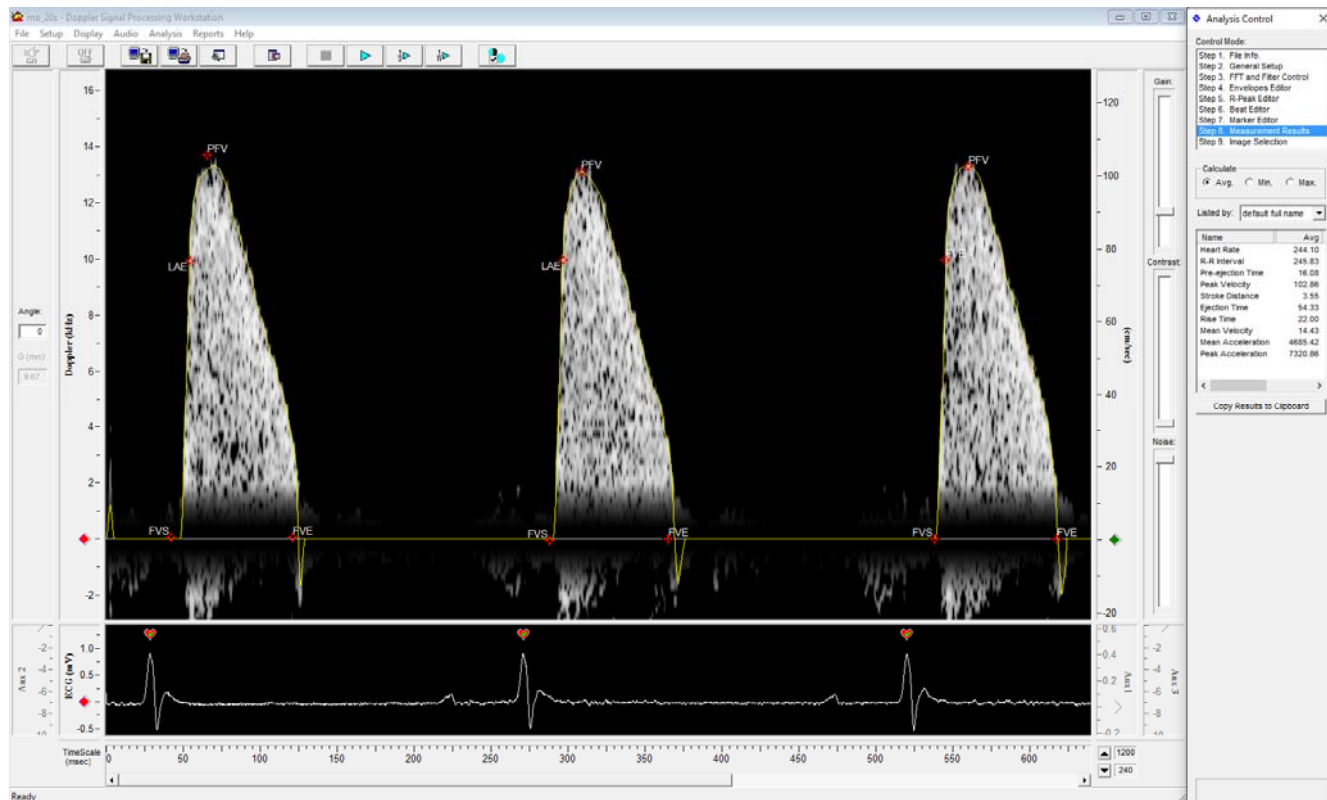
Analysis Procedure For mitral inflow velocity signal of a mouse and (fig. 4b) for the same signal with analysis control window.

1. Open a data file from file menu.

2. Select data type (Doppler or M-mode).

3. If Doppler, select signal type (Aortic, <u>Mitral</u>, Pulse Wave, or Peripheral).

4. Select parameters to be calculated for the chosen signal.

5. Adjust Soft Filter (HPF) & FFT settings as desired.

6. Calculate the envelope. Edit the envelope if necessary. Adjust Gain-Noise-Contrast controls if necessary and re-calculate envelop.

7. Detect R-peaks automatically & manually edit R-peak positions if needed.

8. Select the desired R-peaks to choose the R-R time interval immediately following the selected R-peak. Only the beats in the selected R-R intervals will be available for analysis.

9. Depending on the type of signal the necessary markers are placed to enable the parameter calculations.

10. The calculated parameters are displayed in the result window. Check whether the parameters displayed in Results window have nominal values.

11. If parameters are not nominal, check SD values and repeat the above steps as necessary.

12. If parameters are satisfactory, then send parameters to clipboard for transfer to spreadsheet for statistical analysis.

13. Also, can select report generation (single/dual format).

14. Select the type of report that needs to be generated (graph, text, etc.).

15. Print a hard copy of report or save to a new file (different from data file).

16. Save the data file to the existing file or to a new (name) data file. Steps 13-14 are described in detail in Report Generation chapter.

Figure 4b: Analysis of Mitral Inflow Signal
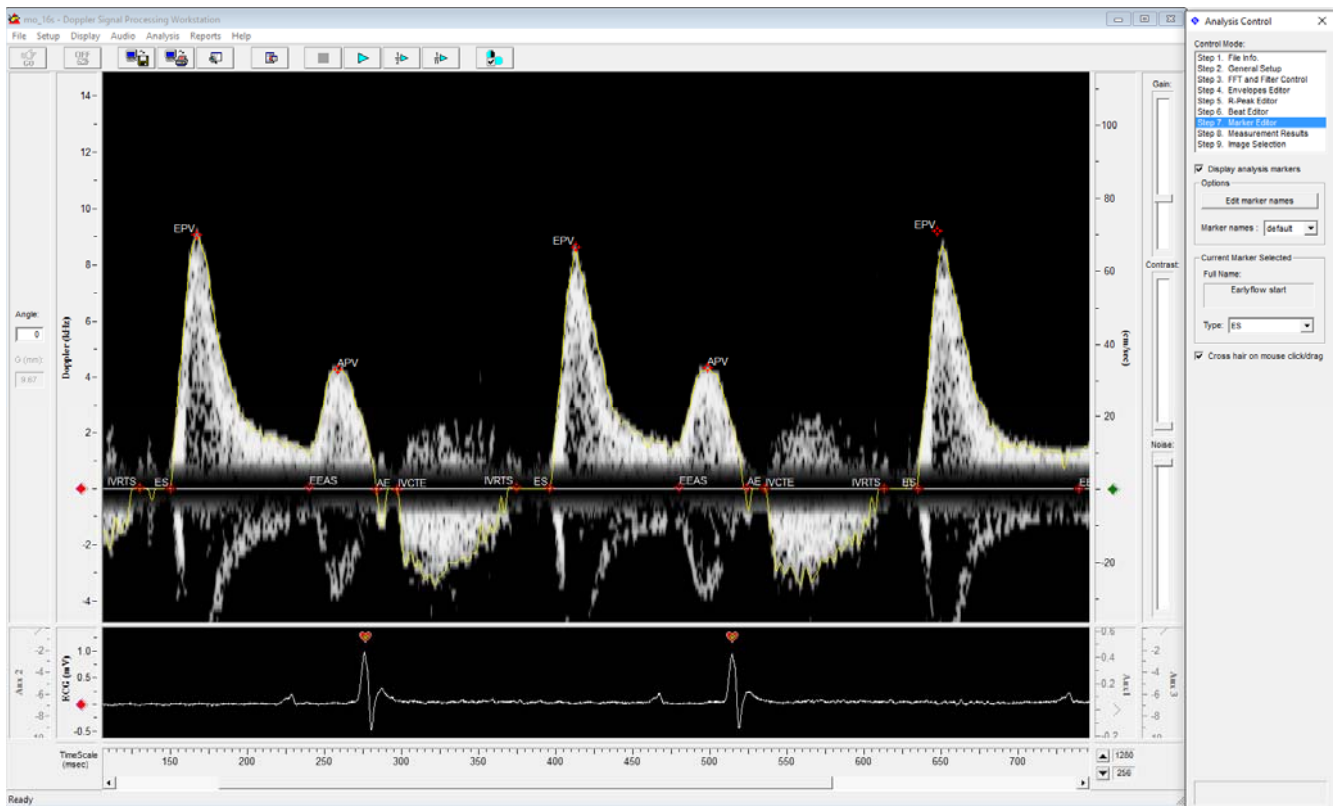
Figures 4b: Analysis of Mitral Inflow signals

Analysis Procedure See fig. 4c for the thoracic aorta velocity signal with analysis control window and the abdominal aorta velocity signal with analysis control window.

1. Open a data file from file menu.

2. Select data type (Doppler or M-mode).

3. If Doppler, select signal type (Aortic, Mitral, _Pulse Wave_, or Peripheral).

4. Select parameters to be calculated for the chosen signal.

5. Adjust Soft Filter (HPF) & FFT settings as desired.

6. Calculate the envelope. Edit the envelope if necessary. Adjust Gain-Noise-Contrast controls if necessary and re-calculate envelop.

7. Detect R-peaks automatically & manually edit R-peak positions if needed.

8. Select the desired R-peaks to choose the R-R time interval immediately following the selected R-peak. Only the beats in the selected R-R intervals will be available for analysis.

9. Depending on the type of signal the necessary markers are placed to enable the parameter calculations.

10. The calculated parameters are displayed in the result window. Check whether the parameters displayed in Results window have nominal values.

11. If parameters are not nominal, check SD values and repeat the above steps as necessary.

12. If parameters are satisfactory, then send parameters to clipboard for transfer to spreadsheet for statistical analysis.

13. Also, can select report generation (single/dual format).

14. Select the type of report that needs to be generated (graph, text, etc.).

15. Print a hard copy of report or save to a new file (different from data file).

16. Save the data file to the existing file or to a new (name) data file. Steps 13-14 are described in detail in Report Generation chapter.

Figure 4c. Analysis of Thoracic (Arch) Aortic & Analysis of Abdominal Aortic Signal
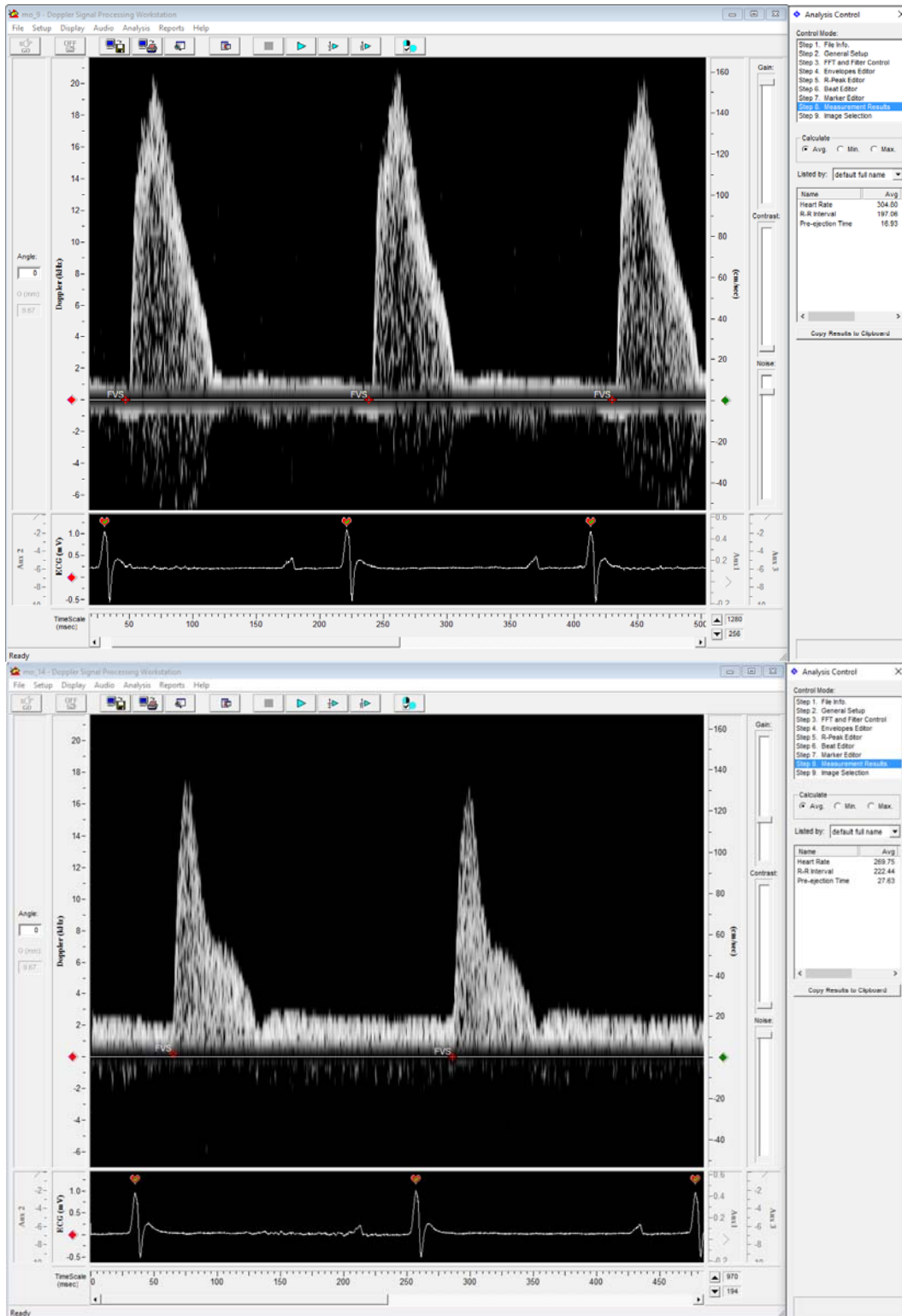
Analysis Procedure For peripheral (carotid) flow velocity signal of a mouse (fig. 4d) with analysis control window.

1. Open a data file from file menu.

2. Select data type (Doppler or M-mode).

3. If Doppler, select signal type (Aortic, Mitral, Pulse Wave, or <u>Peripheral</u>).

4. Select parameters to be calculated for the chosen signal.

5. Adjust Soft Filter (HPF) & FFT settings as desired.

6. Calculate the envelope. Edit the envelope if necessary. Adjust Gain-Noise-Contrast controls if necessary and re-calculate envelop.

7. Detect R-peaks automatically & manually edit R-peak positions if needed.

8. Select the desired R-peaks to choose the R-R time interval immediately following the selected R-peak. Only the beats in the selected R-R intervals will be available for analysis.

9. Depending on the type of signal the necessary markers are placed to enable the parameter calculations.

10. The calculated parameters are displayed in the result window. Check whether the parameters displayed in Results window have nominal values.

11. If parameters are not nominal, check SD values and repeat the above steps as necessary.

12. If parameters are satisfactory, then send parameters to clipboard for transfer to spreadsheet for statistical analysis.

13. Also, can select report generation (single/dual format).

14. Select the type of report that needs to be generated (graph, text, etc.).

15. Print a hard copy of report or save to a new file (different from data file).

16. Save the data file to the existing file or to a new (name) data file. Steps 13-14 are described in detail in Report Generation chapter.

Figure 4d: Analysis of Peripheral (Carotid) Artery Flow Velocity Signal
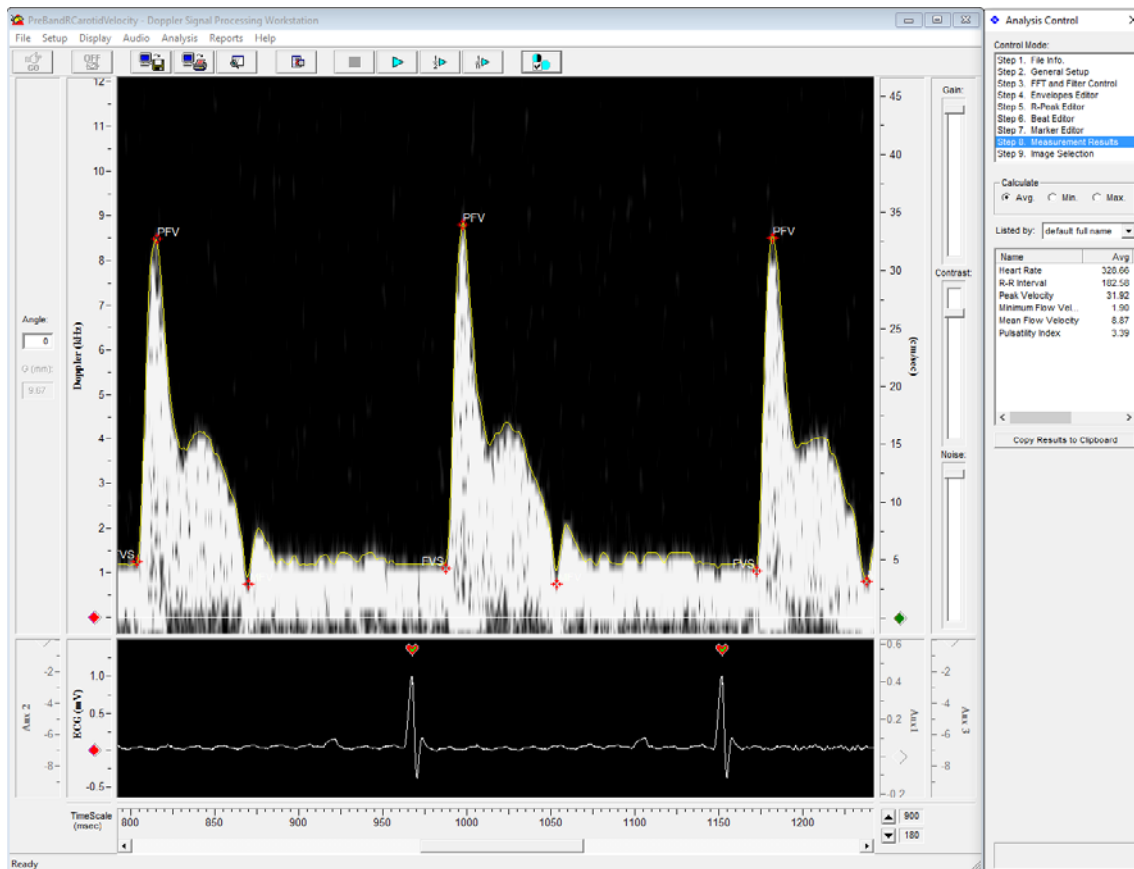
Analysis Procedure For coronary flow velocity signal of a mouse (fig. 4e) with analysis control window.

1. Open a data file from file menu.

2. Select data type (Doppler or M-mode).

3. If Doppler, select signal type (Aortic, Mitral, Pulse Wave, or Peripheral).
    (Here Mitral is selected for Coronary Analysis as specific Coronary analysis case is not available. The mitral markers are used for getting the coronary parameters of peak diastolic coronary flow velocity and area under the coronary diastolic flow velocity curve and diastolic duration).

4. Select parameters to be calculated for the chosen signal (EEAS, APV, & AE are chosen here).

5. Adjust Soft Filter (HPF) & FFT settings as desired.

6. Calculate the envelope. Edit the envelope if necessary. Adjust Gain-Noise-Contrast controls if necessary and re-calculate envelop.

7. Detect R-peaks automatically & manually edit R-peak positions if needed.

8. Select the desired R-peaks to choose the R-R time interval immediately following the selected R-peak. Only the beats in the selected R-R intervals will be available for analysis.

9. Depending on the type of signal the necessary markers are placed to enable the parameter calculations.

10. The calculated parameters are displayed in the result window. Check whether the parameters displayed in Results window have nominal values.

11. If parameters are not nominal, check SD values and repeat the above steps as necessary.

12. If parameters are satisfactory, then send parameters to clipboard for transfer to spreadsheet for statistical analysis.

13. Also, can select report generation (single/dual format).

14. Select the type of report that needs to be generated (graph, text, etc.).

15. Print a hard copy of report or save to a new file (different from data file).

16. Save the data file to the existing file or to a new (name) data file. Steps 13-14 are described in detail in Report Generation chapter.

Figure 4e: Analysis of Coronary Flow Velocity Signal
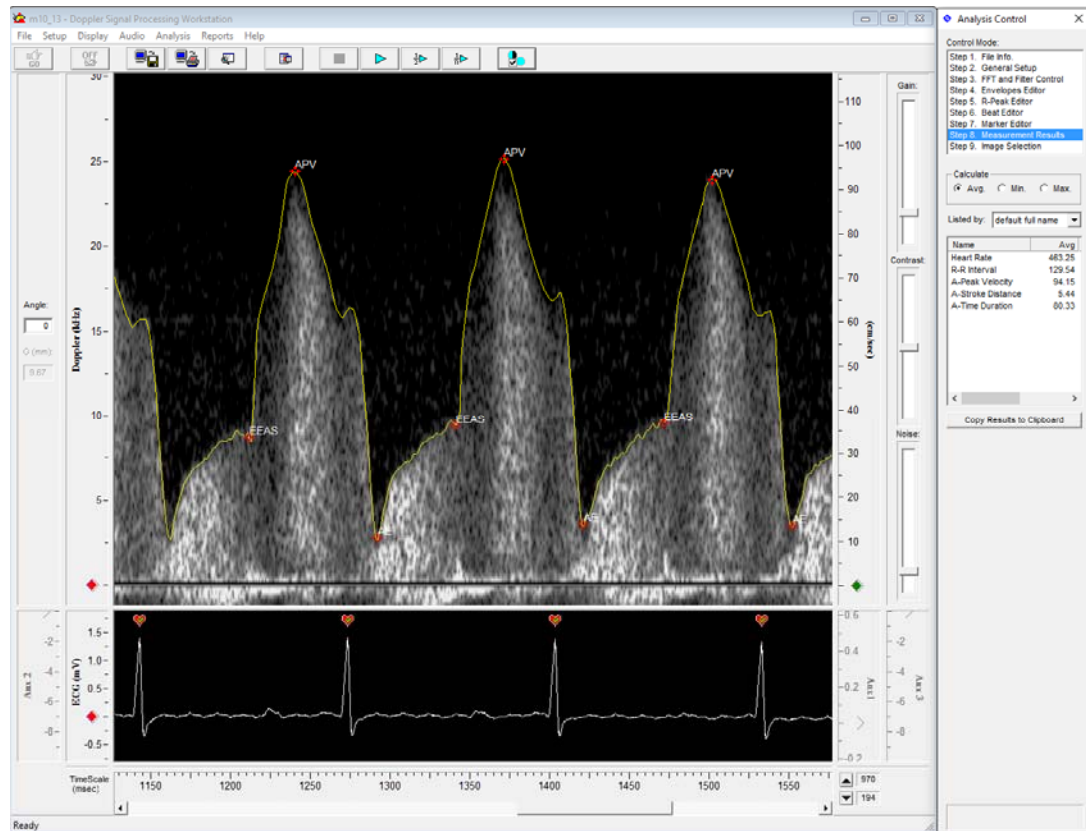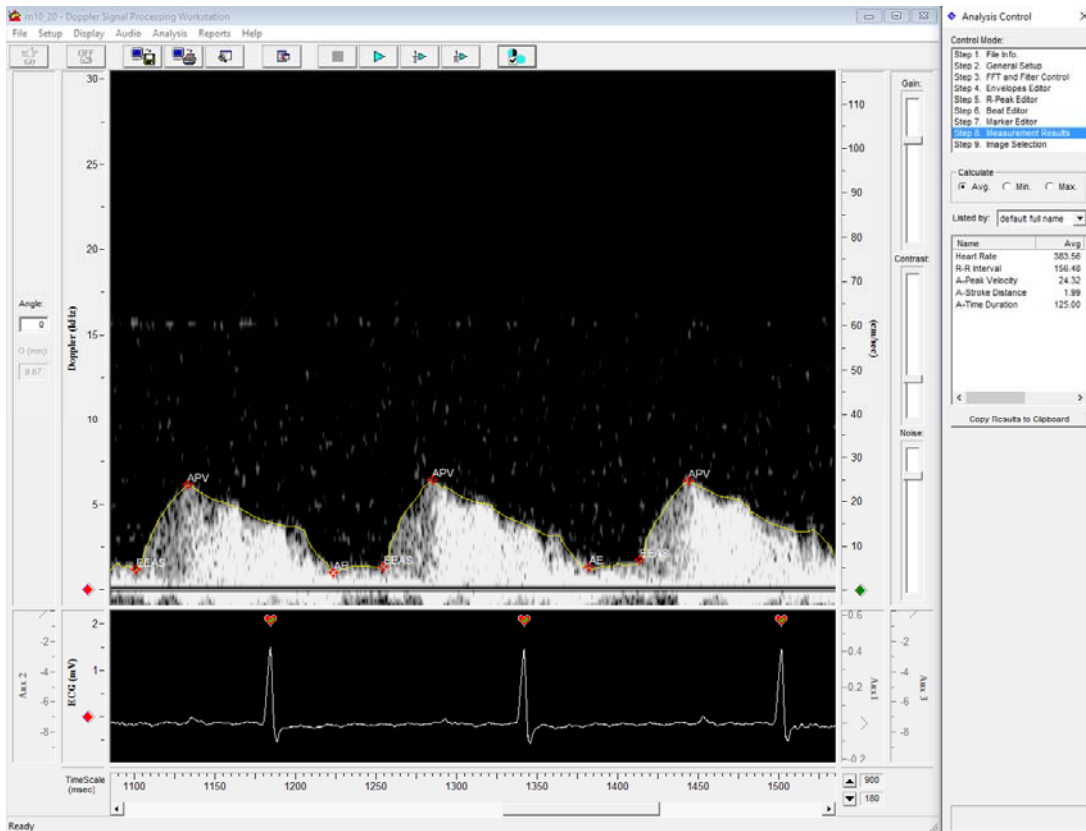
APPLICATIONS AND STUDIES REPORTED

Overview of Applications

1. Cardiac Flow Velocity Measurements

Aortic outflow velocity and Mitral inflow velocity are the two main signals used to study left ventricular systolic and diastolic function, respectively. Measured in ascending aorta or at mitral inlet.

Procedure: The hair on the animal is shaved (or removed by Nair) near the xiphoid and a 10 MHz Doppler probe tip is placed just below the xiphoid and aimed toward the right ear of the mouse. Shown in the figure 1a is the probe orientation for the measurement of aortic outflow signal. A tiny amount of ultrasonic gel is used between the probe tip and the skin surface to obtain a good acoustic coupling. While holding the probe steady with the hand and adjusting the orientation slightly the user can find the aortic outflow signal. As this is being done the user can also adjust the range gate (remotely or with knob on the module) to optimally position the sample volume in the left ventricular outflow tract (LVOT - aortic root/aortic sinus). Typical range for the measurement of aortic outflow from xiphoid is 6-8mm.

Figure 1a. The orientations/positions of Doppler probe on the mouse to get the aortic outflow velocity (left) and mitral inflow velocity (right) signals.

Shown in the figure 1b is a mitral signal (upper part) and an aortic signal (lower part) with a list of all the possible parameters that can be measured. Parameters extracted from mitral flow velocity are used to determine diastolic function and those extracted from aortic flow velocity are used to determine systolic function. Peak aortic velocity is used as an index of cardiac output, or cardiac output can be estimated as [area under aortic curve] x [aortic diameter]. Aortic diameter can

be measured using a high resolution imaging system or estimated using allometric equation (Ascending Aorta Diameter (cm) = $0.41 \times W^{0.36}$; W is body weight in kg, Holt et al. 1981).
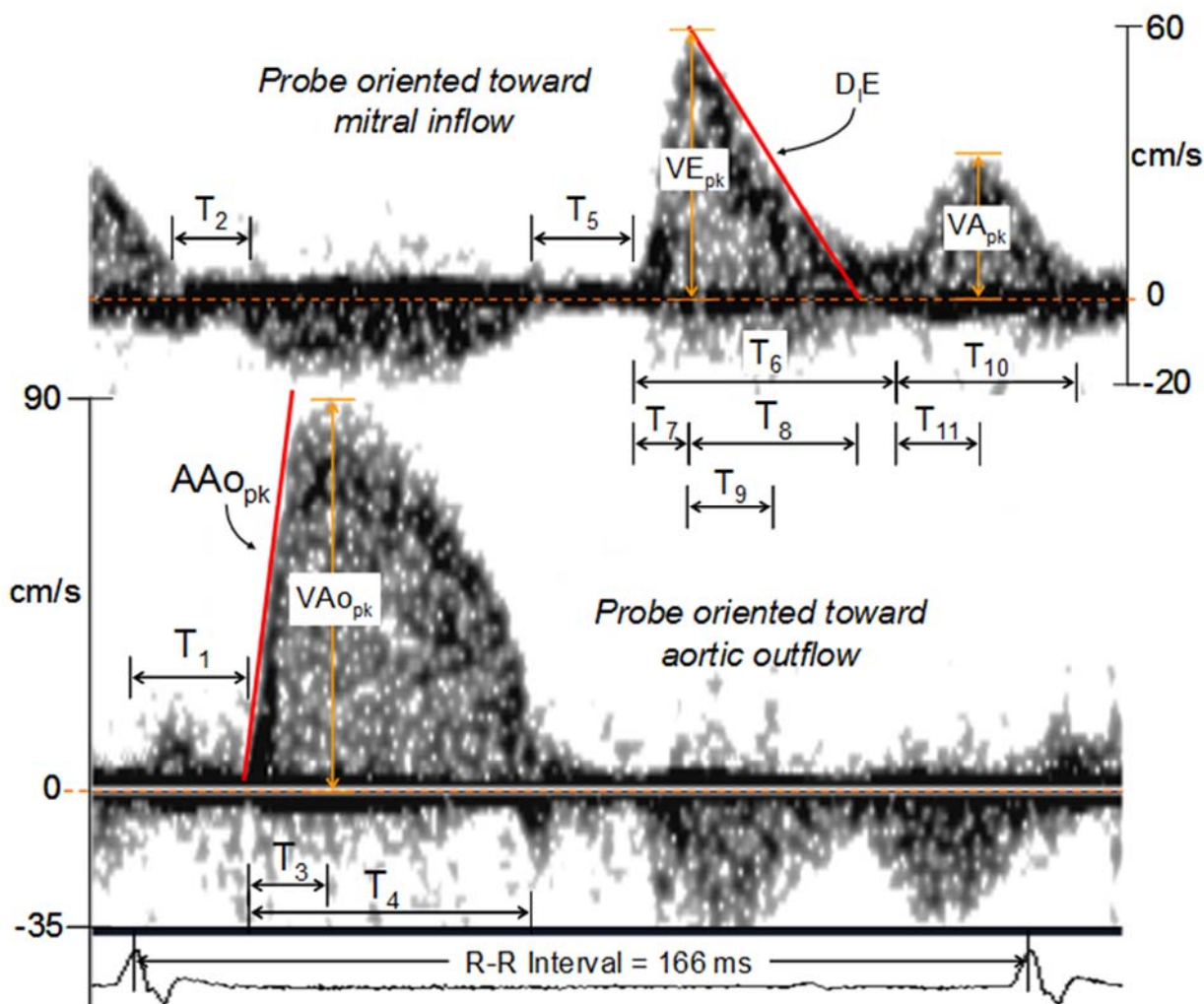
VAo_{pk}	- Peak aortic velocity;	T_4	- Ejection time;
VE_{pk}	- Peak early (E) flow velocity;	T_5	- Isovolumic relaxation time;
VA_{pk}	- Peak atrial flow velocity;	T_6	- Duration of early flow velocity;
AAo_{pk}	- Peak acceleration of aortic velocity;	T_7	- Rise time of early flow velocity;
D_iE	- Linear deceleration of E-flow velocity;	T_8	- E-flow velocity deceleration time;
T_1	- Pre-ejection time;	T_9	- Time from peak-½ peak of D_iE;
T_2	- Isovolumic contraction time;	T_{10}	- Duration of atrial flow velocity;
T_3	- Rise time of aortic velocity;	T_{11}	- Rise time of atria flow velocity;

Figure 1b. The aortic outflow signal and mitral inflow signal with all the parameters that can be extracted and secondary parameters that can be calculated.

2. Pulse Wave Velocity Measurements

Pulse wave velocity (PWV) is defined as the velocity at which the blood pressure/flow/flow velocity pulse that is ejected by the heart travels in the aorta and other vessels. PWV is mostly measured globally as in the aorta (aortic arch to abdominal aorta) but can be measured locally as within the aortic arch, in ascending aorta-to-right carotid, or as in iliac-to-femoral vessels.

Procedure: The hair on the animal is shaved (or removed by Nair) near the base of the left upper limb to measure from the aortic arch and in the lower abdomen (about 4 cm from arch location) to measure from the abdominal aorta (See figure 2a). The flow velocity signals can be measured non-simultaneously with one 20 MHz probe or simultaneously with two 20-MHz probes. To measure the aortic arch velocity signal the 20 MHz Doppler probe tip is placed at the base of the left upper limb, oriented almost parallel to the board surface and aimed toward the upper mid-chest as shown. The abdominal velocity signal is measured with the probe tip placed in the mid lower abdomen and oriented almost vertical. A tiny amount of ultrasonic gel is used between the probe tip and the skin surface to obtain a good acoustic coupling. The probe can be hand-held for non-simultaneous measurement or held with a micropositioner for simultaneous measurement. The range gate can be adjusted (remotely or with knob on the module) to optimally position the sample volume in the respective vessel locations. Typical range for the aortic arch signal is 3-4 mm and abdominal aortic signal is 2-3 mm.

Figure 2a. The orientations/positions of Doppler probe on the mouse to get the aortic arch flow velocity (left) and abdominal aortic flow velocity (right) signals.
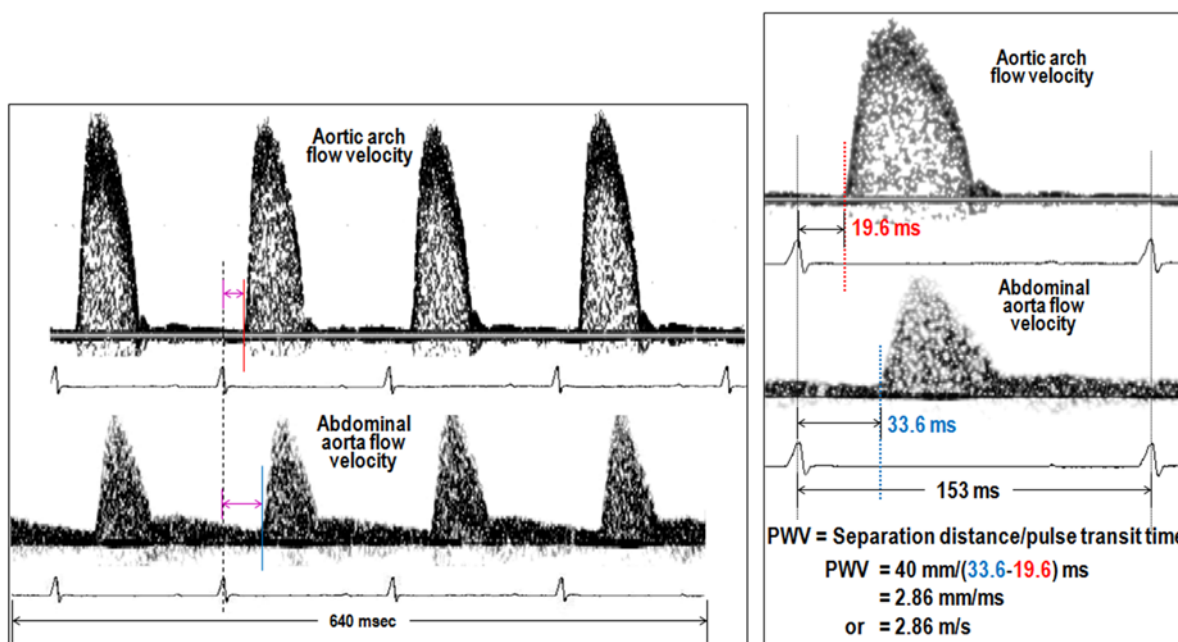
Figure 2b. Aortic arch and abdominal aorta signals with time from the respective R-wave to foot of flow velocity signal (left) and the calculation of PWV from the R-wave based timing. This for non-simultaneous measurement.
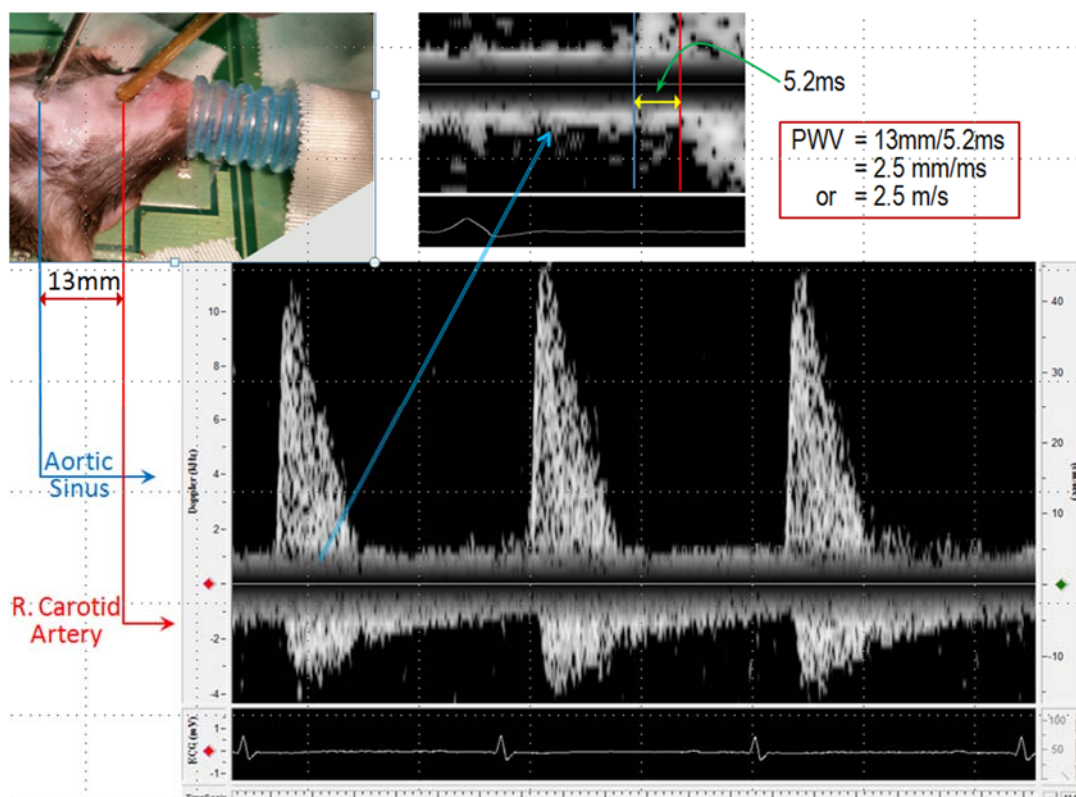
Figure 2c. The combined flow velocity signals from aortic sinus and right carotid artery. Pulse transit time can be calculated as shown without the need for R-wave reference.

3. Transverse Aortic Constriction (TAC) Measurements

Constriction of transverse aorta between the innominate and the left carotid arteries (known as TAC, transverse aortic banding, aortic stenosis) is a common method used to stress/pressure overload the heart. This surgical model of banding the aorta produces cardiac hypertrophy and is used to reveal the phenotypic differences that are masked in genetic mouse models due to compensation. Measurement made in left and right carotid arteries and just distal to the stenosis (stenotic jet velocity).

Procedure: The hair on the animal is shaved (or removed by Nair) on both sides of trachea to measure left and right carotid flow velocity signals and near the base of the left upper limb to measure baseline and stenotic jet velocities from the aortic arch (figure 3a). The flow velocity signals are measured a 20 MHz probe as shown in the figure 3a with the Doppler probe tip on the right side of the trachea to measure right carotid flow velocity and on the left side of the trachea to measure left carotid flow velocity. For aortic arch the Doppler probe is placed at the base of the left upper limb, oriented almost parallel to the board surface and aimed toward the upper mid-chest as shown. A tiny amount of ultrasonic gel is used between the probe tip and the skin surface to obtain a good acoustic coupling. The probe can be held by hand or a micropositioner. The range gate can be adjusted (remotely or with knob on the module) to optimally position the sample volume in the respective vessel locations. Typical range for the aortic arch signal is 3-4 mm and carotid signals is 2-3 mm.
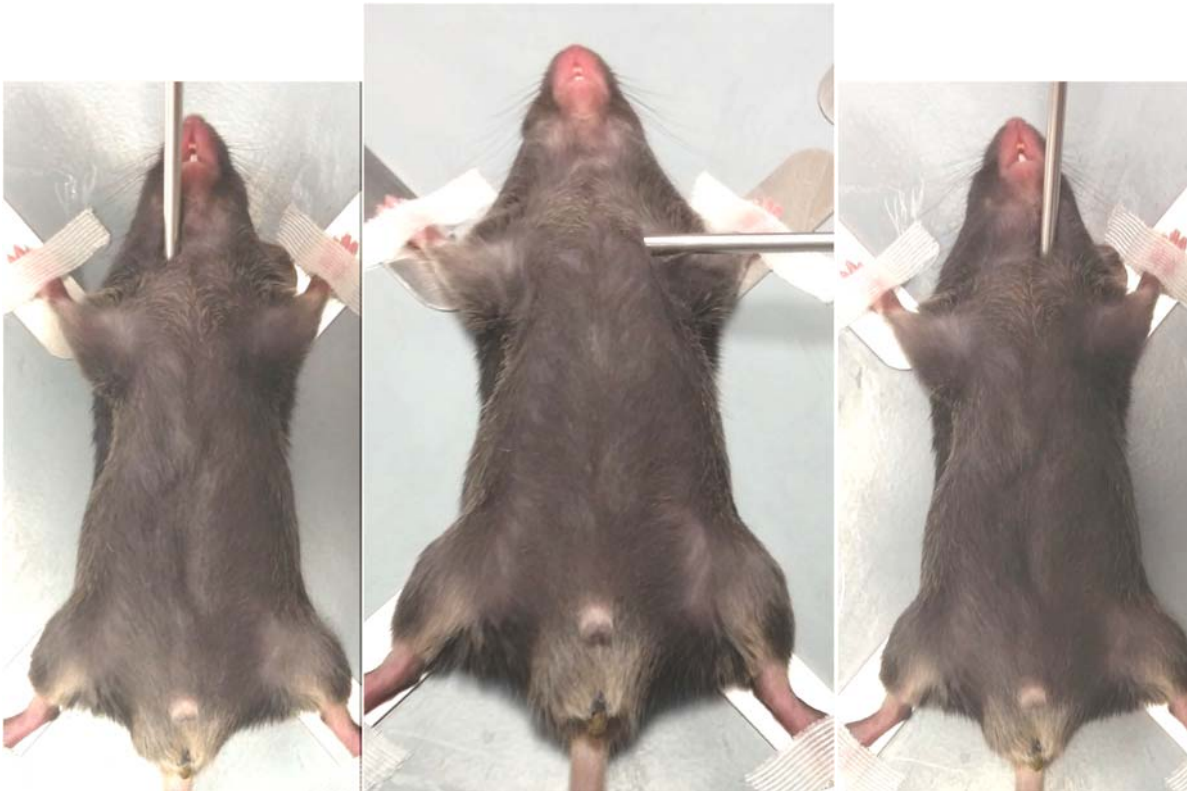
Figure 3a. The orientations/positions of Doppler probe on the mouse to get the right carotid flow velocity (left), aortic arch flow velocity (middle) and left carotid flow velocity (right) signals. Note that probe is oriented at ≈ 45° to flow direction in the carotids.
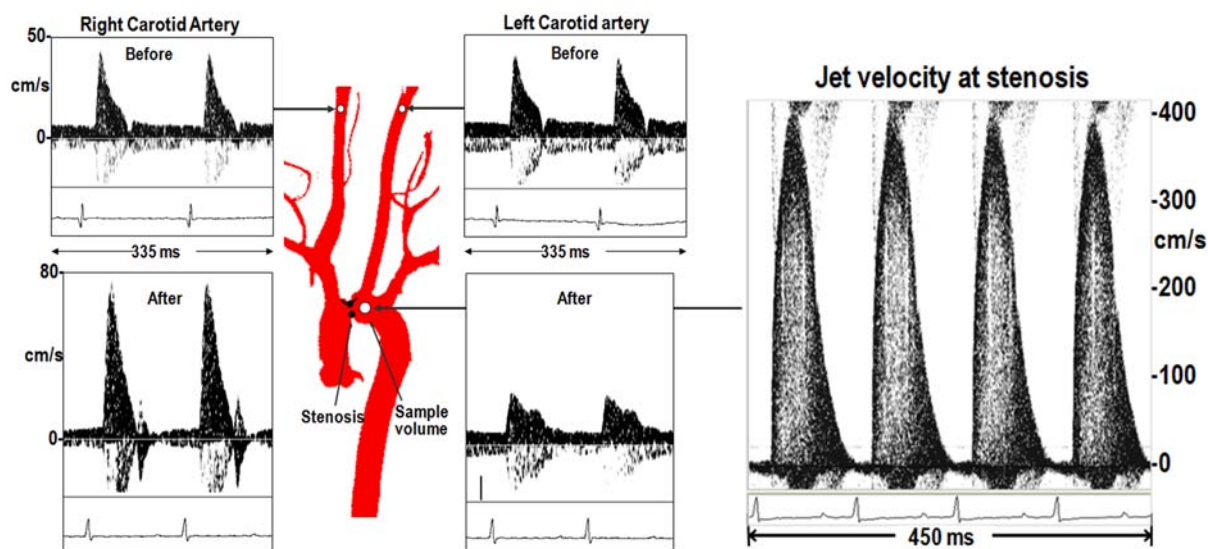
Figure 3b. Right and left carotid artery velocity signals before (left-upper) and after (left-lower) aortic banding in a mouse. The velocity is more pulsatile in right carotid and diminished and continuous in left carotid after banding. The aortic arch flow velocity (right) increased by 4-fold at the stenosis from pre-banding baseline.

4. Coronary Flow Velocity and Coronary Flow Reserve Measurements

Noninvasive coronary flow measurement by ultrasound has been difficult because of the size of the coronary arteries, the depth at which they are located, and their constant motion due to their attachment to the epicardial surface. These measurement however, can be made in mice much more easily than original thought. Baseline coronary blood flow measurement does not provide much information on coronary artery disease and the severity of the disease is estimated using a coronary vasodilator to increase blood flow and then measuring calculating the ratio of maximum flow to baseline flow which is an index of coronary flow reserve.

Procedure: The hair on the animal is shaved (or removed by Nair) at the chest area just below the base of the left upper limb to measure left main coronary flow velocity (figure 4a). The coronary flow velocity signal is measured with a 20 MHz probe as shown with the Doppler probe tip on the chest area between and focused through the 2nd or 3rd intercostal space on the left side of the chest. The Doppler probe is oriented almost parallel to the board surface and aimed toward the upper mid-chest as shown. A tiny amount of ultrasonic gel is used between the probe tip and the skin surface to obtain a good acoustic coupling. Because of the motion of the coronary artery it is suggested that the probe be held with a micropositioner. Once the coronary signal is found the micropositioner can be used to optimize the location of the sample volume in the left main coronary artery. Typical range for the coronary artery signal is 3-4 mm.

Figure 4a. The orientation/position of Doppler probe on the mouse to measure the left main coronary artery flow velocity. The probe is oriented almost parallel to the horizontal surface.
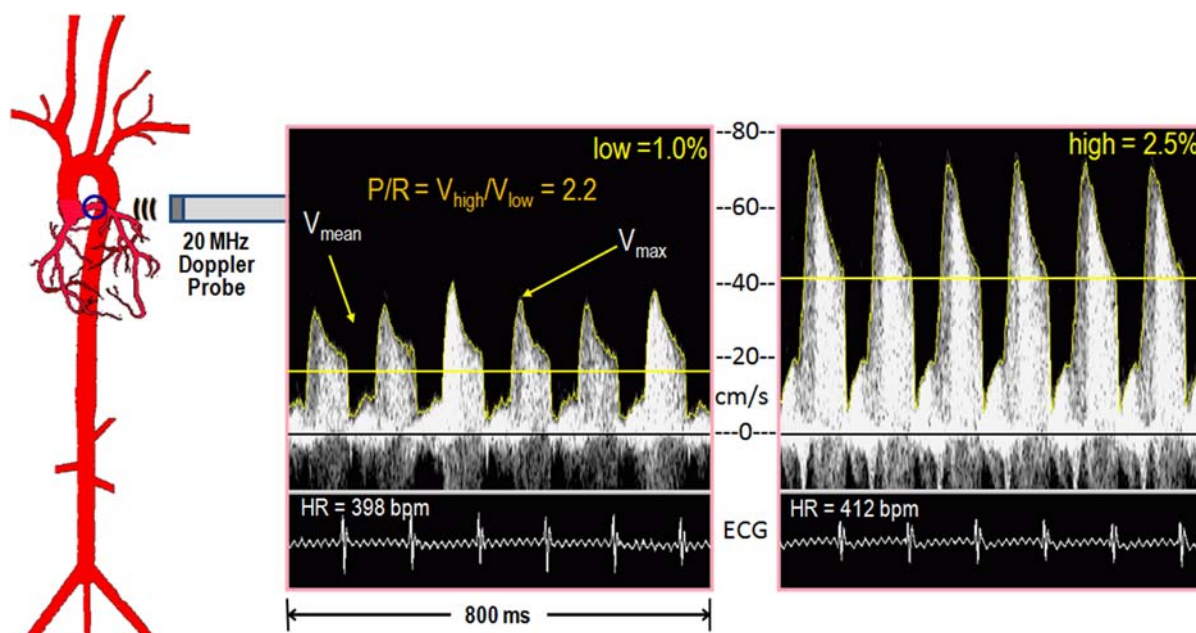
Figure 4b. Coronary artery flow velocity signal at baseline and under hyperemic conditions. The hyperemic flow can be achieved by increasing the level of isoflurane to 2.5% and baseline can be measured after reducing isoflurane level to 1%. Coronary flow velocity reserve is calculated as, CFVR= P/R = V_{high}/V_{low} ≈ 75/34 = 2.2.
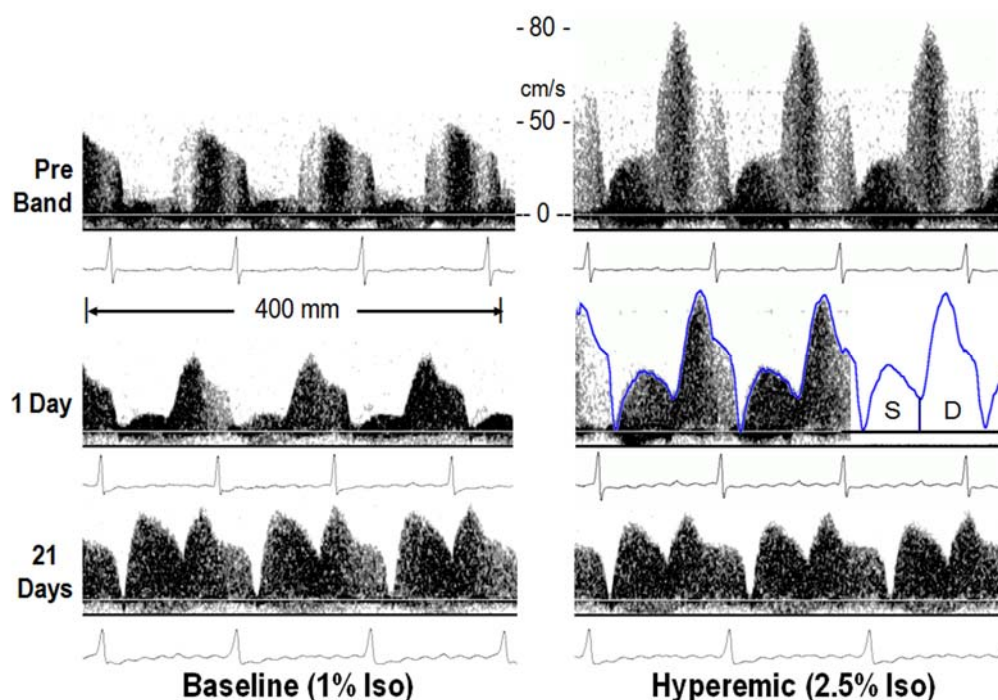
Figure 4c. Coronary artery flow velocity signals before and 1 Day and 21 Days after TAC at low (1%) and high (2.5%) concentrations of isoflurane gas anesthesia. A envelope is shown on the 1 Day hyperemic display showing the systolic (S) and diastolic (D) time-velocity areas used in calculating S/D ratios (Hartley et al. 2008).

5. Peripheral Vessel Flow Velocity Measurements

Noninvasive femoral, iliac, renal flow velocity measurement by ultrasound has been difficult because of the size of the arteries or their anatomical location. Nevertheless these measurements can be made noninvasively transcutaneously by a hand-held Doppler probe in mice with fairly good knowledge of their anatomical location and shape and direction of flow velocity in these vessels. The other option is to measure using an implanted Doppler cuff specifically for vessels of the abdomen such as the ones listed above and others such as portal vein, hepatic artery, celiac artery or even abdominal aorta.

Procedure: For transcutaneous application the hair at the location on the animal is shaved (or removed by Nair) to measure flow velocity signals (example for renal arteries is shown figure in 5a). The left renal artery (LRA) and right renal artery (RRA) flow velocity signals are measured with a 20 MHz Doppler probe tip placed on the abdominal area as shown. The Doppler probe is oriented almost parallel to the board surface. A tiny amount of ultrasonic gel is used between the probe tip and the skin surface to obtain a good acoustic coupling. The renal flows can also be measured with the mouse in the prone position as the renal arteries are closer to the back of the animal. Typical range for the renal artery signals is 2-4 mm. Without flipping the direction of the Doppler probe the renal flow should appear on the opposite sides with the probe tip moved slightly distal/proximal to each and the range adjusted.

Figure 5a. The orientation and position of Doppler probe on the mouse to measure the right renal artery (RRA-1st) and left renal artery (LRA-2nd) in a mouse. Notice that the probe measuring from the RRA is at a higher position than the LRA. Also, the flow in RRA is flowing away from the probe and in LRA is flowing towards the probe. The probe is oriented almost parallel to the horizontal surface.

Procedure for measurements in prone position: The most consistent signals were obtained with the mouse prone and the 20 MHz Doppler probe placed to the right of the spine 5 mm below the last rib and pointed at 90° toward the underlying aorta and 45° to the horizontal. Signals were obtained from the right renal artery at a 2 mm sample volume depth, from the left renal artery across the aorta and slightly caudal at a 4 mm depth, and from the aorta by angling the probe toward the tail (In the mouse the right renal artery is higher than the left renal artery). The peak velocity measured ranges from 50-65 cm/s (this also depends on the measurement angle). The best way to do comparative studies by stabilizing the probe in a holder and measuring the renal signal before and after an intervention. For serial monitoring use the same location and orientation consistently. **Note**: The 3.2 & 3.4 locations could be in the range of 3-4 cm from ear level. The distance between left and right renal arteries in head-tail direction could be within 2-4 mm.

Figure 5b. Left and right renal artery flow velocity signals. Notice that the waveform are in opposite directions. The signals are analyzed as peripheral signals were the area under the curve, the pulsatility index (given as PI=[peakSys-minDias]/meanVel) and the resistivity index (defined as RI= [peakSys-minDias]/minDias).
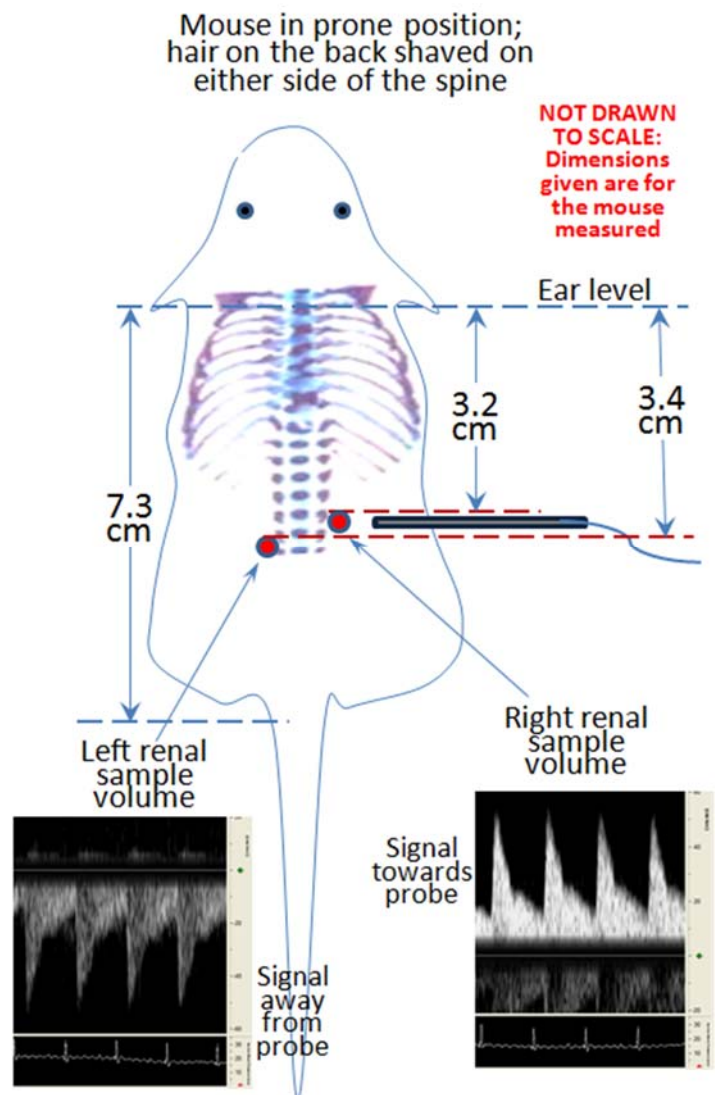
Studies Reported for Each Application

1. Cardiac Flow Velocity Measurements

Applications related to myocardial infarction and left anterior descending (LAD) coronary artery occlusion/reperfusion

One of the most studied area of cardiac function is myocardial infarction caused by permanent occlusion of the coronary or repetitive occlusion and reperfusion to precondition the heart and observe the remodeling characteristics both at the functional level and cellular level.

In studies of permanent occlusion it was shown that peak aortic flow velocity dropped significantly in the first 2 weeks when 2-3 month old mice underwent permanent occlusion of left anterior descending (LAD) coronary artery but AoPV does not decrease further in the following 5-6 months (Michael et al., 1999). Callaerts-Vegh et al., (2003) studied the effects of carvedilol, alprenolol, and ICI-118,551 on cardiac function in mice with permanent occlusion of coronary LAD artery. The cardiac parameters of mitral peak early flow velocity and aortic peak velocity were measured using the Doppler system studies at baseline, first 2 weeks post-occlusion, and 3 weeks after drug treatment. They reported that peak early flow velocity was restored to baseline values when treated with carvedilol, no improvement with ICI-118,551 treatment, and worsened in alprenolol treated. Peak aortic velocity remained same from 2-5 weeks in all groups. This study used Doppler system to demonstrate carvedilol treatment is beneficial in a myocardial damage caused by ischemia in a mice. In a study of cardiac repair in AICAR treated old mice that have undergone using 1-hr LAD occlusion followed by 30-day reperfusion, peak aortic flow velocity, mean acceleration, isovolumic contraction, Isovolumic relaxation, Tei index, and peak early flow velocity as measured by Doppler improved in the AICAR-treated group which had reduced adverse remodeling (Cieslik et al., 2013).

Applications related to aging and myocardial stiffness

In a study of age-associated diastolic dysfunction it was shown that myocardial stiffness increases with age due to increase in matrix metalloproteinase (MMP)-9, an extracellular matrix mediator. In this study peak aortic velocities were measured to determine systolic function and mitral flow velocities were measured to determine diastolic function of the left ventricle in four age groups of wild-type and MMP-9 null mice. The results indicated no changes in aortic peak velocities indicating no changes in systolic function with age. While the mitral early-to-atrial (E/A) flow velocity ratios were reduced in older versus younger WT controls, the E/A ratios remained unchanged in the MMP-9 null mice. This study showed that MMP-9 deletion attenuates the age-related decline in diastolic function (Chiao et al., 2012). Studies of diastolic dysfunction using E/A flow velocity ratios were done in aging mice to examine the role of inflammatory dysregulation in interstitial myocardial fibrosis (Cieslik et al., 2011). Similar studies of diastolic dysfunction were reported in aged mice (Medrano et al. 2015) and in aged MMP-9 null mice (Yabluchanskiy et al., 2014). Diastolic function as measured by E/A flow velocity ratios in the long-lived naked mole-rats was no different between 18–20 year old breeders and non-breeders despite significant differences in estrogen levels. While E/A ratios declined from 1-year to 20-year old female naked mole-rats, they do not exhibit an increased morbidity or mortality with age indicating that these animals may have protective mechanisms from fatal cardiac disease (Grimes et al., 2012).

Applications related to mouse models of heart failure, myocarditis, treatments, and right heart

In mouse models of heart failure, cardiac output estimated using peak aortic flow velocity decreased significantly in caveolin-1 null mice that were exposed to 3 weeks of chronic hypoxia (Cruz et al., 2012). Duerrschmid et al., (2013) showed that Angiotensin-II induces fibroblast maturation from monocytes in the presence of tumor necrosis factor-alpha (TNF) and that mice deficient in both TNF receptor 1 & 2 do not develop cardiac fibrosis in response to Angiotensin-II. Some of the Doppler derived parameters that showed significant differences to support the above observation are early flow linear deceleration time, pre-ejection time, pre-ejection time/ejection time, and Tei index. The virus encephalomyocarditis causes pathogenesis of murine myocarditis which when pretreated with Aprepitant significantly improved heart functions as demonstrated by significantly decreased end systolic diameter and significantly increased peak aortic flow velocity (Robinson et al., 2015). Kelley et al. (2014) used aortic arch flow velocity to estimate cardiac output and pulmonary artery flow velocity to estimate RV cardiac index and pulmonary vascular resistance to study vascular dysfunction and pulmonary hypertension in high-fat diet-induced obesity mouse model.

Applications related to pregnant, embryonic, and newborn mice

The importance of Doppler systems for use in noninvasive cardiac and vascular phenotyping of embryonic and newborn mice was highlighted by Kulandavelu et al., (2006) and pregnant mice by Wong et al., (2002). The utility of the Doppler system in determining the cardiac functional reserve in mice was demonstrated by Vincellete et al., (2006) who reported that despite higher aortic flow velocity and left ventricular contractility, apoE-KO mice had significantly reduced cardiac reserve, as measured by dobutamine stress response, which they suggest could be due to atherosclerosis and endothelial dysfunction that limits blood supply to the heart.

Applications related to transgenic mice with altered cardiac function

Several genetic alterations affect cardiac function. Kelsey et al., (2013) have identified a missense mutation in the KLF3 gene that causes aortic valvular stenosis and embryonic lethality. However, mice that had one mutant copy of KLF3 gene survived into adulthood but had significant cardiac defects that include stenosis of aortic valves, cardiac hypertrophy, and enlarged cardiac chambers. Doppler assessment of cardiac function included peak aortic flow velocity, mitral early flow velocity, isovolumic contraction & relaxation times, ejection time, and Tie index all were significantly altered compared to the wild-type mice which indicates that KLF3 plays an important role in cardiovascular development and function in mice. Another example of genetic alterations affecting cardiac function is the desmin null mouse model which develop cardiomyopathy due to fibrosis, cardiomyocyte death, calcification all leading to heart failure. Weisleder et al., showed that the structural abnormalities that occur in the mitochondria of desmin null mice are the primary cause of cardiomyopathy. They have demonstrated that overexpression of bcl-2 in desmin null heart results in the correction of mitochondrial defects and the related abnormalities leading to significant improvement of cardiac function as evidenced by restoration of peak aortic flow velocity and mean aortic acceleration to normal levels. Reddy et al. (2007) reported that cardiac Doppler indices in growth hormone-releasing hormone receptor null mice (Ghrhr$^{-/-}$; also known as dwarf *Little* mice) revealed significantly diminished systolic and diastolic function when compared to their wild-type littermates at young ages, quite similar to the cardiac function observed in humans with childhood and adulthood onset growth hormone deficiency.

The above are but some of the examples of the usage of the Indus Instruments Doppler system for noninvasive measurement of cardiac function in mice and other small animals. For more details on the system design and applications please refer to Reddy et al. (2005a & 2005b) and Hartley et al. (2000 & 2002, 2011).

References

- Callaerts-Vegh Z, Evans KL, Shipley GL, Davies PJ, Cuba DL, Gurji HA, Giles H, Bond RA. Effects of different beta adrenoceptor ligands in mice with permanent occlusion of the left anterior descending coronary artery. *Br J Pharmacol*, 138:1505-1516, 2003.
- Chiao YA, Ramirez TA, Zamilpa R, Okoronkwo SM, Dai Q, Zhang J, Jin YF, Lindsey ML. Matrix metalloproteinase-9 deletion attenuates myocardial fibrosis and diastolic dysfunction in ageing mice. *Cardiovasc Res*, 96:444-455, 2012.
- Cieslik KA, Taffet GE, Carlson S, Hermosillo J, Trial J, Entman ML.Immune-inflammatory dysregulation modulates the incidence of progressive fibrosis and diastolic stiffness in the aging heart. *J Mol Cell Cardiol*, 50:248-256, 2011.
- Cieslik KA, Taffet GE, Crawford JR, Trial J, Mejia Osuna P, Entman ML.AICAR-dependent AMPK activation improves scar formation in the aged heart in a murine model of reperfused myocardial infarction. *J Mol Cell Cardiol*, 63:26-36, 2013.
- Cruz JA, Bauer EM, Rodriguez AI, Gangopadhyay A, Zeineh NS, Wang Y, Shiva S, Champion HC, Bauer PM. Chronic hypoxia induces right heart failure in caveolin-1-/- mice. *Am J Physiol Heart Circ Physiol*, 302:H2518-H2527, 2012.
- Duerrschmid C, Crawford JR, Reineke E, Taffet GE, Trial J, Entman ML, Haudek SB.TNF receptor 1 signaling is critically involved in mediating angiotensin-II-induced cardiac fibrosis. *J Mol Cell Cardiol*, 57:59-67, 2013.
- Grimes KM, Reddy AK, Lindsey ML, Buffenstein R. And the beat goes on: attenuated cardiovascular aging in the longest-lived rodent, the naked mole-rat. *Am J Physiol Heart Circ Physiol*, 307:H284-H291, 2014.
- Hartley CJ, Reddy AK, Madala S, Martin-McNulty B, Vergona R, Sullivan ME, Halks-Miller M, Taffet GE, Michael LH, Entman ML, Wang Y-X. Hemodynamics changes in apolipoprotein E-knockout mice. *Am J Physiol Heart Circ Physiol*, 279:H2326-H2334, 2000.
- Hartley CJ, Taffet GE, Reddy AK, Entman ML, Michael LH. Noninvasive cardiovascular phenotyping in mice. *Inst Lab Anim Res,* 43:147-158, 2002.
- Hartley CJ, Reddy AK, Madala S, Entman ML, Michael LH, Taffet GE. Doppler velocity measurements from large and small arteries of mice. Review . *Am J Physiol Heart Circ Physiol*, 301: H269-H278, 2011.
- Holt JP, Rhode EA, Holt WW, Kines H.Geometric similarity of aorta, venae cavae, and certain of their branches in mammals. *Am J Physiol*, 241:R100-R104, 1981.
- Kelley EE, Baust J, Bonacci G, Golin-Bisello F, Devlin JE, St Croix CM, Watkins SC, Gor S, Cantu-Medellin N, Weidert ER, Frisbee JC, Gladwin MT, Champion HC, Freeman BA, Khoo NK. Fatty acid nitroalkenes ameliorate glucose intolerance and pulmonary hypertension in high-fat diet-induced obesity. *Cardiovasc Res*, 101:352-363, 2014.
- Kelsey L, Flenniken AM, Qu D, Funnell AP, Pearson R, Zhou YQ, Voronina I, Berberovic Z, Wood G, Newbigging S, Weiss ES, Wong M, Quach I, Yeh SY, Deshwar AR, Scott IC, McKerlie C, Henkelman M, Backx P, Simpson J, Osborne L, Rossant J, Crossley M, Bruneau B, Adamson SL. ENU-induced

mutation in the DNA-binding domain of KLF3 reveals important roles for KLF3 in cardiovascular development and function in mice. *PLoS Genet*, 9:e1003612, 2013.

- Kulandavelu S, Qu D, Sunn N, Mu J, Rennie MY, Whiteley KJ, Walls JR, Bock NA, Sun JC, Covelli A, Sled JG, Adamson SL. Embryonic and neonatal phenotyping of genetically engineered mice. Review article. *ILAR J*, 47:103-117, 2006.
- Medrano G, Hermosillo-Rodriguez J, Pham T, Granillo A, Hartley CJ, Reddy A, Osuna PM, Entman ML, Taffet GE.Left Atrial Volume and Pulmonary Artery Diameter Are Noninvasive Measures of Age-Related Diastolic Dysfunction in Mice. J Gerontol A Biol Sci Med Sci. glv143, [In Press] 2015.
- Michael LH, Ballantyne CM, Zachariah JP, Gould KE, Pocius JS, Taffet GE, Hartley CJ, Pham TT, Daniel SL, Funk E, Entman ML. Myocardial infarction and remodeling in mice: effect of reperfusion. *Am J Physiol Heart Circ Physiol*, 277:H660-H668, 1999.
- Reddy AK, Amador-Noguez D, Darlington GJ, Scholz BA, Michael LH, Hartley CJ, Entman ML, Taffet GE. Cardiac function in young and old *Little* mice. *J Gerontol Biol Sci Med Sci,* 62A:1319-1325, 2007.
- Reddy AK, Jones AD, Martono C, Caro WA, Madala S, Hartley CJ. Pulsed Doppler signal processing for use in mice: Design and evaluation. *IEEE Trans Biomed Eng*, 52:1764-1770, 2005.
- Reddy AK, Taffet GE, Li, Y-H, Lim S-W, Pham TT, Pocius JS, Entman ML, Michael LH, Hartley CJ. Pulsed Doppler signal processing for use in mice: Applications. *IEEE Trans Biomed Eng*, 52:1771-1783, 2005.
- Robinson P, Taffet GE, Engineer N, Khumbatta M, Firozgary B, Reynolds C, Pham T, Bulsara T, Firozgary G. Substance P Receptor Antagonism: A Potential Novel Treatment Option for Viral-Myocarditis. *Biomed Res Int*, 2015:645153, 2015.
- Vincelette J, Martin-McNulty B, Vergona R, Sullivan ME, Wang YX.Reduced cardiac functional reserve in apolipoprotein E knockout mice. *Transl Res*, 148:30-36, 2006.
- Weisleder N, Taffet GE, Capetanaki Y. Bcl-2 overexpression corrects mitochondrial defects and ameliorates inherited desmin null cardiomyopathy, *PNAS*, 101:769-774, 2004.
- Wong AY, Kulandavelu S, Whiteley KJ, Qu D, Langille BL, Adamson SL. Maternal cardiovascular changes during pregnancy and postpartum in mice. *Am J Physiol Heart Circ Physiol*, 282:H918-H925, 2002.
- Yabluchanskiy A, Ma Y, Chiao YA, Lopez EF, Voorhees AP, Toba H, Hall ME, Han HC, Lindsey ML, Jin YF. Cardiac aging is initiated by matrix metalloproteinase-9-mediated endothelial dysfunction. *Am J Physiol Heart Circ Physiol*, 306:H1398-H1407, 2014.

2. Pulse Wave Velocity Measurements

Studies of aortic/arterial/vascular stiffness

Pulse wave velocity (PWV) is used as an indicator of the compliance or stiffness of the vessel segment between the two sites of measurement. Vessel compliance or stiffness can be affected by several factors such as aging, hypertension, atherosclerosis, and several conditions that affect the structure of the vessel wall. PWV in general is not affected by changes in heart rate. However, PWV measured using non-simultaneous method is prone error if transients occurs in the R-R interval.

Several disease or genetic conditions, aging, and drug or other pharmacological interventions affect vessel stiffness. These include - Aging, Gender, Obesity, Diabetes, Atherosclerosis, Hypertension, Oxidative stress, Antioxidant intervention, Nitric oxide deficiency, Angiotensin-II induced hypertension, Endothelial dysfunction, Tissue transglutaminase activity, L-NAME treatment in ArgII KO mice, calcium/calmodulin-dependent kinase II (CaMKII) inhibition in VSMCs, Klotho+/- haploinsufficient mice, Mitochondrial function, Spermidine, Nitrite therapy, Leptin, . All the studies presented below have used the Indus Instruments Mouse Doppler to measure PWV to determine the extent of aortic/arterial stiffness.

Applications related to aortic/arterial stiffness, treatments in oxidative stress, endothelial dysfunction, and transgenic animals

The influence of mitochondrial oxidative stress on aortic stiffness was demonstrated in a mouse model of superoxide dismutase 2 (SOD2+/-). With age these mice had increased collagen I expression, disintegrated elastic lamellae, and increased smooth muscle cell apoptosis all resulting in increased aortic stiffness as measured by PWV when compared to aged-matched wildtype mice (Zhou et al., 2012). In another study it was shown that the antioxidant enzyme superoxide dismutase (SOD) mimetic TEMPOL reversed the age-associated increases in collagen, endothelial dysfunction, and aortic PWV in old rats (Fleenor et al. 2012). Spermidine, an anti-aging process autophagy nutrient, was shown to increase NO bioavailability, reduce oxidative stress, alter structural factors, and enhance autophagy thereby reducing arterial stiffness as measured by PWV (LaRocca et al, 2013). Another study showed that endothelial NOS is uncoupled in mice exposed to cigarette smoke leading to endothelial dysfunction and vascular stiffness and that this process is prevented by deletion of Arg2 (Sikka et al. 2013).

Endothelial dysfunction and arterial stiffening that occurs with age related oxidative stress was shown to be reduced with short-term nitrite therapy as evidenced by lowered PWV in old animals that have undergone nitrite therapy (Sindler et al, 2011). Vendrov et al (2015) demonstrated that inhibition of NOX1/2 NADPH oxidase by genetic deletion of p47phox, in Apoe-/- mice reduces the generation of vascular reactive oxygen species and atherosclerosis at young age. They showed that under hyperlipidemic conditions at old age it is NOX4 and mitochondrial oxidative stress that are mediators of cardiovascular disease. MitoTEMPO treatment in these mice reduced vascular ROS levels and atherosclerosis and improved vascular function by reducing stiffness as measured by PWV. Walker et al. (2015) demonstrated that aortic stiffness can increase oxidative stress and lower NO bioavailability causing endothelial dysfunction in cerebral arteries using the mouse model of elastin heterozygote mice (Eln+/–) and it wild-type (Eln+/+) counterpart. They also showed that incubation of cerebral artery in superoxide scavenger TEMPOL improved endothelial function in cerebral arteries.

Applications related to aortic/arterial stiffness, treatments in atherosclerosis, endothelial dysfunction, and transgenic animals

Chatterjee et al. (2014) demonstrated that inhibition of glycosphingolipid synthesis in the cell membrane prevents atherosclerosis and reduces arterial stiffness as measured by aortic PWV in rabbits and apolipoprotein E null mice. They showed that ApoE null fed with western diet had higher aortic PWV, intima-media thickening, oxidized low-density lipoprotein, Ca2+ deposits, and glucosylceramide and lactosylceramide synthase activity all of which were reduced or prevented with the administration of an inhibitor of glycosphingolipid synthesis, D-threo-1-phenyl-2-decanoylamino-3-morpholino-1-propanol (D-PDMP) in vehicle (5% Tween-80 in PBS). In young low-density lipoprotein receptor-deficient (LDLr null) mice Du et al. (2015) showed that aortic perivascular adipose tissue promotes aortic stiffness and remodeling. LDLr null mice had stiffer aortas (as assessed by aortic PWV) and had higher intrinsic mechanical stiffness due to increased collagen type I and advanced glycation end products. Wang et al. (2005) showed that administration of Fasudil inhibits Rho-kinase and prevents abdominal aortic aneurysm (AAA) caused by Angiotensin II infusion in apolipoprotein E null mice. They report that AAA is associated with an increase in proteolysis and apoptosis. The effects of Angiotensin II and Fasudil administration were measured using aortic PWV.

Applications related to hypertension, leptin, pulse diets, obesity, and diabetes

Dietary changes to control hypertension has been suggested as an alternative to pharmacological treatments that currently unable to sufficiently control blood pressure. Diets that include a significant amount of pulses are being investigated for their possible effects on hypertension apart from obesity and diabetes. Hanson et al. (2014) conducted a study, in which spontaneously hypertensive rats (SHR) were fed pulse based diet for 4 weeks. They found that lentil based diet reduced blood pressure, decreased the aortic media thickness, aorta media:lumen ratio, and lowered cholesterol levels when compared to controls but with no effect on PWV. One of the main roles of leptin is to regulate body weight through control of metabolic rate and satiety, but it also plays a role in maintaining vascular tone. Investigations by Sikka et al. (2010) showed that aortic stiffness assessed by PWV was higher in leptin deficient ob/ob mice which was reversed with leptin treatment. They also reported that WT mice treated with a leptin antagonist had increased aortic stiffness without any change in body weight, thereby demonstrating that leptin plays a key role in maintaining aortic compliance. In another study DeMarco et al. (2015) demonstrated that administration of Spironolactone, a mineralocorticoid receptor agonist, diminished the enhanced activation of vascular mineralocorticoid receptors (which impairs insulin signaling, induces oxidative stress, inflammation, and maladaptive immune responses) and prevented stiffening (assessed using PWV) of the aorta and the femoral arteries in western diet fed obese female mice.

Applications related to nitric oxide, endothelial dysfunction, tissue transglutaminase activity, angiotensin II, arginase II, and calcium/calmodulin-dependent kinase II

The relationship between NO deficiency, Angiotensin II and arterial stiffness was investigated by Fitch et al. (2006) by measuring aortic stiffness using PWV in angiotensin II administered control mice and mice treated with L-NAME, which is a NO synthase (NOS) inhibitor. The mice that received both L-NAME and Angiotensin II had significantly higher collagen and lower elastin in their aortic wall indicating that a significant increase in aortic stiffness. The arterial wall structure and function is regulated by nitric oxide and the tissue transglutaminase catalyzes the cross-linking of matrix proteins to increase aortic stiffness. The role of NO derived by endothelial NO synthase (eNOS) in regulating

transglutaminase function was studied by Jung et al. (2013). Aortic stiffness as measured by PWV increased in the eNOS null mice and confirmed by ex-vivo tensile testing. Pressure-dimension analysis showed that the carotid arteries of the eNOS null were also stiffer.

The enzyme arginase that is expressed in vascular endothelial cells is known to alter NOS-3 activity via the regulation of intracellular L-arginine. Lim et al. (2007) conducted a study to demonstrate that vascular endothelial production is reciprocally regulated by mitochondrial arginase II. They did this using a mouse model of arginase II knockout which had significant reduced aortic stiffness as measured by PWV which was reversed by the administration of L-NAME. Thus they showed that NO production, vascular endothelial function, and vascular stiffness are regulated by mitochondrial arginase II via modulation of NOS-3 activity. In another study Prasad et al. (2015) demonstrated that inhibition of calcium/calmodulin-dependent kinase II in vascular smooth muscle cells results in the protection of aortic wall from angiotensin II related changes in wall structure and function. Aortic stiffness as measured by PWV was unchanged in TG SM-CaMKIIN (hemagglutinin-tagged CaMKIIN transgene) mice.

Aging, nitric oxide, endothelial dysfunction, mitochondrial function

Aging is associated with alterations in extracellular matrix, collagen and elastin, protein cross-linking via advanced glycation end products, all leading to increases in aortic stiffness. Henson et al. (2014) demonstrated that age-related aortic stiffness as measured by PWV is worsened by high-fat diet in older animals and Lin et al. (2016) showed that in mouse model of haplodeficiency of Klotho (KL+/−; an anti-aging gene) high-fat diet not only worsens but also accelerates arterial stiffening as evidenced by increased PWV within 5 weeks. Chen et al. (2015) reported that aortic media in Klotho deficient mice have increased levels of collagen and decreased levels of elastin along with increases in matrix metalloproteinases all indicative of increased arterial stiffness. These mice when treated with with eplerenone (aldosterone receptor blocker) had lower PWV indicating that arterial stiffness was eliminated. This indicates that arterial stiffening in klotho deficient mice perhaps involves aldosterone-mediated upregulation of scleraxis leading to increased collagen-1 and induction of autophagy leading decreased elastin levels (Chen et al., 2015). Cardiovascular aging is associated with endothelial dysfunction and increased arterial stiffness. Soucy et al. (2006) investigated the effects of aging on aortic stiffness and shear stress-induced endothelial nitric oxide (NO) signaling in young and old rats. Arterial stiffness as assessed by PWV, in old rats and in rats treated with *N-nitro-L-arginine methyl ester* was significantly greater versus young rats. They observed similar increases in PWV in eNOS-knockout mice compared to wild-type mice. One of the underlying mechanisms that affect arterial stiffness is mitochondrial function. LaRocca et al. (2014) studied the role mitochondria play in aging arteries and how it affects stiffness. They showed that with age mice had impaired mitochondrial quality control mediators, increased activation of the mitochondrial redox/stress sensor p66shc, higher superoxide production and greater arterial stiffness (as evidenced higher PWV) all of which were reversed when old mice were administered a nutraceutical, trehalose. They conclude that that age-associated mitochondrial stress/dysfunction contributes to aortic stiffening.

The above are but some of the examples of the usage of the Indus Instruments Doppler system for noninvasive measurement of cardiac function in mice and other small animals. For more details on the system design and applications please refer to Reddy et al. (2005a, 2005b, 2009, 2014) and Hartley et al. (2000, 2002, 2010, 2011).

References

- Chatterjee S, Bedja D, Mishra S, Amuzie C, Avolio A, Kass DA, Berkowitz D, Renehan M. Inhibition of glycosphingolipid synthesis ameliorates atherosclerosis and arterial stiffness in apolipoprotein E-/- mice and rabbits fed a high-fat and -cholesterol diet. *Circulation*, 129:2403-2413, 2014.
- Chen K, Zhou X, Sun Z. Haplodeficiency of klotho gene causes arterial stiffening via upregulation of scleraxis expression and induction of autophagy. *Hypertension*, 66:1006-1013, 2015.
- DeMarco VG, Habibi J, Jia G, Aroor AR, Ramirez-Perez FI, Martinez-Lemus LA, Bender SB, Garro M, Hayden MR, Sun Z, Meininger GA, Manrique C, Whaley-Connell A, Sowers JR. Low-dose mineralocorticoid receptor blockade prevents western diet-induced arterial stiffening in female mice. *Hypertension*, 66:99-107, 2015.
- Du B, Ouyang A, Eng JS, Fleenor BS. Aortic perivascular adipose-derived interleukin-6 contributes to arterial stiffness in low-density lipoprotein receptor deficient mice. *Am J Physiol Heart Circ Physiol*, 308:H1382-1390, 2015.
- Fitch RM, Rutledge JC, Wang YX, Powers AF, Tseng JL, Clary T, Rubanyi GM. Synergistic effect of angiotensin II and nitric oxide synthase inhibitor in increasing aortic stiffness in mice. *Am J Physiol Heart Circ Physiol*, 290:H1190-H1198, 2006.
- Fleenor BS, Seals DR, Zigler ML, Sindler AL. Superoxide-lowering therapy with TEMPOL reverses arterial dysfunction with aging in mice. *Aging Cell*, 11:269-276, 2012.
- Hanson MG, Zahradka P, Taylor CG. Lentil-based diets attenuate hypertension and large-artery remodelling in spontaneously hypertensive rats. *Br J Nutr*, 111:690-698, 2014.
- Hartley CJ, Reddy AK, Madala S, Entman ML, Michael LH, Taffet GE. Doppler velocity measurements from large and small arteries of mice. *Am J Physiol Heart Circ Physiol*, 301:H269-H278, 2011.
- Hartley CJ, Reddy AK, Madala S, Entman ML, Taffet GE. Feasibility of Doppler velocity measurements to estimate volume pulsations of an arterial segment. *Ultrasound Med Biol*, 36:1169-1175, 2010.
- Hartley CJ, Reddy AK, Madala S, Martin-McNulty B, Vergona R, Sullivan ME, Halks-Miller M, Taffet GE, Michael LH, Entman ML, Wang Y-X. Hemodynamics changes in apolipoprotein E-knockout mice. *Am J Physiol Heart Circ Physiol*, 279:H2326-H2334, 2000.
- Hartley CJ, Taffet GE, Reddy AK, Entman ML, and Michael LH. Noninvasive cardiovascular phenotyping in mice. *Inst Lab Anim Res*, 43:147-158, 2002.
- Henson GD, Walker AE, Reihl KD, Donato AJ, Lesniewski LA. Dichotomous mechanisms of aortic stiffening in high-fat diet fed young and old B6D2F1 mice. *Physiol Rep*, 2:e00268, 2014.
- Jung SM, Jandu S, Steppan J, Belkin A, An SS, Pak A, Choi EY, Nyhan D, Butlin M, Viegas K, Avolio A, Berkowitz DE, Santhanam L. Increased tissue transglutaminase activity contributes to central vascular stiffness in eNOS knockout mice. *Am J Physiol Heart Circ Physiol*, 305:H803-H810, 2013.
- LaRocca TJ, Gioscia-Ryan RA, Hearon CM Jr, Seals DR.The autophagy enhancer spermidine reverses arterial aging. *Mech Ageing Dev*, 134:314-320, 2013.
- LaRocca TJ, Hearon CM Jr, Henson GD, Seals DR. Mitochondrial quality control and age-associated arterial stiffening. *Exp Gerontol*, 58:78-82, 2014.
- Lim HK, Lim HK, Ryoo S, Benjo A, Shuleri K, Miriel V, Baraban E, Camara A, Soucy K, Nyhan D, Shoukas A, Berkowitz DE. Mitochondrial arginase II constrains endothelial NOS-3 activity. *Am J Physiol Heart Circ Physiol*, 293:H3317-3324, 2007.
- Lin Y, Chen J, Sun Z. Antiaging gene klotho deficiency promoted high-fat diet-induced arterial stiffening via inactivation of AMP-activated protein kinase. *Hypertension*, 67:564-573, 2016.

- Prasad AM, Morgan DA, Nuno DW, Ketsawatsomkron P, Bair TB, Venema AN, Dibbern ME, Kutschke WJ, Weiss RM, Lamping KG, Chapleau MW, Sigmund CD, Rahmouni K, Grumbach IM. Calcium/calmodulin-dependent kinase II inhibition in smooth muscle reduces angiotensin II-induced hypertension by controlling aortic remodeling and baroreceptor function. *J Am Heart Assoc*, 4:e001949, 2015.
- Reddy AK, Hartley CJ, Thuy T. Pham, Darlington G, Entman ML, Taffet GE. Young Little mice express a premature cardiovascular aging phenotype. *J Gerontol A Biol Sci Med Sci*, 69:152-159, 2014.
- Reddy AK, Jones AD, Martono C, Caro WA, Madala S, Hartley CJ. Pulsed Doppler signal processing for use in mice: Design and evaluation. *IEEE Trans Biomed Eng*, 52:1764-1770, 2005a.
- Reddy AK, Madala S, Jones AD, Caro WA, Eberth JF, Pham TT, Taffet GE, Hartley CJ. Multi-channel pulsed Doppler signal processing for vascular measurements in mice. *Ultrasound Med Biol*, 35:2042-2054, 2009.
- Reddy AK, Taffet GE, Li, Y-H, Lim S-W, Pham TT, Pocius JS, Entman ML, Michael LH, Hartley CJ. Pulsed Doppler signal processing for use in mice: Applications. *IEEE Trans Biomed Eng*, 52:1771-1783, 2005b.
- Sikka G, Pandey D, Bhuniya AK, Steppan J, Armstrong D, Santhanam L, Nyhan D, Berkowitz DE. Contribution of arginase activation to vascular dysfunction in cigarette smoking. *Atherosclerosis*, 231:91-94, 2013.
- Sikka G, Yang R, Reid S, Benjo A, Koitabashi N, Camara A, Baraban E, O'Donnell CP, Berkowitz DE, Barouch LA. Leptin is essential in maintaining normal vascular compliance independent of body weight. *Int J Obesity*, 34:203-206, 2010.
- Sindler AL, Fleenor BS, Calvert JW, Marshall KD, Zigler ML, Lefer DJ, Seals DR. Nitrite supplementation reverses vascular endothelial dysfunction and large elastic artery stiffness with aging. *Aging Cell*, 10:429-437, 2011.
- Soucy KG, Lim HK, Attarzadeh DO, Santhanam L, Kim JH, Bhunia AK, Sevinc B, Ryoo S, Vazquez ME, Nyhan D, Shoukas AA, Berkowitz DE. Dietary inhibition of xanthine oxidase attenuates radiation-induced endothelial dysfunction in rat aorta. *J Appl Physiol (1985)*, 108:1250-1258, 2010.
- Soucy KG, Ryoo S, Benjo A, Lim HK, Gupta G, Sohi JS, Elser J, Aon MA, Nyhan D, Shoukas AA, Berkowitz DE. Impaired shear stress-induced nitric oxide production through decreased NOS phosphorylation contributes to age-related vascular stiffness. *J Appl Physiol (1985)*, 101:1751-1759, 2006.
- Tuday EC, Meck JV, Nyhan D, Shoukas AA, Berkowitz DE. Microgavity-induced changes in aortic stiffness and their role in orthostatic intolerance. *J Appl Physiol (1985)*, 102:853-858, 2007.
- Tuday EC, Nyhan D, Shoukas AA, Berkowitz DE. Simulated microgravity-induced aortic remodeling. *J Appl Physiol (1985)*, 106:2002-2008, 2009.
- Vendrov AE, Vendrov KC, Smith A, Yuan J, Sumida A, Robidoux J, Runge MS, Madamanchi NR. NOX4 NADPH oxidase-dependent mitochondrial oxidative stress in aging-associated cardiovascular disease. *Antioxid Redox Signal*, 23:1389-1409, 2015.
- Walker AE, Henson GD, Reihl KD, Morgan RG, Dobson PS, Nielson EI, Ling J, Mecham RP, Li DY, Lesniewski LA, Donato AJ. Greater impairments in cerebral artery compared with skeletal muscle feed artery endothelial function in a mouse model of increased large artery stiffness. *J Physiol*, 593:1931-1943, 2015.
- Wang YX, Martin-McNulty B, da Cunha V, Vincelette J, Lu X, Feng Q, Halks-Miller M, Mahmoudi M, Schroeder M, Subramanyam B, Tseng JL, Deng GD, Schirm S, Johns A, Kauser K, Dole WP, Light DR.

Fasudil, a Rho-kinase inhibitor, attenuates angiotensin II-induced abdominal aortic aneurysm in apolipoprotein E-deficient mice by inhibiting apoptosis and proteolysis. *Circulation*, 111:2219-2226, 2005.

- Zhou RH, Vendrov AE, Tchivilev I, Niu XL, Molnar KC, Rojas M, Carter JD, Tong H, Stouffer GA, Madamanchi NR, Runge MS. Mitochondrial oxidative stress in aortic stiffening with age: the role of smooth muscle cell function. *Arterioscler Thromb Vasc Biol*, 32:745-755, 2012.

3. Transverse Aortic Constriction (TAC) Measurements

Numerous transgenic or mutant mouse models of cardiovascular diseases develop compensatory mechanisms that mask the phenotypic differences maintaining many cardiovascular parameters. Therefore, resting values for these and other physiological parameters may be nearly normal and often need interventions to reveal phenotypic differences.

A common surgical intervention for stressing the heart is a pressure overload model produced by constricting the aorta between the innominate artery and the left carotid artery in mice was developed by Rockman et al. (1993) and this aortic banding model produces cardiac hypertrophy in mice. All the studies summarized below used the Doppler system to qualify and quantify the levels of pressure-overload that TAC generated.

RCA, LCA, and stenotic jet flow velocity in TAC mouse model, validation of simplified Bernoulli's equation, TAC studies in aging & doxorubicin mouse models

Li et al. (2003a) has conducted a study to investigate the relationship between flow velocity changes in the right and left carotid arteries (RCA & LCA) to the extent of cardiac hypertrophy and to the flow velocity patterns in abdominal aorta (ABA) in mice with transverse aortic constriction (TAC). They found that post-TAC peak RCA velocity increased significantly, peak LCA velocity and peak ABA velocity decreased significantly with no change in mean velocities of RCA, LCA and ABA which they attribute to adaptation of the peripheral arteries to maintain normal cerebral and peripheral perfusion. They reported that RCA/LCA peak velocity ratio at 1-day post-TAC was significantly correlated with the heart weight/body weight ratio at 7-days post-TAC. Additionally they found that RCA/LCA peak velocity ratio had a significant positive correlation peak stenotic jet velocity. They also validated that peak stenotic jet velocity can be used to estimate pressure gradient across the stenosis noninvasively in mice using the simplified Bernoulli equation ($P=4V^2$; where P is in *mmHg* and V is in *m/s*). On a follow-up study Li et al. (2003b) demonstrated that there is an age-related delay i n vascular adaptation in older mice as take longer time than young mice to adapt and establish adequate mean flow velocity in the carotid arteries. This is evidenced by the lower RCA/LCA mean velocity ratio and higher pulsatility index ratio at 1-day post-TAC in older mice with these differences disappearing at 7-days post-TAC. Using a mouse TAC model the same group demonstrated the utility of recombinant thrombomodulin protein administration in preventing the progression of left ventricular contractile dysfunction and in decreasing the apoptosis induced by doxorubicin (Li et al. 2010).

TAC in mouse models of heart failure

Patients with end-stage heart failure had downregulation of GTPase Rnd3 (Rho family guanosine triphosphate) transcripts. The consequence of Rnd3 regulation in heart failure was investigated by Yue et al. (2014) by subjecting the haploinsufficient Rnd3$^{+/-}$ mice to pressure overload by transverse aortic constriction (TAC). The resulting apoptosis, increased caspase-3 activity, and elevated Rho kinase activity were reversed by fasudil treatment followed by partially improved cardiac function. They concluded that haploinsufficient Rnd3$^{+/-}$ mice are predisposed to hemodynamic stress and that overactivation of Rho kinase activity is in part responsible for the development of apoptotic cardiomyopathy in these mice.

TAC and cardiac hypertrophy in mouse models of gender and parent-of-origin

Using TAC Barrick et al. (2007) demonstrated C57BL/6J mice developed eccentric hypertrophy characterized by systolic dysfunction and right heart failure and 129S1 gradually developed concentric hypertrophy characterized by preserved systolic function. With their findings of dominance of genetic susceptibility to initial concentric hypertrophy over eccentric hypertrophy they suggest that investigators should be cautious in their interpretation of outcomes in TAC studies when mice of mixed genetic backgrounds are used. Barrick et al. (2009) followed up this study by looking at gender and parent-of-origin effects on pressure-overload response to TAC. They found that 5-weeks post-TAC, female 129B6F1 mice had much larger hearts than female 129 and B6129F1 mice indicating that offspring of B6 male mice are more vulnerable to TAC produced cardiac hypertrophy than offspring of 129 males. They conclude that the the traits of the 129 resistance factor or the B6 susceptibility factor are active only when inherited from respective fathers. This study also serves to caution the investigators about the vulnerabilities of of the usage of C57BL/6 and 129S1 strains to generate genetically engineered mice to study pressure-overload.

TAC in mouse model of steroid receptor coactivator-2 deficiency

Cardiac failure in humans is often associated with decrease in the transcriptional regulator steroid receptor coactivator-2 (SRC-2), perhaps due to its role as an important regulator of the adult heart gene expression profile (Reineke et al. 2012). The lack of heart weight changes or alterations in cardiac function in SRC-2 null mice may be due to compensatory mechanisms. Reineke et al. (2014) showed that SRC-2 null mice had stress-induced cardiac dysfunction when subjected to TAC but did not exhibit the mass and dimension changes observed with hypertrophy. They also observed that the molecular signaling known to activate hypertrophy was blunted and concluded that SRC-2 plays a role in maintaining a steady-state adult heart transcriptional profile and that its deletion interferes with the timing and integration needed to respond efficiently to stress.

Progression and regression mouse model of TAC

Stansfield et al. (2007) have developed a unique mouse model of pressure-overload/relief to study the regression of left ventricular hypertrophy to mimic the effects of removing the excessive load such as stenotic valve replacement and treatment of hypertension. They subjected mice to 4-weeks of TAC using a minimally invasive slipknot technique followed by the removal of the band and observed the progression and regression using carotid Doppler velocity ratios which reverted to normal values after the removal of the band. Additionally they reported that hypertrophic response assessed through heart weight/body weight ratios, histology, cardiac dimensions, hypertrophic gene expression, regressed within 1 week and remained at those levels for up to 4 weeks.

Ascending aortic constriction rat model of cardiac hypertrophy

Most small animal models of pressure-overload use the TAC method. However, in a study conducted for her Dissertation Vela (2010) used a more severe pressure-overload rat model that was banded at the ascending aorta before the innominate. While the stenotic jet velocity seen were similar to those observed in mice with TAC, the peak carotid velocity ratios were reversed with right carotid velocity having a diminished peaks and left carotid velocity was more pulsatile.

TAC mouse model with treatment by genetic alteration

Yang et al. (2014) demonstrated that deficiency of Munc13-4 (a limiting factor in vesicular priming and fusion) in mice (Unc13-dJinx) had a regression of cardiac hypertrophy after 5-weeks in response to TAC in contrast with WT type mice which had sustained cardiac hypertrophy. They showed cardiac hypertrophy was partially restored upon administration of WT platelets or platelet releasate in Unc13-dJinx mice. This study shows that Munc13-4 deficiency may represent a novel target for preventing long-term left ventricular hypertrophy.

Please refer to the reports by several other investigators have used Indus Doppler system in other TAC related studies (Hartley et al. 2008, Yue 2015, Baskin 2012, Yang 2012, Yang et al. 2012).

References

- Barrick CJ, Dong A, Waikel R, Corn D, Yang F, Threadgill DW, Smyth SS. Parent-of-origin effects on cardiac response to pressure overload in mice. *Am J Physiol Heart Circ Physiol*, 297:H1003-H1009, 2009.
- Barrick CJ, Rojas M, Schoonhoven R, Smyth SS, Threadgill DW. Cardiac response to pressure overload in 129S1/SvImJ and C57BL/6J mice: temporal- and background-dependent development of concentric left ventricular hypertrophy. Am J Physiol Heart Circ Physiol. 2007 May;*Am J Physiol Heart Circ Physiol*, 292:H2119-H2130, 2007.
- Baskin KK. Regulation of protein degradation in the heart by amp-activated protein kinase. *PhD Dissertation*, The University of Texas Health Science Center at Houston and MD Anderson Cancer Center Graduate School of Biomedical Sciences, Houston, TX, 2012.
- Hartley CJ, Reddy AK, Madala S, Michael LH, Entman ML, Taffet GE, Doppler estimation of reduced coronary flow reserve in mice with pressure overload cardiac hypertrophy. *Ultrasound Med Biol*, 34:892-901, 2008.
- Li Y-H, Reddy AK, Taffet GE, Michael LH, Entman ML, Hartley CJ. Peripheral vascular adaptations to transverse aortic banding in mice. *Ultrasound in Medicine and Biology*, 29(9):1281-1289, 2003a.
- Li Y-H, Reddy AK, Ochoa LN, Pham TT, Hartley CJ, Michael LH, Entman ML, Taffet GE. Effect of age on peripheral vascular response to transverse aortic banding in mice. *Journal of Gerontology Biological Sciences*, 58A (10):895-899, 2003b.
- Li YH, Chung HC, Luo CY, Chao TH, Shyu KG, Shi GY, Wu HL.Thrombomodulin is upregulated in cardiomyocytes during cardiac hypertrophy and prevents the progression of contractile dysfunction. *J Card Fail*, 16:980-990, 2010.
- Reineke EL, York B, Stashi E, Chen X, Tsimelzon A, Xu J, Newgard CB, Taffet GE, Taegtmeyer H, Entman ML, O'Malley BW. SRC-2 coactivator deficiency decreases functional reserve in response to pressure overload of mouse heart. *PLoS One*, 7:e53395, 2012.
- Stansfield WE, Rojas M, Corn D, Willis M, Patterson C, Smyth SS, Selzman CH.Characterization of a model to independently study regression of ventricular hypertrophy. *J Surg Res*, 142:387-393, 2007.
- Vela D. Dynamic Remodeling of the Stressed Heart: Role of Protein Degradation Pathways. *MS Thesis*, The University of Texas Health Science Center at Houston and MD Anderson Cancer Center Graduate School of Biomedical Sciences, Houston, TX, 2010.
- Yang F, Dong A, Ahamed J, Sunkara M, Smyth SS. Granule cargo release from bone marrow-derived cells sustains cardiac hypertrophy. *Am J Physiol Heart Circ Physiol*, 307:H1529-H1538, 2014.

- Yang F, Dong A, Mueller P, Caicedo J, Sutton AM, Odetunde J, Barrick CJ, Klyachkin YM, Abdel-Latif A, Smyth SS. Coronary artery remodeling in a model of left ventricular pressure overload is influenced by platelets and inflammatory cells. *PLoS One*,7:e40196, 2012.
- Yang F. Inflammatory interactions and secretion in cardiac remodeling. *PhD Dissertation*, University of Kentucky, Lexington, KY, 2012.
- Yue X, Yang X, Lin X, Yang T, Yi X, Dai Y, Guo J, Li T, Shi J, Wei L, Fan GC, Chen C, Chang J. Rnd3 haploinsufficient mice are predisposed to hemodynamic stress and develop apoptotic cardiomyopathy with heart failure. *Cell Death Dis*, 5:e1284, 2014.
- Yue X. Mechanistic study of rnd3 in cardiomyopathy. *PhD Dissertation*, Texas A&M University Graduate and Professional Studies, College Station, TX, 2015.

4. Coronary Flow Velocity and Coronary Flow Reserve Measurements

Coronary flow reserve (CFR) measurement method and CFR in various mouse models

The non-image guided coronary flow velocity measurement method was reported by Hartley et al. (2007). In this study, isoflurane, a commonly used anesthetic agent, which is also a potent coronary vasodilator, was used to to assess CFR in mice. In humans, CFR is reduced with age, coronary artery disease and other cardiac pathologies. Hartley et al. (2007) used the Indus Doppler system to determine CFR in mouse models that mimic some of the above human conditions. Mice were anesthetized with low (1%) and high (2.5%) levels of isoflurane to generate baseline (B) and hyperemic (H) coronary flows, respectively. Using a 20-MHz Doppler probe that was held with a micromanipulator and aimed toward the origin of the left main coronary artery to measure peak diastolic coronary flow velocity during the B and H conditions in young (6 wk), old (2 yr), and old apolipoprotein-E null (ApoE$^{-/-}$; 2 yr) atherosclerotic mice. For each group an average value of H/B ratio was calculated and compared. They reported that the differences in B velocities and H/B between young and old and between old and APOE$^{-/-}$ were significant but no differences observed in H velocities. Therefore the high H/B in old mice was a result of lower B flow velocity rather than higher H flow velocity. On the other hand, ApoE$^{-/-}$ mice have higher B and H velocities, perhaps due to coronary lesions. They conclude that the combination of Doppler ultrasound and isoflurane based coronary vasodilation allows for a convenient noninvasive method to estimate coronary reserve in mice.

Hartley et al. (2008) studied the effect of TAC induced pressure overload cardiac hypertrophy in mice on CFR Using the 20-MHz Indus Doppler ultrasound the left main coronary flow velocity was measured at baseline (B) and at hyperemia (H) induced by low (1%) and high (2.5%) isoflurane gas anesthesia at pre-TAC and at 1-day, 7-day, and 21-day post-TAC. The jet flow velocity was measured just distal to the stenosis and pressure drop was estimated by using approximate Bernoulli's equation (PmmHg=4V^2; Vm/s, validated in mice by Li et al. 2003). The pressure drop progressively increased from ≈50 mmHg at 1-day post-TAC to ≈75 mmHg at 21-day post-TAC. Also, CFR (H/B) dropped progressively from ≈3.2 pre-TAC to ≈2.2 (1-day), ≈1.7 (7-day), and ≈1.4 (21-day) post-TAC. Hartley et al. (2008) are the first group to report a significant and progressive increase in the coronary systolic/diastolic velocity ratio from 0.17 pre-TAC to 0.91 21-day post-TAC and to report a serial measurement of CFR demonstrating that CFR is virtually eliminated in TAC induced mice after 21-day of cardiac remodeling.

Coronary flow reserve in cardiac failure from cancer treatment

Many cancer treatments eliminate the risk of death only to create another, the heart failure. In his dissertation work, Rodriguez (2015) reported that sunitinib chemotherapy disrupted the function of coronary arteries as measured by coronary flow reserve. This was shown using four different coronary vasodilators with different mechanisms of operation - isoflurane, acetylcholine, adenosine, and sodium nitroprusside. Rodriguez (2015) also demonstrated that the coronary dysfunction was due to loss of pericyte caused by Sunitinib which inhibited PDGFRβ. This was proved by treatment with CP-67345, a potent PDGFRβ inhibitor, that resulted in declines in coronary flow reserve. Coronary flow reserve that was diminished in mice treated with sunitinib for 14 days, improved significantly when treated with sunitinib+thalidomide from day 15 to day 28.

Coronary flow reserve in control and sham mice that have undergone TAC

Transverse aortic constriction is used to study the development of cardiac hypertrophy in many mice studies. Barrick et al. (2007) reported that mice that have undergone TAC also have perivascular inflammation and thickening of the coronary artery media, in addition to myocardial fibrosis. Yang et al. (2012) demonstrated that perivascular inflammation indeed is associated with remodeling in coronary arteries and correlated with declines in coronary flow reserve in TAC induced wild type mice compared to that in sham operated control mice.

Coronary flow reserve in mouse model mimicking of human heart failure

The observation of decrease in a small GTPase, Rnd3, an endogenous inhibitor of Rho Kinase 1 (ROCK1) in end-stage heart failure patients led Yue (2015) to investigate the role of Rnd3 in the heart. To this end, a Rnd3 null mouse line was generated which was resulted in embryonic lethality in these mice with elevated Rock1 activity leading to severe cardiac apoptosis at the E10.5 stage. So, haploinsufficient Rnd3 (Rnd3+/-) mice that survived to adulthood were generated and when subjected to TAC resulted in ROCK1 activation and cardiomyocyte apoptosis with reduced capillary numbers and sizes and reduced coronary flow reserve. A double knockout mouse line with Rnd3+/-ROCK1-/- background rescued the phenotype partially.

References

- Barrick CJ, Rojas M, Schoonhoven R, Smyth SS, Threadgill DW (2007). Cardiac response to pressure overload in 129S1/SvImJ and C57BL/6J mice: temporal- and background-dependent development of concentric left ventricular hypertrophy. *Am J Physiol Heart Circ Physiol*, 292:H2119-H2130, 2007.
- Hartley CJ, Reddy AK, Madala S, Entman ML, Michael LH, Taffet GE. Doppler velocity measurements from large and small arteries of mice. Review . *Am J Physiol Heart Circ Physiol*, 301: H269-H278, 2011.
- Hartley CJ, Reddy AK, Madala S, Michael LH, Entman ML, Taffet GE, Doppler estimation of reduced coronary flow reserve in mice with pressure overload cardiac hypertrophy. *Ultrasound Med Biol*, 34:892-901, 2008.
- Hartley CJ, Reddy AK, Madala S, Michael LH, Entman ML, Taffet GE. Effects of isoflurane on coronary blood flow velocity in young, old, and ApoE$^{-/-}$ mice measured by Doppler ultrasound. *Ultrasound Med Biol*, 33:512-521, 2007.
- Li Y-H, Reddy AK, Taffet GE, Michael LH, Entman ML, Hartley CJ. Peripheral vascular adaptations to transverse aortic banding in mice. *Ultrasound in Medicine and Biology*, 29(9):1281-1289, 2003.
- Rodriguez MR. Sunitinib-induced cardiotoxicity exposes microvascular and metabolic derangements in the failing heart. PhD Thesis.The University of Texas Health Science Center at Houston and MD Anderson Cancer Center Graduate School of Biomedical Sciences, Houston, TX, 2015.
- Yang F, Dong A, Mueller P, Caicedo J, Sutton AM, Odetunde J, Barrick CJ, Klyachkin YM, Abdel-Latif A, Smyth SS. Coronary artery remodeling in a model of left ventricular pressure overload is influenced by platelets and inflammatory cells. *PLoS One*, 7:e40196, 2012.
- Yang F. Inflammatory interactions and secretion in cardiac remodeling. *PhD Dissertation*, University of Kentucky, Lexington, KY, 2012.
- Yue X. Mechanistic study of rnd3 in cardiomyopathy. *PhD Dissertation*, Texas A&M University Graduate and Professional Studies, College Station, TX, 2015.

5. Peripheral Vessel Flow Velocity Measurements

Diabetic nephropathy chronic kidney disease

Lin et al. (2013) used renal flow velocity measurements to study diabetic nephropathy in the mouse deficient in the anti-aging gene, Klotho, which is primarily expressed in kidneys since Klotho was diminished in kidneys of diabetic nephropathy patients. Klotho deficient mice were made diabetic with injections of streptozotocin and renal blood flow were measured. They report that neither Klotho deficiency nor 3 to 5 week streptozotocin administration affected renal blood flow which perhaps may indicate that short-term treatment by streptozotocin does not result in renal hemodynamic changes. Thus they conclude that renal ischemia may have caused early diabetic nephropathy in Klotho deficient mice as indicated by the enhancement of both TGF1 and mTOR signaling in kidneys.

Studies of Vascular Injury: Many Doppler measurements of peripheral vessels involve studies of vascular injury models. The saphenous vein is most often used vessel to study the vascular injury and thrombosis formation/anti-coagulation.

Coagulation studies in hemophilia B mice

Buyue et al (2008) hypothesized that coagulation response is regulated by factor IXa heparin-binding exosite. To test this, they studied the effect of mutations that enhanced (R170A) or reduced (R233A) stability of the protease factor VIIIa A2 domain interaction on thrombin generation initiated by tissue factor and factor IXa. These evaluations were done by bleeding from a saphenous vein incision or by FeCl3-induced saphenous vein thrombosis in the factor IX-deficient plasma hemophilia B mouse compared to wildtype mice. They observed a 2-3 fold increase in factor IXa R170A in peak thrombin concentration and 5-fold increase in flow velocity measured using 20 MHz Doppler. On the other hand they observed that factor IXa R233A was blunted and delayed in the hemophilia B mice. Additionally, the average time to hemostasis after saphenous vein incision and the occlusion time post-FeCl3-induced saphenous vein injury decreased with factor IX replacement. The observed results indeed confirm that coagulation response is regulated by factor IXa heparin-binding exosite and therefore could be used as a novel antithrombotic target.

Coagulation abnormalities

Identifying coagulation abnormalities in patients with combined bleeding and thrombosis history is clinically challenging. Marchi et al. (2012) investigated the pathophysiologic mechanisms of dysregulated coagulation in a patient with coagulation abnormalities that included hematomas, retinal artery occlusion/thrombosis, transient cerebral ischemia, and poor wound healing. They demonstrated that in an arterial injury model, hypofibrinogenemic mice ($Fgn^{+/-}$) infused with FVIII demonstrated significantly shorter vessel occlusion times, as measured by Doppler flow velocity, than saline-infused $Fgn^{+/-}$ mice. Their results suggest the bleeding and thrombosis combination is perhaps due to combination of hypofibrinogenemia and hypercoagulability of plasma.

Aging & cellular senescence in mice overexpressing p16INK4a and vascular injury model

Vascular dysfunction with aging is associated with cellular senescence resulting from upregulation of the cell cycle inhibitor, p16INK4a, which promotes senescence with aging. Cardenas et al. (2011) investigated the role of p16INK4a overexpression with aging in venous thrombosis. They

subjected the p16INK4a overexpression mouse model to 4 types of vascular injuries that include induction of thrombus formation in saphenous vein with (a) ferric chloride & (b) Rose Bengal, examination of thrombus resolution through with (c) ferric chloride plus vascular ligation, and (d) administration of lipopolysaccharide to initiate inflammation-induced vascular dysfunction. They demonstrated that the vessels of p16INK4a overexpression mice occluded faster than those of control mice in type (a) ferric chloride and type (b) Rose Bengal tests. Additionally, they reported that thrombus resolution (c) was slower in the p16INK4a overexpression mice than in the controls and that the p16INK4a overexpression mice had enhanced generation of thrombin generation with lipopolysaccharide treatment. The time-to-occlusion measurements were made from Doppler flow velocity signals.

Thrombosis in cancer

Trousseau syndrome refers to the venous thromboembolism (VTE) that occurs in cancer and the rates of VTE depend on the type of cancer. Wang et al. (2012) investigated the role of tissue factor (TF), a transmembrane protein, which activates the coagulation cascade in patients of pancreatic cancer. They used a xenograft mouse model with four variations of human pancreatic tumors to study the role of TF in activated coagulation and its reversal with human TF inhibition. Of the four they found that only two of the variations expressed TF and activated coagulation which was reversed with an anti-human TF Ab. They created a 90% stenosed inferior vena cava model and a ferric chloride induced saphenous vein thrombosis and monitored blood flow with a 20 MHz Doppler flow. The absence of blood flow for a minute was defined as occlusion and the time from injury-to-cessation of blood flow was defined as time-to-occlusion. They observed that mice with TF expression had increased thrombosis in a saphenous vein model but not in in the inferior vena cava stenosis model when compared to control mice.

Post-angioplasty restenosis in a hypercholesterolemic rabbit model with and without COX-1 gene

Post-angioplasty restenosis is a major problem in patients of coronary artery disease. Liu et al. (2005) investigated the effectiveness of Cyclooxygenase-1 (COX-1) gene transduction on prostacyclin, an antithrombotic molecule and a vasodilator, which can play a role in preventing post-angioplasty restenosis in a rabbit model of hypercholesterolemia. They injured one of the carotid artery with the other serving as control and then performed local gene transduction with and without COX-1 gene. After 28 days of treatment, blood flow velocity as measured by Doppler was restored in arteries treated with COX-1 but not in sham treated arteries. Their observations suggested that COX-1 prevented restenosis after injury and the arteries had larger lumen area.

Arterial tortuosity models

Tortuosity of arteries is caused by aging, genetic defects, and other diseases. While in vitro and modeling studies by several researchers have shown that buckling of the arteries may lead to tortuous arteries, Zhang et al. (2014) developed an in vivo buckling model of the rat carotid artery. They transplanted the left carotid arteries to the right side to effect buckling under in vivo pressure. They observed significant buckling in the carotid artery 1- week post-surgery, with altered wall stress and significant increases in cell proliferation and matrix metalloprotinease-2 (MMP-2) expression. The tortuosity of the grafts increased without any changes in vessel dimensions, blood pressure, or flow velocity (measured by 20 MHz Doppler).

Muscular dystrophy and ischemia

Zhang et al. (2103) investigated whether neuronal nitric oxide synthase (nNOS) binding mini-dystrophin expression restored with gene therapy can mitigate muscle ischemia and injury in Duchenne muscular dystrophy (DMD). In this study they used a mouse model of DMD and a mouse model of dystrophin deficiency and performed gene transfer experiments. After four months of treatment they observed an increase in muscle force, lack of injury from eccentric contraction, reduction in histopathology, and attenuation of adrenergic vasoconstriction as measured by Doppler.

References

- Buyue Y, Whinna HC, Sheehan JP. The heparin-binding exosite of factor IXa is a critical regulator of plasma thrombin generation and venous thrombosis. *Blood*, 112:3234-3241, 2008.
- Cardenas JC, Owens AP3rd, Krishnamurthy J, Sharpless NE, Whinna HC, Church FC. Overexpression of the cell cycle inhibitor p16INK4a promotes a prothrombotic phenotype following vascular injury in mice. *Arterioscler Thromb Vasc Biol*, 31:827-833, 2011.
- Lin Y, Kuro-o M, Sun Z. Genetic deficiency of anti-aging gene *klotho* exacerbates early nephropathy in STZ-induced diabetes in male mice. *Endocrinology*, 154:3855-3863, 2013.
- Liu Q, Chen ZQ, Bobustuc GC, McNatt JM, Segall H, Pan S, Willerson JT, Zoldhelyi P. Local gene transduction of cyclooxygenase-1 increases blood flow in injured atherosclerotic rabbit arteries. *Circulation*, 111:1833-1840, 2005.
- Marchi R, Walton BL, McGary CS, Lin FC, Ma AD, Pawlinski R, Mackman N, Campbell RA, Di Paola J, Wolberg AS. Dysregulated coagulation associated with hypofibrinogenaemia and plasma hypercoagulability: implications for identifying coagulopathic mechanisms in humans. *Thromb Haemost*, 108:516-526, 2012.
- Wang JG, Geddings JE, Aleman MM, Cardenas JC, Chantrathammachart P, Williams JC, Kirchhofer D, Bogdanov VY, Bach RR, Rak J, Church FC, Wolberg AS, Pawlinski R, Key NS, Yeh JJ, Mackman N. Tumor-derived tissue factor activates coagulation and enhances thrombosis in a mouse xenograft model of human pancreatic cancer. *Blood*, 119:5543-5552, 2012.
- Zhang J, Liu Q, Han HC.An *in vivo* rat model of artery buckling for studying wall remodeling. *Ann Biomed Eng*, 42:1658-1667, 2014.
- Zhang Y, Yue Y, Li L, Hakim CH, Zhang K, Thomas GD, Duan D. Dual AAV therapy ameliorates exercise-induced muscle injury and functional ischemia in murine models of Duchenne muscular dystrophy. *Hum Mol Genet*, 22:3720-3729, 2013.

List of All References with Links

1. Ahmad, N., Bygrave, M., Chhem, R., Hoffman, L., Welch, I., Grange, R., Fenster, A., Hill, D., Lee, T. Y., High-frequency ultrasound to grade disease progression in murine models of Duchenne muscular dystrophy. *J Ultrasound Med*, 28 (6) 707-16, 2009. link
2. Ahmad, N., Bygrave, M., De Zordo, T., Fenster, A., Lee, T. Y., Detecting degenerative changes in myotonic murine models of Duchenne muscular dystrophy using high-frequency ultrasound. *J Ultrasound Med*, 29 (3) 367-75, 2010. link
3. Allen, R. A., Wu, W., Yao, M., Dutta, D., Duan, X., Bachman, T. N., Champion, H. C., Stolz, D. B., Robertson, A. M., Kim, K., Isenberg, J. S., Wang, Y., Nerve regeneration and elastin formation within poly(glycerol sebacate)-based synthetic arterial grafts one-year post-implantation in a rat model. *Biomaterials*, 35 (1) 165-73, 2014. link
4. Amundsen, B. H., Ericsson, M., Seland, J. G., Pavlin, T., Ellingsen, O., Brekken, C., A comparison of retrospectively self-gated magnetic resonance imaging and high-frequency echocardiography for characterization of left ventricular function in mice. *Lab Anim*, 45 (1) 31-7, 2011. link
5. Andrukhova, O., Slavic, S., Zeitz, U., Riesen, S. C., Heppelmann, M. S., Ambrisko, T. D., Markovic, M., Kuebler, W. M., Erben, R. G.,Vitamin D is a regulator of endothelial nitric oxide synthase and arterial stiffness in mice. *Mol Endocrinol*, 28 (1) 53-64, 2014. link
6. Bachman, T. N., Bursic, J. J., Simon, M. A., Champion, H. C., A Novel Acquisition Technique to Utilize Swan-Ganz Catheter data as a Surrogate for High-fidelity Micromanometry within the Right Ventricle and Pulmonary Circuit. *Cardiovasc Eng Technol*, 4 (2) 183-191, 2013. link
7. Barreto-Torres, Giselle, Javadov, Sabzali, Possible Role of Interaction between PPARα and Cyclophilin D in Cardioprotection of AMPK against In Vivo Ischemia-Reperfusion in Rats. *PPAR Research*, 201612, 2016. link
8. Barrick, C. J., Dong, A., Waikel, R., Corn, D., Yang, F., Threadgill, D. W., Smyth, S. S., Parent-of-origin effects on cardiac response to pressure overload in mice. *Am J Physiol Heart Circ Physiol*, 297 (3) H1003-9, 2009. link
9. Barrick, C. J., Roberts, R. B., Rojas, M., Rajamannan, N. M., Suitt, C. B., O'Brien, K. D., Smyth, S. S., Threadgill, D. W., Reduced EGFR causes abnormal valvular differentiation leading to calcific aortic stenosis and left ventricular hypertrophy in C57BL/6J but not 129S1/SvImJ mice. *Am J Physiol Heart Circ Physiol*, 297 (1) H65-75, 2009. link
10. Barrick, C. J., Rojas, M., Schoonhoven, R., Smyth, S. S., Threadgill, D. W., Cardiac response to pressure overload in 129S1/SvImJ and C57BL/6J mice: temporal- and background-dependent development of concentric left ventricular hypertrophy. *Am J Physiol Heart Circ Physiol*, 292 (5) H2119-30, 2007. link
11. Biswas, Dipankar, Transition to turbulence in non-Newtonian fluids: An in-vitro study using pulsed Doppler ultrasound for biological flows. 2014. link
12. Boesen, E. I., Crislip, G. R., Sullivan, J. C., Use of ultrasound to assess renal reperfusion and P-selectin expression following unilateral renal ischemia. *Am J Physiol Renal Physiol*, 303 (9) F1333-40, 2012. link
13. Brennan, M. P., Sinusas, A. J., Horvath, T. L., Collins, J. G., Harding, M. J., Correlation between body weight changes and postoperative pain in rats treated with meloxicam or buprenorphine. *Lab Anim (NY)*, 38 (3) 87-93, 2009. link

14. Broberg, C. S., Pantely, G. A., Barber, B. J., Mack, G. K., Lee, K., Thigpen, T., Davis, L. E., Sahn, D., Hohimer, A. R., Validation of the myocardial performance index by echocardiography in mice: a noninvasive measure of left ventricular function. *J Am Soc Echocardiogr*, 16 (8) 814-23, 2003. link

15. Brown, A. S., Leamen, L., Cucevic, V., Foster, F. S., Quantitation of hemodynamic function during developmental vascular regression in the mouse eye. *Invest Ophthalmol Vis Sci*, 46 (7) 2231-7, 2005. link

16. Buyue, Y., Whinna, H. C., Sheehan, J. P., The heparin-binding exosite of factor IXa is a critical regulator of plasma thrombin generation and venous thrombosis. *Blood*, 112 (8) 3234-41, 2008. link

17. Callaerts-Vegh, Z., Evans, K. L., Shipley, G. L., Davies, P. J., Cuba, D. L., Gurji, H. A., Giles, H., Bond, R. A., Effects of different beta adrenoceptor ligands in mice with permanent occlusion of the left anterior descending coronary artery. *Br J Pharmacol*, 138 (8) 1505-16, 2003. link

18. Cardenas, J. C., Owens, A. P., 3rd, Krishnamurthy, J., Sharpless, N. E., Whinna, H. C., Church, F. C., Overexpression of the cell cycle inhibitor p16INK4a promotes a prothrombotic phenotype following vascular injury in mice. *Arterioscler Thromb Vasc Biol*, 31 (4) 827-33, 2011. link

19. Casey, David, Characterization of Transition to Turbulence for Blood in an Eccentric Stenosis Under Steady Flow Conditions. 2014. link

20. Chatterjee, S., Bedja, D., Mishra, S., Amuzie, C., Avolio, A., Kass, D. A., Berkowitz, D., Renehan, M., Inhibition of glycosphingolipid synthesis ameliorates atherosclerosis and arterial stiffness in apolipoprotein E-/- mice and rabbits fed a high-fat and -cholesterol diet. *Circulation*, 129 (23) 2403-13, 2014. link

21. Chiao, Y. A., Ramirez, T. A., Zamilpa, R., Okoronkwo, S. M., Dai, Q., Zhang, J., Jin, Y. F., Lindsey, M. L., Matrix metalloproteinase-9 deletion attenuates myocardial fibrosis and diastolic dysfunction in ageing mice. *Cardiovasc Res*, 96 (3) 444-55, 2012. link

22. Chintalgattu, V., Ai, D., Langley, R. R., Zhang, J., Bankson, J. A., Shih, T. L., Reddy, A. K., Coombes, K. R., Daher, I. N., Pati, S., Patel, S. S., Pocius, J. S., Taffet, G. E., Buja, L. M., Entman, M. L., Khakoo, A. Y., Cardiomyocyte PDGFR-beta signaling is an essential component of the mouse cardiac response to load-induced stress. *J Clin Invest*, 120 (2) 472-84, 2010. link

23. Cieslik, K. A., Taffet, G. E., Carlson, S., Hermosillo, J., Trial, J., Entman, M. L., Immune-inflammatory dysregulation modulates the incidence of progressive fibrosis and diastolic stiffness in the aging heart. *J Mol Cell Cardiol*, 50 (1) 248-56, 2011. link

24. Cieslik, K. A., Taffet, G. E., Crawford, J. R., Trial, J., Mejia Osuna, P., Entman, M. L., AICAR-dependent AMPK activation improves scar formation in the aged heart in a murine model of reperfused myocardial infarction. *J Mol Cell Cardiol*, 6326-36, 2013. link

25. Cruz, J. A., Bauer, E. M., Rodriguez, A. I., Gangopadhyay, A., Zeineh, N. S., Wang, Y., Shiva, S., Champion, H. C., Bauer, P. M.,Chronic hypoxia induces right heart failure in caveolin-1-/- mice. *Am J Physiol Heart Circ Physiol*, 302 (12) H2518-27, 2012. link

26. deAlmeida, A. C., van Oort, R. J., Wehrens, X. H., Transverse aortic constriction in mice. *J Vis Exp* (38) 2010. link

27. Donato, A. J., Walker, A. E., Magerko, K. A., Bramwell, R. C., Black, A. D., Henson, G. D., Lawson, B. R., Lesniewski, L. A., Seals, D. R., Life-long caloric restriction reduces oxidative stress and preserves nitric oxide bioavailability and function in arteries of old mice. *Aging Cell*, 12 (5) 772-83, 2013. link

28. Du, B., Ouyang, A., Eng, J. S., Fleenor, B. S., Aortic perivascular adipose-derived interleukin-6 contributes to arterial stiffness in low-density lipoprotein receptor deficient mice. *Am J Physiol Heart Circ Physiol*, 308 (11) H1382-90, 2015. link

29. Duerrschmid, C., Crawford, J. R., Reineke, E., Taffet, G. E., Trial, J., Entman, M. L., Haudek, S. B., TNF receptor 1 signaling is critically involved in mediating angiotensin-II-induced cardiac fibrosis. *J Mol Cell Cardiol*, 5759-67, 2013. [link]

30. Eberth, John Francis, Arterial biomechanics and the influences of pulsatility on growth and remodeling. 2008. [link]

31. Eberth, J. F., Gresham, V. C., Reddy, A. K., Popovic, N., Wilson, E., Humphrey, J. D., Importance of pulsatility in hypertensive carotid artery growth and remodeling. *J Hypertens*, 27 (10) 2010-21, 2009. [link]

32. Fitch, R. M., Rutledge, J. C., Wang, Y. X., Powers, A. F., Tseng, J. L., Clary, T., Rubanyi, G. M., Synergistic effect of angiotensin II and nitric oxide synthase inhibitor in increasing aortic stiffness in mice. *Am J Physiol Heart Circ Physiol*, 290 (3) H1190-8, 2006. [link]

33. Flenniken, A. M., Osborne, L. R., Anderson, N., Ciliberti, N., Fleming, C., Gittens, J. E., Gong, X. Q., Kelsey, L. B., Lounsbury, C., Moreno, L., Nieman, B. J., Peterson, K., Qu, D., Roscoe, W., Shao, Q., Tong, D., Veitch, G. I., Voronina, I., Vukobradovic, I., Wood, G. A., Zhu, Y., Zirngibl, R. A., Aubin, J. E., Bai, D., Bruneau, B. G., Grynpas, M., Henderson, J. E., Henkelman, R. M., McKerlie, C., Sled, J. G., Stanford, W. L., Laird, D. W., Kidder, G. M., Adamson, S. L., Rossant, J., A Gja1 missense mutation in a mouse model of oculodentodigital dysplasia. *Development*, 132 (19) 4375-86, 2005. [link]

34. George, Brian Patrick, Experimental and Computational Modeling of Ultrasound Correlation Techniques. 2010. [link]

35. Grimes, K. M., Lindsey, M. L., Gelfond, J. A., Buffenstein, R., Getting to the heart of the matter: age-related changes in diastolic heart function in the longest-lived rodent, the naked mole rat. *J Gerontol A Biol Sci Med Sci*, 67 (4) 384-94, 2012. [link]

36. Grimes, K. M., Reddy, A. K., Lindsey, M. L., Buffenstein, R., And the beat goes on: maintained cardiovascular function during aging in the longest-lived rodent, the naked mole-rat. *Am J Physiol Heart Circ Physiol*, 307 (3) H284-91, 2014. [link]

37. Gurha, P., Wang, T., Larimore, A. H., Sassi, Y., Abreu-Goodger, C., Ramirez, M. O., Reddy, A. K., Engelhardt, S., Taffet, G. E., Wehrens, X. H., Entman, M. L., Rodriguez, A., microRNA-22 promotes heart failure through coordinate suppression of PPAR/ERR-nuclear hormone receptor transcription. *PloS one*, 8 (9) e75882, 2013. [link]

38. Hanson, M. G., Zahradka, P., Taylor, C. G., Lentil-based diets attenuate hypertension and large-artery remodelling in spontaneously hypertensive rats. *Br J Nutr*, 111 (4) 690-8, 2014. [link]

39. Hartley, C., Reddy, A., Entman, M., Michael, L., Taffet, G., Madala, S., Characterization of arterial wave propagation and reflection in mice. *Conf Proc IEEE Eng Med Biol Soc*, 1601-4, 2005. [link]

40. Hartley, C. J., Reddy, A. K., Madala, S., Entman, M. L., Michael, L. H., Taffet, G. E., Noninvasive ultrasonic measurement of arterial wall motion in mice. *Am J Physiol Heart Circ Physiol*, 287 (3) H1426-32, 2004. [link]

41. Hartley, C. J., Reddy, A. K., Madala, S., Entman, M. L., Michael, L. H., Taffet, G. E., Doppler velocity measurements from large and small arteries of mice. *Am J Physiol Heart Circ Physiol*, 301 (2) H269-78, 2011. [link]

42. Hartley, C. J., Reddy, A. K., Madala, S., Entman, M. L., Taffet, G. E., Feasibility of dual Doppler velocity measurements to estimate volume pulsations of an arterial segment. *Ultrasound Med Biol*, 36 (7) 1169-75, 2010. [link]

43. Hartley, C. J., Reddy, A. K., Madala, S., Martin-McNulty, B., Vergona, R., Sullivan, M. E., Halks-Miller, M., Taffet, G. E., Michael, L. H., Entman, M. L., Wang, Y. X., Hemodynamic changes in apolipoprotein E-knockout mice. *Am J Physiol Heart Circ Physiol*, 279 (5)H2326-34, 2000. [link](#)

44. Hartley, C. J., Reddy, A. K., Madala, S., Michael, L. H., Entman, M. L., Taffet, G. E., Effects of isoflurane on coronary blood flow velocity in young, old and ApoE(-/-) mice measured by Doppler ultrasound. *Ultrasound Med Biol*, 33 (4) 512-21, 2007. [link](#)

45. Hartley, C. J., Reddy, A. K., Madala, S., Michael, L. H., Entman, M. L., Taffet, G. E., Doppler estimation of reduced coronary flow reserve in mice with pressure overload cardiac hypertrophy. *Ultrasound Med Biol*, 34 (6) 892-901, 2008. [link](#)

46. Hartley, C. J., Reddy, A. K., Michael, L. H., Entman, M. L., Chintalagattu, V., Khakoo, A. Y., Taffet, G. E., Coronary flow reserve in mice: effects of age, coronary disease, and vascular loading. *Conf Proc IEEE Eng Med Biol Soc*, 20103780-3, 2010. [link](#)

47. Hartley, C. J., Reddy, A. K., Michael, L. H., Entman, M. L., Taffet, G. E., Coronary flow reserve as an index of cardiac function in mice with cardiovascular abnormalities. *Conf Proc IEEE Eng Med Biol Soc*, 20091094-7, 2009. [link](#)

48. Hartley, C. J., Taffet, G. E., Reddy, A. K., Entman, M. L., Michael, L. H., Noninvasive cardiovascular phenotyping in mice. *ILAR J*, 43 (3)147-58, 2002. [link](#)

49. Haudek, S. B., Cheng, J., Du, J., Wang, Y., Hermosillo-Rodriguez, J., Trial, J., Taffet, G. E., Entman, M. L., Monocytic fibroblast precursors mediate fibrosis in angiotensin-II-induced cardiac hypertrophy. *J Mol Cell Cardiol*, 49 (3) 499-507, 2010. [link](#)

50. Henson, G. D., Walker, A. E., Reihl, K. D., Donato, A. J., Lesniewski, L. A., Dichotomous mechanisms of aortic stiffening in high-fat diet fed young and old B6D2F1 mice. *Physiol Rep*, 2 (3) e00268, 2014. [link](#)

51. Jin, Changzhu, Three dimensional wall motion of the carotid artery investigated by high-frequency ultrasound. 2014. [link](#)

52. Jung, S. M., Jandu, S., Steppan, J., Belkin, A., An, S. S., Pak, A., Choi, E. Y., Nyhan, D., Butlin, M., Viegas, K., Avolio, A., Berkowitz, D. E., Santhanam, L., Increased tissue transglutaminase activity contributes to central vascular stiffness in eNOS knockout mice. *Am J Physiol Heart Circ Physiol*, 305 (6) H803-10, 2013. [link](#)

53. Kass, D. J., Rattigan, E., Kahloon, R., Loh, K., Yu, L., Savir, A., Markowski, M., Saqi, A., Rajkumar, R., Ahmad, F., Champion, H. C., Early treatment with fumagillin, an inhibitor of methionine aminopeptidase-2, prevents Pulmonary Hypertension in monocrotaline-injured rats. *PloS one*, 7 (4) e35388, 2012. [link](#)

54. Kelley, E. E., Baust, J., Bonacci, G., Golin-Bisello, F., Devlin, J. E., St Croix, C. M., Watkins, S. C., Gor, S., Cantu-Medellin, N., Weidert, E. R., Frisbee, J. C., Gladwin, M. T., Champion, H. C., Freeman, B. A., Khoo, N. K., Fatty acid nitroalkenes ameliorate glucose intolerance and pulmonary hypertension in high-fat diet-induced obesity. *Cardiovasc Res*, 101 (3) 352-63, 2014. [link](#)

55. Kim, J. H., Bugaj, L. J., Oh, Y. J., Bivalacqua, T. J., Ryoo, S., Soucy, K. G., Santhanam, L., Webb, A., Camara, A., Sikka, G., Nyhan, D., Shoukas, A. A., Ilies, M., Christianson, D. W., Champion, H. C., Berkowitz, D. E., Arginase inhibition restores NOS coupling and reverses endothelial dysfunction and vascular stiffness in old rats. *J Appl Physiol (1985)*, 107 (4) 1249-57, 2009. [link](#)

56. Kulandavelu, Shathiyah, Cardiovascular, utero-and fetoplacental function in mice during normal pregnancy and in the absence of endothelial nitric oxide synthase (eNOS). 2010. [link](#)

57. Kulandavelu, S., Qu, D., Sunn, N., Mu, J., Rennie, M. Y., Whiteley, K. J., Walls, J. R., Bock, N. A., Sun, J. C., Covelli, A., Sled, J. G., Adamson, S. L., Embryonic and neonatal phenotyping of genetically engineered mice. *ILAR J*, 47 (2) 103-17, 2006. link

58. LaRocca, T. J., Gioscia-Ryan, R. A., Hearon, C. M., Jr., Seals, D. R., The autophagy enhancer spermidine reverses arterial aging. *Mech Ageing Dev*, 134 (7-8) 314-20, 2013. link

59. LaRocca, T. J., Hearon, C. M., Jr., Henson, G. D., Seals, D. R., Mitochondrial quality control and age-associated arterial stiffening. *Exp Gerontol*, 5878-82, 2014. link

60. Li, Han, Role of Spongiotrophoblast VEGFA during Pregnancy. 2011. link

61. Li, Jinghong, Friedrich, Craig R, Keynton, Robert S, Design and fabrication of a miniaturized, integrated, high-frequency acoustical lens transducer system. *J Micromech Microeng*, 12 (3) 219, 2002. link

62. Li, Y. H., Chung, H. C., Luo, C. Y., Chao, T. H., Shyu, K. G., Shi, G. Y., Wu, H. L., Thrombomodulin is upregulated in cardiomyocytes during cardiac hypertrophy and prevents the progression of contractile dysfunction. *J Card Fail*, 16 (12) 980-90, 2010. link

63. Li, Y. H., Reddy, A. K., Ochoa, L. N., Pham, T. T., Hartley, C. J., Michael, L. H., Entman, M. L., Taffet, G. E., Effect of age on peripheral vascular response to transverse aortic banding in mice. *J Gerontol A Biol Sci Med Sci*, 58 (10) B895-9, 2003. link

64. Li, Y. H., Reddy, A. K., Taffet, G. E., Michael, L. H., Entman, M. L., Hartley, C. J., Doppler evaluation of peripheral vascular adaptations to transverse aortic banding in mice. *Ultrasound Med Biol*, 29 (9) 1281-9, 2003. link

65. Lim, H. K., Ryoo, S., Benjo, A., Shuleri, K., Miriel, V., Baraban, E., Camara, A., Soucy, K., Nyhan, D., Shoukas, A., Berkowitz, D. E., Mitochondrial arginase II constrains endothelial NOS-3 activity. *Am J Physiol Heart Circ Physiol*, 293 (6) H3317-24, 2007. link

66. Lin, Y., Kuro-o, M., Sun, Z., Genetic deficiency of anti-aging gene klotho exacerbates early nephropathy in STZ-induced diabetes in male mice. *Endocrinology*, 154 (10) 3855-63, 2013. link

67. Marchi, R., Walton, B. L., McGary, C. S., Lin, F. C., Ma, A. D., Pawlinski, R., Mackman, N., Campbell, R. A., Di Paola, J., Wolberg, A. S., Dysregulated coagulation associated with hypofibrinogenaemia and plasma hypercoagulability: implications for identifying coagulopathic mechanisms in humans. *Thromb Haemost*, 108 (3) 516-26, 2012. link

68. Michael, L. H., Ballantyne, C. M., Zachariah, J. P., Gould, K. E., Pocius, J. S., Taffet, G. E., Hartley, C. J., Pham, T. T., Daniel, S. L., Funk, E., Entman, M. L., Myocardial infarction and remodeling in mice: effect of reperfusion. *Am J Physiol*, 277 (2 Pt 2) H660-8, 1999.link

69. Namiranian, K., Lloyd, E. E., Crossland, R. F., Marrelli, S. P., Taffet, G. E., Reddy, A. K., Hartley, C. J., Bryan, R. M., Jr., Cerebrovascular responses in mice deficient in the potassium channel, TREK-1. *Am J Physiol Regul Integr Comp Physiol*, 299 (2)R461-9, 2010. link

70. Reddy, A., Pham, T., Michael, L., Taffet, G., Hartley, C., Is aortic impedance altered in dwarf mice?. *Conf Proc IEEE Eng Med Biol Soc*, 1605-6, 2005. link

71. Reddy, AK, Taffet, GE, Prchal, JF, Michael, LH, Entman, ML, Hartley, CJ, Effect of cellular elements on pressure-velocity relationship in mice. *Engineering in Medicine and Biology Society, 2004. IEMBS'04. 26th Annual International Conference of the IEEE*, 23720-3722, 2004. link

72. Reddy, A. K., Amador-Noguez, D., Darlington, G. J., Scholz, B. A., Michael, L. H., Hartley, C. J., Entman, M. L., Taffet, G. E., Cardiac function in young and old Little mice. *J Gerontol A Biol Sci Med Sci*, 62 (12) 1319-25, 2007. link

73. Reddy, A. K., Hartley, C. J., Pham, T. T., Darlington, G., Entman, M. L., Taffet, G. E., Young little mice express a premature cardiovascular aging phenotype. *J Gerontol A Biol Sci Med Sci*, 69 (2) 152-9, 2014. link

74. Reddy, A. K., Li, Y. H., Pham, T. T., Ochoa, L. N., Trevino, M. T., Hartley, C. J., Michael, L. H., Entman, M. L., Taffet, G. E., Measurement of aortic input impedance in mice: effects of age on aortic stiffness. *Am J Physiol Heart Circ Physiol*, 285 (4) H1464-70, 2003. link

75. Reddy, Anilkumar K, Li, Yi-Heng, Pham, Thuy T, Taffet, George E, Michael, Lloyd H, Entman, Mark L, Hartley, Craig J, Indices of aortic stiffness in mice. *Engineering in Medicine and Biology Society, 2003. Proceedings of the 25th Annual International Conference of the IEEE*, 1276-278, 2003. link

76. Reddy, A. K., Madala, S., Jones, A. D., Caro, W. A., Eberth, J. F., Pham, T. T., Taffet, G. E., Hartley, C. J., Multichannel pulsed Doppler signal processing for vascular measurements in mice. *Ultrasound Med Biol*, 35 (12) 2042-54, 2009. link

77. Reddy, A. K., Namiranian, K., Lloyd, E. E., Bryan, R. M., Taffet, G. E., Hartley, C. J., Effect of isoflurane on aortic impedance in mice. *Conf Proc IEEE Eng Med Biol Soc*, 20091104-5, 2009. link

78. Reddy, A. K., Taffet, G. E., Hartley, C. J., Aortic impedance in Little mice. *Conf Proc IEEE Eng Med Biol Soc*, 20081397-8, 2008. link

79. Reddy, A. K., Taffet, G. E., Li, Y. H., Lim, S. W., Pham, T. T., Pocius, J. S., Entman, M. L., Michael, L. H., Hartley, C. J., Pulsed Doppler signal processing for use in mice: applications. *IEEE Trans Biomed Eng*, 52 (10) 1771-83, 2005. link

80. Reddy, A. K., Taffet, G. E., Madala, S., Michael, L. H., Entman, M. L., Hartley, C. J., Noninvasive blood pressure measurement in mice using pulsed Doppler ultrasound. *Ultrasound Med Biol*, 29 (3) 379-85, 2003. link

81. Reddy, A. K., Taffet, G. E., Prchal, J. F., Michael, L. H., Entman, M. L., Hartley, C. J., Effect of cellular elements on pressure-velocity relationship in mice. *Conf Proc IEEE Eng Med Biol Soc*, 53720-2, 2004. link

82. Robinson, P., Taffet, G. E., Engineer, N., Khumbatta, M., Firozgary, B., Reynolds, C., Pham, T., Bulsara, T., Firozgary, G., Substance P receptor antagonism: a potential novel treatment option for viral-myocarditis. *Biomed Res Int*, 2015645153, 2015. link

83. Santhanam, L., Tuday, E. C., Webb, A. K., Dowzicky, P., Kim, J. H., Oh, Y. J., Sikka, G., Kuo, M., Halushka, M. K., Macgregor, A. M., Dunn, J., Gutbrod, S., Yin, D., Shoukas, A., Nyhan, D., Flavahan, N. A., Belkin, A. M., Berkowitz, D. E., Decreased S-nitrosylation of tissue transglutaminase contributes to age-related increases in vascular stiffness. *Circ Res*, 107 (1) 117-25, 2010. link

84. Sikka, G., Pandey, D., Bhuniya, A. K., Steppan, J., Armstrong, D., Santhanam, L., Nyhan, D., Berkowitz, D. E., Contribution of arginase activation to vascular dysfunction in cigarette smoking. *Atherosclerosis*, 231 (1) 91-4, 2013. link

85. Sikka, G., Yang, R., Reid, S., Benjo, A., Koitabashi, N., Camara, A., Baraban, E., O'Donnell, C. P., Berkowitz, D. E., Barouch, L. A., Leptin is essential in maintaining normal vascular compliance independent of body weight. *Int J Obes (Lond)*, 34 (1) 203-6, 2010. link

86. Soucy, K. G., Lim, H. K., Attarzadeh, D. O., Santhanam, L., Kim, J. H., Bhunia, A. K., Sevinc, B., Ryoo, S., Vazquez, M. E., Nyhan, D., Shoukas, A. A., Berkowitz, D. E., Dietary inhibition of xanthine oxidase attenuates radiation-induced endothelial dysfunction in rat aorta. *J Appl Physiol (1985)*, 108 (5) 1250-8, 2010. link

87. Soucy, K. G., Lim, H. K., Benjo, A., Santhanam, L., Ryoo, S., Shoukas, A. A., Vazquez, M. E., Berkowitz, D. E., Single exposure gamma-irradiation amplifies xanthine oxidase activity and induces endothelial dysfunction in rat aorta. *Radiat Environ Biophys*, 46 (2)179-86, 2007. link

88. Soucy, K. G., Lim, H. K., Kim, J. H., Oh, Y., Attarzadeh, D. O., Sevinc, B., Kuo, M. M., Shoukas, A. A., Vazquez, M. E., Berkowitz, D. E.,HZE 56Fe-ion irradiation induces endothelial dysfunction in rat aorta: role of xanthine oxidase. *Radiat Res*, 176 (4) 474-85, 2011. link

89. Soucy, K. G., Ryoo, S., Benjo, A., Lim, H. K., Gupta, G., Sohi, J. S., Elser, J., Aon, M. A., Nyhan, D., Shoukas, A. A., Berkowitz, D. E.,Impaired shear stress-induced nitric oxide production through decreased NOS phosphorylation contributes to age-related vascular stiffness. *J Appl Physiol (1985)*, 101 (6) 1751-9, 2006. link

90. Stansfield, W. E., Rojas, M., Corn, D., Willis, M., Patterson, C., Smyth, S. S., Selzman, C. H.,Characterization of a model to independently study regression of ventricular hypertrophy. *J Surg Res*, 142 (2) 387-93, 2007. link

91. Steppan, J., Tran, H., Benjo, A. M., Pellakuru, L., Barodka, V., Ryoo, S., Nyhan, S. M., Lussman, C., Gupta, G., White, A. R., Daher, J. P., Shoukas, A. A., Levine, B. D., Berkowitz, D. E., Alagebrium in combination with exercise ameliorates age-associated ventricular and vascular stiffness. *Exp Gerontol*, 47 (8) 565-72, 2012. link

92. Thakker, G. D., Frangogiannis, N. G., Bujak, M., Zymek, P., Gaubatz, J. W., Reddy, A. K., Taffet, G., Michael, L. H., Entman, M. L., Ballantyne, C. M., Effects of diet-induced obesity on inflammation and remodeling after myocardial infarction. *Am J Physiol Heart Circ Physiol*, 291 (5) H2504-14, 2006. link

93. Tuday, E. C., Meck, J. V., Nyhan, D., Shoukas, A. A., Berkowitz, D. E., Microgravity-induced changes in aortic stiffness and their role in orthostatic intolerance. *J Appl Physiol (1985)*, 102 (3) 853-8, 2007. link

94. Tuday, E. C., Nyhan, D., Shoukas, A. A., Berkowitz, D. E., Simulated microgravity-induced aortic remodeling. *J Appl Physiol (1985)*,106 (6) 2002-8, 2009. link

95. Vela, Deborah,Dynamic Remodeling of the Stressed Heart: Role of Protein Degradation Pathways. 2010. link

96. Vendrov, A. E., Vendrov, K. C., Smith, A., Yuan, J., Sumida, A., Robidoux, J., Runge, M. S., Madamanchi, N. R., NOX4 NADPH Oxidase-Dependent Mitochondrial Oxidative Stress in Aging-Associated Cardiovascular Disease. *Antioxid Redox Signal*, 23 (18) 1389-409, 2015. link

97. Vincelette, J., Martin-McNulty, B., Vergona, R., Sullivan, M. E., Wang, Y. X., Reduced cardiac functional reserve in apolipoprotein E knockout mice. *Transl Res*, 148 (1) 30-6, 2006. link

98. Walker, A. E., Henson, G. D., Reihl, K. D., Morgan, R. G., Dobson, P. S., Nielson, E. I., Ling, J., Mecham, R. P., Li, D. Y., Lesniewski, L. A., Donato, A. J., Greater impairments in cerebral artery compared with skeletal muscle feed artery endothelial function in a mouse model of increased large artery stiffness. *J Physiol*, 593 (8) 1931-43, 2015. link

99. Wang, J. G., Geddings, J. E., Aleman, M. M., Cardenas, J. C., Chantrathammachart, P., Williams, J. C., Kirchhofer, D., Bogdanov, V. Y., Bach, R. R., Rak, J., Church, F. C., Wolberg, A. S., Pawlinski, R., Key, N. S., Yeh, J. J., Mackman, N., Tumor-derived tissue factor activates coagulation and enhances thrombosis in a mouse xenograft model of human pancreatic cancer. *Blood*, 119 (23) 5543-52, 2012. link

100. Wang, Yi-Xin,Measurement of pulse wave velocity. *A Handbook of Mouse Models of Cardiovascular Disease*245-254, 2006. link

101. Wang, Y. X., da Cunha, V., Martin-McNulty, B., Vincelette, J., Li, W., Choy, D. F., Halks-Miller, M., Mahmoudi, M., Schroeder, M., Johns, A., Light, D. R., Dole, W. P., Inhibition of Rho-kinase by fasudil attenuated angiotensin II-induced cardiac hypertrophy in apolipoprotein E deficient mice. *Eur J Pharmacol*, 512 (2-3) 215-22, 2005. link

102.   Wang, Y. X., Martin-McNulty, B., da Cunha, V., Vincelette, J., Lu, X., Feng, Q., Halks-Miller, M., Mahmoudi, M., Schroeder, M., Subramanyam, B., Tseng, J. L., Deng, G. D., Schirm, S., Johns, A., Kauser, K., Dole, W. P., Light, D. R., Fasudil, a Rho-kinase inhibitor, attenuates angiotensin II-induced abdominal aortic aneurysm in apolipoprotein E-deficient mice by inhibiting apoptosis and proteolysis. *Circulation*, 111 (17) 2219-26, 2005. link

103.   Weisleder, N., Taffet, G. E., Capetanaki, Y., Bcl-2 overexpression corrects mitochondrial defects and ameliorates inherited desmin null cardiomyopathy. *Proc Natl Acad Sci U S A*, 101 (3) 769-74, 2004. link

104.   Wong, A. Y., Kulandavelu, S., Whiteley, K. J., Qu, D., Langille, B. L., Adamson, S. L., Maternal cardiovascular changes during pregnancy and postpartum in mice. *Am J Physiol Heart Circ Physiol*, 282 (3) H918-25, 2002. link

105.   Xu, J., Lin, S. C., Chen, J., Miao, Y., Taffet, G. E., Entman, M. L., Wang, Y., CCR2 mediates the uptake of bone marrow-derived fibroblast precursors in angiotensin II-induced cardiac fibrosis. *Am J Physiol Heart Circ Physiol*, 301 (2) H538-47, 2011. link

106.   Yabluchanskiy, A., Ma, Y., Chiao, Y. A., Lopez, E. F., Voorhees, A. P., Toba, H., Hall, M. E., Han, H. C., Lindsey, M. L., Jin, Y. F., Cardiac aging is initiated by matrix metalloproteinase-9-mediated endothelial dysfunction. *Am J Physiol Heart Circ Physiol*, 306 (10) H1398-407, 2014. link

107.   Yang, Fanmuyi, Inflammatory interactions and secretion in cardiac remodeling. 2012. link

108.   Yang, F., Dong, A., Ahamed, J., Sunkara, M., Smyth, S. S., Granule cargo release from bone marrow-derived cells sustains cardiac hypertrophy. *Am J Physiol Heart Circ Physiol*, 307 (10) H1529-38, 2014. link

109.   Yang, F., Dong, A., Mueller, P., Caicedo, J., Sutton, A. M., Odetunde, J., Barrick, C. J., Klyachkin, Y. M., Abdel-Latif, A., Smyth, S. S.,Coronary artery remodeling in a model of left ventricular pressure overload is influenced by platelets and inflammatory cells. *PloS one*,7 (8) e40196, 2012. link

110.   Yang, R., Sikka, G., Larson, J., Watts, V. L., Niu, X., Ellis, C. L., Miller, K. L., Camara, A., Reinke, C., Savransky, V., Polotsky, V. Y., O'Donnell, C. P., Berkowitz, D. E., Barouch, L. A., Restoring leptin signaling reduces hyperlipidemia and improves vascular stiffness induced by chronic intermittent hypoxia. *Am J Physiol Heart Circ Physiol*, 300 (4) H1467-76, 2011. link

111.   Yue, Xiaojing, Mechanistic Study of Rnd3 in Cardiomyopathy. 2015. link

112.   Yue, X., Yang, X., Lin, X., Yang, T., Yi, X., Dai, Y., Guo, J., Li, T., Shi, J., Wei, L., Fan, G. C., Chen, C., Chang, J., Rnd3 haploinsufficient mice are predisposed to hemodynamic stress and develop apoptotic cardiomyopathy with heart failure. *Cell Death Dis*, 5e1284, 2014.link

113.   Zhang, J., Liu, Q., Han, H. C., An in vivo rat model of artery buckling for studying wall remodeling. *Ann Biomed Eng*, 42 (8) 1658-67,2014. link

114.   Zhang, Y., Yue, Y., Li, L., Hakim, C. H., Zhang, K., Thomas, G. D., Duan, D., Dual AAV therapy ameliorates exercise-induced muscle injury and functional ischemia in murine models of Duchenne muscular dystrophy. *Hum Mol Genet*, 22 (18) 3720-9, 2013. link

115.   Zhou, R. H., Vendrov, A. E., Tchivilev, I., Niu, X. L., Molnar, K. C., Rojas, M., Carter, J. D., Tong, H., Stouffer, G. A., Madamanchi, N. R., Runge, M. S., Mitochondrial oxidative stress in aortic stiffening with age: the role of smooth muscle cell function. *Arterioscler Thromb Vasc Biol*, 32 (3) 745-55, 2012. link

116.   Zhou, Y. Q., Foster, F. S., Parkes, R., Adamson, S. L., Developmental changes in left and right ventricular diastolic filling patterns in mice. *Am J Physiol Heart Circ Physiol*, 285 (4) H1563-75, 2003. link

117.	Zhou, Y. Q., Foster, F. S., Qu, D. W., Zhang, M., Harasiewicz, K. A., Adamson, S. L., Applications for multifrequency ultrasound biomicroscopy in mice from implantation to adulthood. *Physiol Genomics*, 10 (2) 113-26, 2002. [link](#)